ELECTRONIC, OPTICAL AND ATOMISTIC STUDIES OF $PtSb_2$ AND $PtBi_2$

By

Samuel Seshupo Mangwejane

A dissertation submitted in fulfillment of the requirements for the degree of

Master of Science in the Faculty of Sciences,Health and Agriculture

University of Limpopo

Turfloop Campus (Former University of the North)

South Africa

February 2005

Supervisor: Prof. P.E. Ngoepe

Co-Supervisor: Prof. S.C. Parker

DECLARATION

I declare that the dissertation hereby submitted to the University of Limpopo for the degree of Master of Science has not been previously submitted by me for a degree at this or any other university; that it is my work in design and execution, and that all material contained therein has been duly acknowledged.

Samuel Seshupo Mangwejane

Date

University of Limpopo

STUDIES OF $PtSb_2$ AND $PtBi_2$ USING AB INITIO TECHNIQUES AND ATOMISTIC SIMULATION

By Samuel Seshupo Mangwejane

ACKNOWLEDGMENTS

I wish to express my sincere gratitude to my advisors, Professor P.E. Ngoepe and Professor S.C. Parker, for their excellent guidance and support during this research. I wish to thank Dr H.M. Sithole for stimulating discussions and support during the stages of this research. I would like to thank my numerous friends at the University of Limpopo especially my fellow students in the Materials Modelling Centre (MMC).

Acknowledgements are also in order for financial received from National Research Foundation and allowances from The Royal Society (UK) and The Royal Institution of Great Britain (UK) and the University of Bath for hosting me during the visits of the summer of 2001 and winter of 2003.

I am grateful to my family for always being there for me. They were a constant source of encouragement and dedicate this thesis to the memory of my late mother Mrs. Irene Monqo and my grand parents.

ABSTRACT

Platinum group minerals are abundant in South Africa. Platinum is of great significance in catalytic applications and many other medical and pharmaceutical industries.

Our studies of $PtSb_2$ and $PtBi_2$ were carried out using Density Functional Techniques, including LDA and GGA methods. We investigated the pressure dependences of lattice parameters and bond lengths of the materials. All these properties were shown to decrease with increasing pressure, in a linear fashion. Other features that were studied are the electronic properties like density of states (DOS) and optical properties to determine the type of material being studied.

A set of interatomic potentials has been derived for the study of bulk and surface properties of $PtSb_2$ using the GULP code (General Utility Lattice Program). These potentials have proved to be reliable since they reproduced bulk properties of $PtSb_2$ such as lattice parameters and elastic constants. As there are no experimental studies on surfaces we have been able, for the first time, to calculate surface energies for the low index surfaces and found out that the most stable surface is the {100} Sb terminated one, with the energy of 0.933 $J.m^{-2}$ and the least stable is the {111} Sb terminated surface with the energy of 2.586 $J.m^{-2}$.

Science: the study of how nature behaves

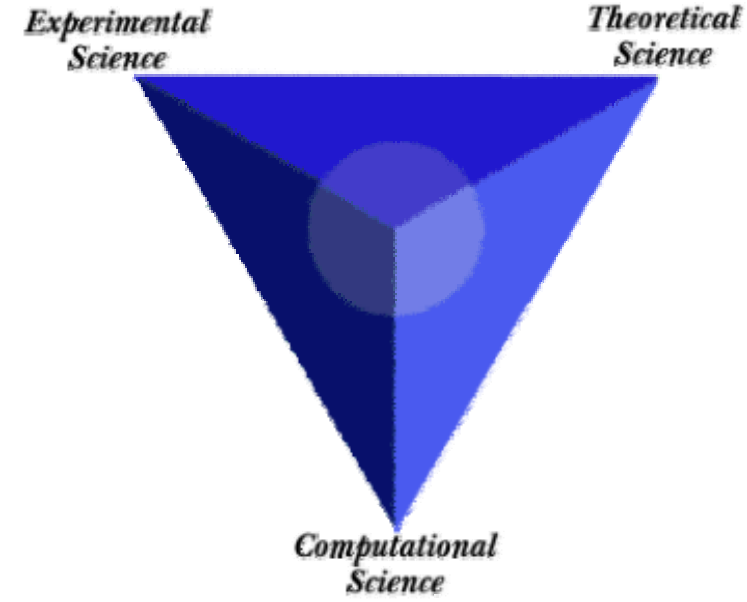

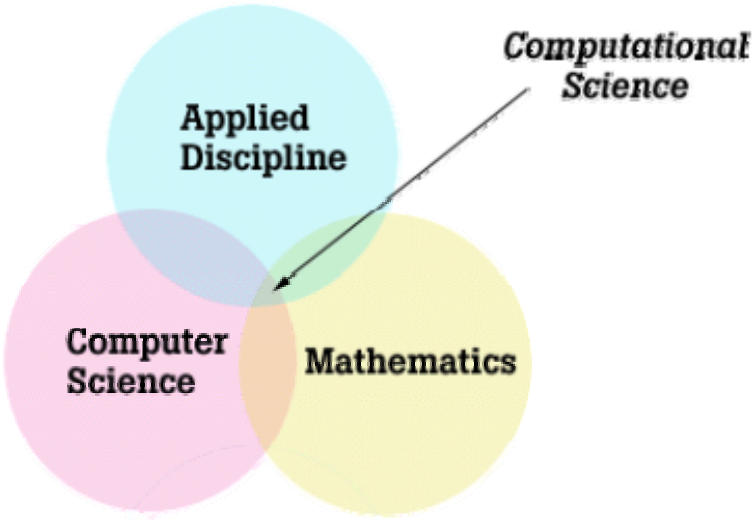

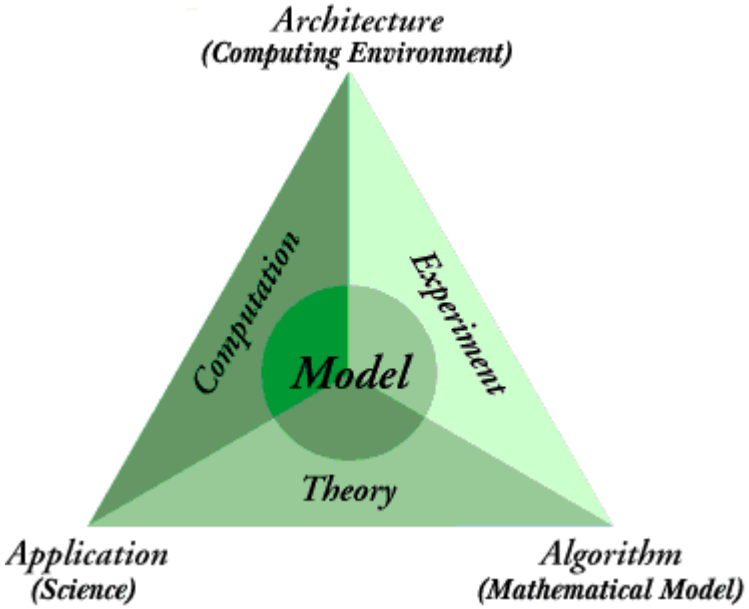
Architecture
(Computing Environment)
Computation
Experiment
Model
Theory
Application
(Science)
Algorithm
(Mathematical Model)

Table of Contents

List of Figures

List of Tables

Chapter 1

Introduction

1.1 General Introduction

In the past decade, there has been a considerable increase in the computational study of materials and the efficiency of the methods employed has improved with the passing of time. Studies are carried out using ab initio methods and atomistic methods, which have different advantages in the results that they produce. The other difference comes from the fact that ab-initio calculations take a lot of computational time and that the atomistic methods do not last long to complete.

1.2 Structural Aspects

The space group of pyrite is T_h^6 (Pa-3) where the four metal atoms are located at 4(a) positions: (0,0,0), (0,1/2,1/2), (1/2,0,1/2) and (1/2,1/2,0) and the eight antimony atoms are in 8(c) positions: ±(u,u,u) , ±(u+1/2,1/2-u,-u), ±(-u,u+1/2,1/2-u) and ±(1/2-u,-u,u+1/2). There are additional symmetry positions (24d) (x,y,z) with x=0.31681,y=0.09448 and z=0.21362. The internal parameter of $PtSb_2$ is u=0.375Å and the lattice parameter of the unit cell a=6.44 Å [Emtage et al, 1965] obtained from experimental measurements. $PtBi_2$ has the internal parameter of 0.3725 Å from calculations and the experimental lattice parameter is 6.625 Å [http://webmineral.com/data/Insizwaite.shtml]

These structures have a pyrite form and therefore their space group is 205 in the crystallographic table. They have the same form as the sodium chloride structure, but have a dimer of Sb_2 (Bi_2). This feature makes the bond between the Sb (Bi) to be more covalent.

The melting point of $PtSb_2$ is estimated to be around 1500K, which indicates that it takes a lot of energy to dissociate this structure. The melting temperature gives a guide as to the strength of the material and therefore its crystal energy or lattice energy.

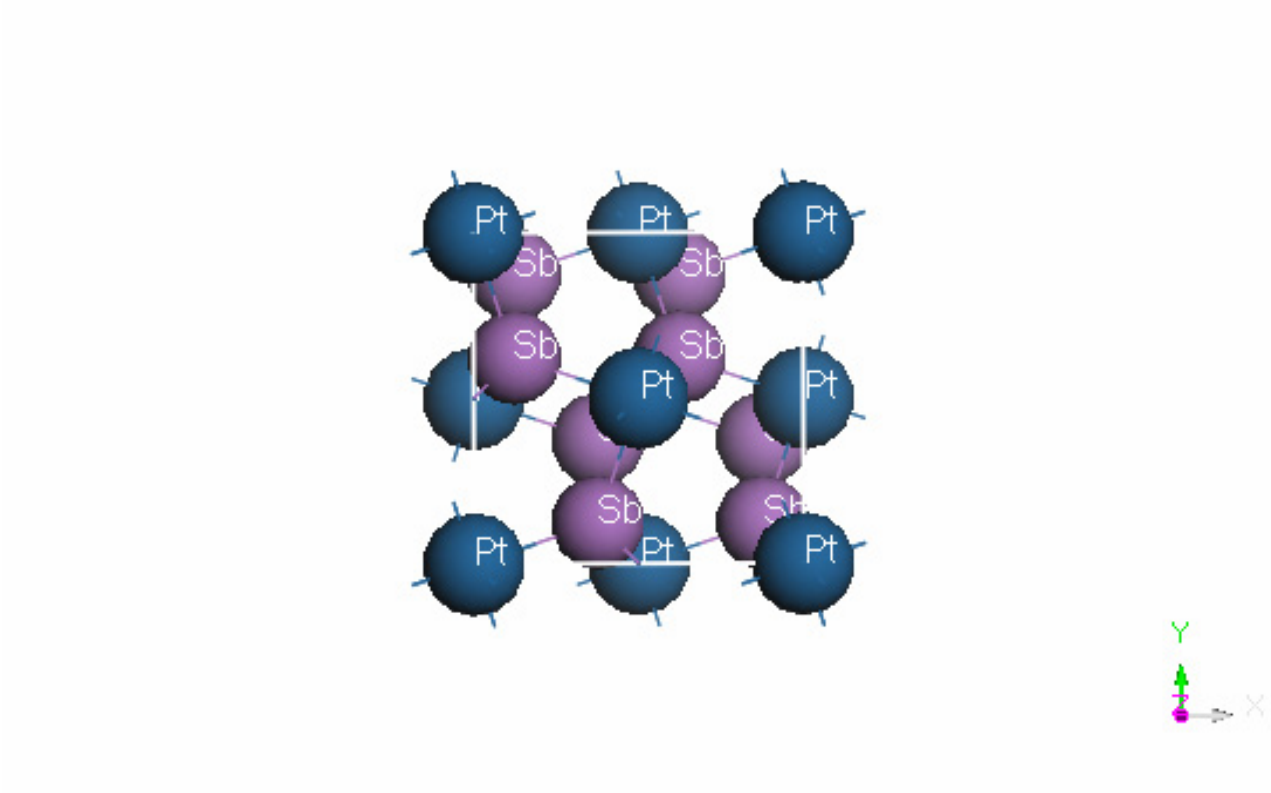

Figure 1: A two dimensional pyrite-structured $PtSb_2$

1.2.1 $PtSb_2$

The pyrite crystal is best described in terms of the NaC1 structure with the sublattices occupied by platinum atoms and the centres of gravity of antimony and bismuth atoms pairs, respectively. The dumbbells are antimony (Sb) along the [111] direction. Whereas the antimony/bismuth atoms are tetrahedrally co-ordinated by one antimony/bismuth and three platinum atoms, the six nearest neighbour antimony/bismuth atoms at each platinum site form slightly deformed octahedra. Due to the deformations of the octahedra, the local

symmetry at the sites is reduced from cubic (0h) to trigonal (C3i). The distorted $PtSb_2$ octahedra are interlinked by common corners and, due to the formation of the <111> antimony pairs, have rotated away from the cartesian axes by about 23. For a two-dimensional crystal the situation is sketched in figure 1 above. Obviously the formation of the <111> arresting pairs does not destroy the square planar coordination of the platinum atoms. Instead the squares built by the antimony atoms just shrink and rotate. Since the orientation of dumbbells conforms to the cubic point group, the underlying Bravais lattice is not longer face centered but simple cubic and the unit cell comprises four formula units. Yet as will be seen below, some features of the electronic structure my still be understood in terms of the face-centered-cubic (fcc) lattice.

1.2.2 $PtBi_2$

$PtBi_2$ have a lot in common with $PtSb_2$ in terms of atomic arrangement and the space group. It has the pyrite structure, but it is metallic in nature. It is of hydrothermal origin, in a vein cutting massif pyrrhotite ore, mostly found in South Africa. The lattice parameter of this compound is a = 6.625 Å and the volume 290.78 $Å^3$ determined experimentally. Calculated density is given as 13.01 g/ $Å^3$. This material has a tin white colour [http://webmineral.com/data/Insizwaite.shtml]. A lot has to be researched and investigated about this compound, as there are no known studies carried out on it thus far.

1.3 Literature Review

Compounds with the pyrite structure especially FeS_2 have been studied extensively both experimentally [Deer et al 1992, Eyert et al 1998, Jaegerman and Tributsch 1993, Ennaoui and Tributsch 1984] and theoretically [Temmerman et al, Zhao et al 1993]. $PtSb_2$ and $PtBi_2$, are found in platinum ores and have a similar structure. Little experimental work has been

carried out on these compounds. Recent *ab initio* TB-LMTO and pseudopotential planewave studies have shown that FeS_2 [Sithole, 2000] and $PtAs_2$ [Ntoahae et al, 1999] are semiconductors with an indirect bandgaps of 0.75 and 0.34 eV respectively. In the case of $PtAs_2$, the As (4s) states form a separate bonding-antibonding gap at high binding energy similar to those of S (3S0) states in pyrite FeS_2. The semiconductor gap was found to originate from the Pt (5d) and As (4p) hybridization effect. Furthermore, the lattice parameter was predicted quite well, without even relaxing the internal parameter. Full relaxation of volume and internal parameters of iron pyrite and marcasite FeS_2, were also carried out using plane-wave pseudopotential methods [Sithole, 2000]. It was found that the internal parameter of pyrite decreases with increasing hydrostatic compression and P-V equation of state fell slightly closer to the experimental curve that the previous unrelaxed TB-LMTO calculations [Sithole, 2000].

On the atomistic simulations a new model has been derived for pyrite [de Leeuw et al 2000, Sithole et al 2003] and marcasite FeS_2 [Sithole et al 2000], and has reproduced bulk and surface properties of these materials quite well at both high pressures and temperatures. In the current work full relaxation and pressure dependent calculations of the lattice and internal parameters, together with charge distributions, density of states and optical properties will be carried out using plane-wave pseudopotential (PWP) methods.

1.3.1 Structural Properties

Structural properties of a material tell us about the strength of the material. These are more pronounced when they are being studied under extreme conditions of high pressure and high temperature. Also the colour of materials might give an indication as to what type of material we are studying.

1.3.2 Electronic and Optical Properties

Electronic properties of a material help us to consider the material under three main groups, namely, metals, semiconductors and insulators. The existence and size of the energy gap (the gap between the highest occupied orbitals and the lowest unoccupied orbital) determines the type of material. In the case of a metal there is no gap as there is overlap of the orbitals, but for semiconductors and insulators there is a gap but is large in insulators. For $PtSb_2$ work has been carried out experimentally, and it was found that it has a narrow band gap of about 0.11 eV [Emtage et al 1965]. The room-temperature elastic-coefficient values calculated from sound-velocity measurements made by the pulse-echo technique are from Damon et al (1965) and are given in Table 2. Little is known about the compound $PtBi_2$.

1.3.3 Short review of techniques

Recent technological developments have led to increasing demands for the materials with special properties. Accordingly, qualitatively new classes of materials have emerged with properties that are fascinating for both scientists and engineers. The dominating approach in studying materials is experiments. However, the possibilities to study materials properties from the first-principles electronic theory were enormously enhanced when the density functional theory (DFT) was formulated by Kohn and co-workers in the mid-60's. At the same time, rapid progress is taking place in the field of numerical computations. These put on the agenda the possibility of ab initio design of structural materials.

In the past twenty years Catlow and co-workers in the field of computer modelling have pioneered the study in atomistic modelling, including Molecular Dynamics. The principle techniques used in the simulation field are energy minimisation, molecular dynamics and Monte Carlo [Catlow and Kotomin, 1990].

Computer simulation studies provide reliable models at the atomistic level by shedding insight and understanding of simulated systems, assist in the interpretation of experimental data and also by providing numerical data on important parameters difficult to measure using experiment. In molecular dynamics, the work of Catlow is very profound, as it involves the use of interatomic potentials. Much of this work involves the calculation of surface energies, temperature dependency of materials and other interesting properties, like diffusion of molecules.

An atomistic simulation involves potential functions and their evaluation. The potential energy function expresses the energy of an assembly of atoms or ions as a function of their nuclear coordinates. Many successes of this method can be found in the reference given above which are benchmarked with experiment. Extensive work has also been done by people involved in the development of the theory like Wimmer (1985), Perdew (1986) and Payne (1992).

Figures 2 and 3 give an overview on the evolution of computational approaches and the choices of the techniques that are being routinely used in the study of materials and their properties.

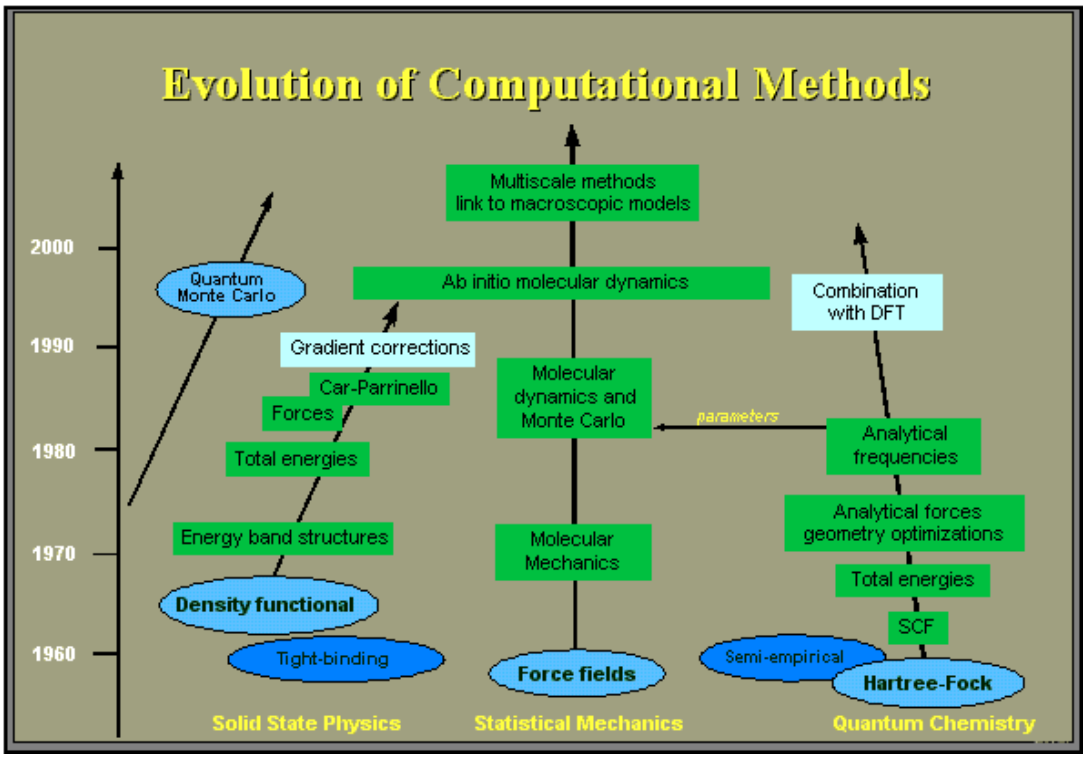

Figure 2: Evolution of computational approaches

1.4 Intentions of the Study

The aim of this work is to study the structures of $PtSb_2$ and $PtBi_2$ using ab-initio and atomistic simulations. It will be indicated in the subsequent sections the kinds of methods that are traditionally used. We will derive inter-atomic potentials for the study of the bulk structure and surface properties, including the calculation of surface energies. Our work on atomistic simulations will entail subjecting our materials to high temperatures and pressures to find what effect that will have, as they are found in ores under these extreme conditions.

For studies involving ab initio techniques, we will be focusing our attention on determining the structural, electronic and optical properties of $PtSb_2$ and $PtBi_2$.

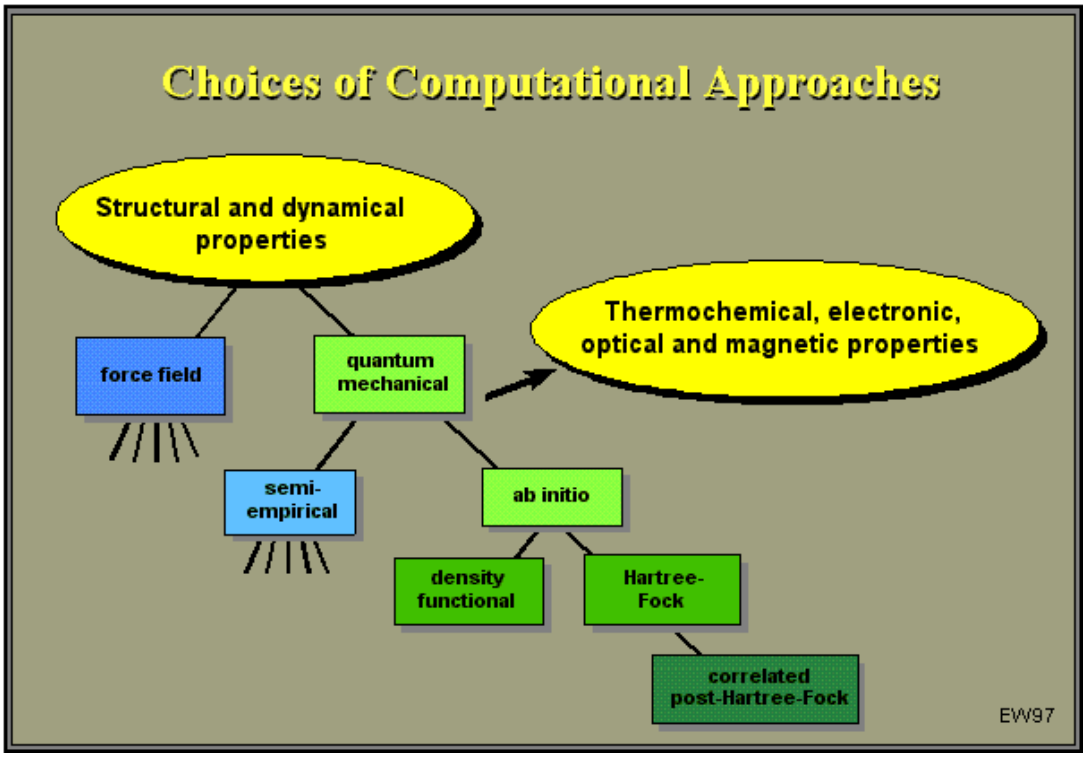

Figure 3: Choices of computational methods

1.5 Outline of the Study

In chapter 1 there will be topics on literature review, the structure and general aspects including the introduction. Chapter 2 will deal with the theoretical basis (foundation), concentrating initially on density functional theory. In chapter 3 we will give the results for our structural, electronic and optical calculations obtained using CASTEP. Chapter 4 focuses on potential models that we will employ in the derivation of interatomic potentials and the calculation of surface energies. In chapter 5 a conclusion is given together with the appendix and references.

Chapter 2
Theoretical Methods

General Introduction

Simulation methods are an ideal tool to understand and predict the properties of matter at the atomistic level. There are various theoretical methods available for the investigation of different properties of materials, and these include ab initio (e.g. Density Functional Theory, Hartree-Fock, semi-empirical and classical empirical methods. The first method is about treating the system involving the electron (all-electron) and forming the functionals (pseudopotentials) for calculations of a myriad of properties of interest. The third focuses on the interatomic potentials derived for the attainment of more or fewer properties as the above but with less computational effort and time invested.

2.1 Ab initio methods

Ab initio, from Latin meaning from first principles, is a group of methods in which molecular structures can be calculated using nothing but the Schrödinger equation, the values of the fundamental constants and the atomic numbers of the atoms present. In this case, no empirical data is used. These methods include density functional theory, Hartree-Fock methods and post-Hartree-Fock methods, which are described in the subsequent subsections.

2.1.1 Formalism of Density Functional Theory

Shortly after the formulation of quantum mechanics in the mid 1920's, Thomas (1926) and Fermi (1928) introduced the idea of expressing the total energy of a system as a functional of the total electron density. Because of the crude treatment of the kinetic energy term, i. e. the absence of molecular orbitals, the accuracy of these early attempts was far from satisfactory. It was not until the 1960's that an exact theoretical framework called Density Functional

Theory (DFT) was formulated by Hohenberg and Kohn and Kohn and Sham (1965) that provided the foundation for accurate calculations. Earlier, motivated by the search for practical electronic structure calculations, [Slater, 1951] had developed an approach, later to become the Xα method [Slater, 1974] which was originally intended as an approximation to Hartree-Fock theory. Today, the Xα method is generally viewed as a simplified form or precursor of density functional theory.

In contrast to the Hartree-Fock picture, which begins conceptually with a description of individual electrons interacting with the nuclei and all other electrons in the system, density functional theory starts with a consideration of the entire electron system. In density functional theory, the total energy is decomposed into three contributions, a kinetic energy, a Coulomb energy due to classical electrostatic interactions among all charged particles in the system, and a term called the exchange-correlation energy that captures all many-body interactions. This decomposition is formally exact, but the actual expressions for the many-body exchange and correlation interactions are unknown.

The Local Density Approximation (LDA) turned out to be computationally convenient and surprisingly accurate. In this approximation, the exchange-correlation energy is taken from the known results of the many-electron interactions in an electron system of constant density (homogeneous electron gas). The LDA amounts to the following picture: at each point in a molecule or solid there exists a well defined electron density; it is assumed that an electron at such a point experiences the same many-body response by the surrounding electrons as if the density of these surrounding electrons had the same value throughout the entire space as at the point of the reference electron. The exchange-correlation energy of the total molecule or solid is then the integral over the contributions from each volume element.

The contributions are different from each volume element depending on the local electron density. The LDA is exact for a perfect metal (which has a constant electron density) and becomes less accurate for systems with varying electron density. Remarkably, the LDA is also quite well suited for systems with a high electron density such as transition metals. In DFT, the total electron density is decomposed into one-electron densities, which are constructed from one-electron wave functions. These one-electron wave functions are similar to those of Hartree-Fock theory. For molecular systems, DFT leads to a molecular orbital (MO) picture in analogy to the Hartree-Fock approach.

DFT has been successfully extended to open-shell systems and magnetic solids [von Barth and Hedin, 1972; Gunnarsson et al, 1972]. In these cases, the local exchange-correlation energy depends not only on the local electron density, but also on the local spin density (which is the difference between the electron density of spin-up electrons and that of spin-down electrons). The resulting generalization of LDA is called local spin density approximation (LSDA).

A priori it is not clear which of the two pictures, the Hartree-Fock approach or the local density functional approach gives better results. In fact, the applicability of the Hartree-Fock picture vs. the local (spin) density approximation depends on the effective range of many-body interactions between electrons. If these interactions are of dimensions of several interatomic distances, then the Hartree-Fock description is better. The mathematical objects used in Hartree-Fock based approaches to describe these many-body or electron correlation effects are molecular orbitals which are quite large, extending over many interatomic distances. If, however, these many-body effects are of a more short-range nature, perhaps smaller than interatomic distances, then the local density approximation is more appropriate. In such a case, a description of these short-range phenomena with large mathematical objects

such as molecular orbitals is extremely slowly converging. As quantum chemists are painfully aware of, this is indeed the case with configuration interaction methods.

Experience shows that for many systems including metals, transition metal compounds, but also organic and inorganic molecules, the LDA gives surprisingly good results, especially for the prediction of structural properties. Configuration interaction expansions, on the other hand, are known for their notoriously slow convergence. This may be taken as evidence of the more local character of many-body interactions for many systems of interest.

2.1 2 Evolution of DFT methods

Prior to the developments of density functional theory, the calculation of energy band structures for crystalline solids had become a major goal of computational solid state physics. During the 1960's, when quantum chemists began systematic Hartree-Fock studies on small molecules, energy band structure calculations of solids were possible only for simple systems such as crystals of copper and silicon containing one or a few atoms per unit cell. The aims of these efforts in solid-state physics were different from those of quantum chemistry. Whereas quantum chemistry focused on the ab initio determination of molecular structures and energies, the goal of energy band structure calculations for solids was the understanding of conducting and insulting behaviour, the elucidation of the types of bonding, the prediction of electronic excitations such as energy band gaps, and the interpretation of photoexcitation spectra.

To this end, semiempirical pseudopotential theory [Phillips, 1958; Cohen and Heine, 1970] became a successful and pragmatic approach especially for semiconductors. All-electron band structure calculations were applied mostly to transition metals and their compounds. Initially, these calculations were carried out non-self-consistently. For a given crystal

structure and atomic positions in the lattice, a crystal potential was constructed from superposed atomic densities and the energy bands evaluated for selected points in momentum space without improving the electron density through a self-consistency procedure. The shape of the crystal potential was simplified in the form of a "muffin-tin" potential [Slater, 1937] with a spherical symmetric potential around the atoms and a constant potential between the atomic spheres. For close-packed structures such as fcc Cu, this is an excellent approximation and substantially simplifies the calculation of the energy bands. During the 1960's, self-consistency was introduced still using the simplified "muffin-tin" potential. Around 1970, self-consistent muffin-tin energy band structure calculations were possible for systems containing a few atoms per unit cell.

At that time, quantum chemists had already recognized the power of total energies as a tool for geometry optimisation of molecules and had developed analytic energy gradients (forces) that greatly facilitated geometry optimisations. Shape approximations to the potential are questionable for open molecular structures and hence the use of the muffin-tin approximation in the form of the so-called multiple-scattering X-alpha method [Slater, 1974] for molecules and clusters met with scepticism among many ab initio quantum chemists.

In computational solid state physics, total energy calculations as a predictive tool for crystal structures and elastic properties of solids came into general use only in the mid to late 1970's, which was almost 10 years later than the corresponding development in Hartree-Fock theory for molecules.

By 1970, density functional theory had become a widely accepted many-body approach for first-principles calculations on solids, superseding the X-alpha-approach. Initially, energy band structure methods such as the augmented plane wave (APW) method [Slater, 1937] and the Korringa-Kohn-Rostoker (KKR) method [Korringa, 1947; Kohn and Rostoker, 1954]

were very tedious since the system of equations to be solved in each iterative step of the self-consistency procedure were non-linear (the matrix elements depended on the energy). Furthermore, the computer hardware at that time was limited both in processor speed, but perhaps even more by memory size. A major step forward was the introduction of linearized methods, especially the linearized augmented plane wave (LAPW) method [Koelling and Arbman, 1975; Andersen, 1975] and the linearized muffin-tin orbital (LMTO) method [Andersen, 1975].

By 1980, quantum chemists had developed analytical second derivatives in Hartree-Fock theory for the investigation of structural and vibrational properties of molecules. During the same time, computational solid state physicists worked on the formulation of all-electron self-consistent methods without muffin-tin shape approximations, such as the full-potential linearized augmented plane wave (FLAPW) method with total energy capabilities as reviewed by Wimmer et al (1985). Analytic first derivatives (forces) within solid state calculations were first introduced in pseudopotential plane wave methods as reviewed by Payne et al (1992) and only fairly recently in other solid-state methods. Larger unit cells of bulk solids with more degrees of freedom and especially the investigation of surfaces required tools for predicting the position of atoms, for example in the case of surface reconstructions. Hence, total energy and force methods for solids and surfaces became more urgent.

In solid state calculations, the emphasis had shifted from the prediction of electronic structure effects for a given atomic arrangement to the prediction of structural and energetic properties as revealed by novel techniques such as extended x-ray absorption fine structure spectroscopy (EXAFS) and the scanning tunnelling microscope (STM). Pseudopotential theory, originally used in the form of a parameterised semiempirical approach for calculating

energy band structures of semiconductors, had been developed into a first-principles method with rigorous procedures to construct reliable pseudopotentials [Bachelet et al, 1982]. Pseudopotentials turned out to be particularly elegant and useful for the investigation of main-group element semiconductors.

Using the pseudopotential plane wave approach, Car and Parrinello (1985) made an important step in the unification of electronic structure theory and statistical mechanics. In this approach, it is possible to simulate the motions of the atomic nuclei, as they would occur, for example, in a chemical reaction while at the same time relaxing the electronic structure, all within a single theoretical framework. Until then, molecular dynamics had been mostly the domain of empirical force field approaches, which are not intended for describing the formation, and breaking of chemical bonds.

Density functional theory, originally intended for metallic solid state systems, turned out to be also surprisingly successful for describing the structure and energetics of molecules. First clear evidence for the capabilities of the local density functional approach for molecular systems was given already in the 1970's, but only recent systematic calculations on a large number of typical molecules together with the introduction of gradient corrected density functionals [Perdew, 1986; Becke, 1988] have made density functional theory an accepted approach for quantum chemistry [Labanowski and Andzelm, 1991]. These capabilities of density functional theory as tool for molecular and chemical problems are remarkable, since the theory was originally developed as approach in solid-state physics.

2.1.3 Assessment of DFT methods

In view of the criteria introduced earlier, the status of density functional calculations for solids, surfaces, and molecules can be characterized as follows.

Capability

Like Hartree-Fock methods, density functional calculations provide structural, energetic, and vibrational properties. More than Hartree-Fock calculations, density functional calculations enable also the prediction of electronic, optical, and magnetic properties of condensed phases.

Generality

The density functional approach is applicable to all atoms of the periodic table provided relativistic effects are taken into account for heavier elements such as third-row transition metals, rare earths, and actinides. The approach can be used for metallic, covalent, and ionic bonds. Its greatest strength is metallic condensed systems, yet its range includes as well organic molecules. With the inclusion of gradient corrections for the exchange-correlation term, even weaker interactions such as hydrogen bonds can be reasonably well described. Furthermore, so-called "difficult" molecules such as ozone seem to be treated by density functional methods with the same level of accuracy as other molecules. Within molecular applications, the approach is particularly useful for organometallic systems. Thus, in terms of generality and robustness, density functional theory seems to be superior to the Hartree-Fock approach.

Local density functional calculations do encounter problems for narrow-gap insulators and certain oxides. The LDA tends to overemphasize the metallic character and one needs to be careful in the interpretation of the density functional one-electron energies. Furthermore, weaker bonds such as hydrogen bonds are significantly overestimated in the LDA. The primary results of density functional calculations are the electron density, the spin density, the total energy, and the one-particle energies and wave functions. From these quantities, one

can derive important electronic, optic and magnetic properties including dipole (and higher) moments, polarizabilities and hyper-polarizabilities, and magnetic moments. LDA calculations for systems in their electronic ground state can be used to estimate electronic excitation energies including work functions, optical and UV spectra, and core level spectra for solids, surfaces, and molecules.

Accuracy

Quite consistently, for a great number of strong bonds in solids, molecules, and surfaces, interatomic equilibrium distances are predicted by precise density functional calculations to within about 0.02 Å of experiment; bond angles and dihedral angles are found within a few degrees of their experimental values. Within the local density approximation, binding energies are typically overestimated, sometimes by as much as a factor of two. Inclusion of non-local gradient corrections [Perdew, 1986; Becke, 1988] improves the values of binding energies and brings them to within about 10 kJ/mol of experiment.

The results obtained at this level of theory are comparable with sophisticated correlated quantum mechanical methods such as coupled cluster theory. Vibrational frequencies are predicted to within 10-50 cm^{-1}. At present, there is no clear theoretical path that would allow the systematic improvement of the accuracy of density functional methods. This is a major conceptual difference to Hartree-Fock based methods, where at least in principle there is a way for systematic improvements. Practical density functional calculations involve numerical integrations in addition to the evaluation of analytical expressions. These numerical integrations introduce a numerical noise that can be noticed, for example, in geometry optimisations of highly flexible molecules.

By increasing the size of the numerical grid, this numerical noise can be controlled, albeit at the expense of computational effort. This is in contrast to Hartree-Fock methods, which are usually implemented in a completely analytical way. Thus, the numerical precision of Hartree-Fock calculations is limited by the machine precision (typically 14 decimal figures) whereas the precision of density functional calculations is governed by the grid resolution. One could argue that if a theory has a certain intrinsic error compared with experiment, any computational approach that gives results within that error range is acceptable and any improvement in numerical precision has no physical meaning. On the other hand, it can be desirable, for example in the investigation of subtle trends, to have a high numerical precision.

System size

Density functional calculations are possible for systems of the order of 100 atoms. By exploring point-group symmetry, calculations for clusters of over 1000 atoms have been demonstrated for fixed geometries. While the self-consistent-field procedure converges typically in 10-20 iterations for organic materials and semiconductors, metallic systems and especially magnetic transition metals such as Fe and Ni are very difficult to converge. In practice, this limits the size of systems that can be treated to perhaps less than 50 atoms per unit cell or cluster.

Tractable time scale

With the work of Car and Parrinello, density functional calculations have become possible for studying dynamic phenomena. However, for a system with about 100 atoms, accurate density functional calculations are about 1000 times slower than force field calculations, thus reducing the accessible time scales to the range of picoseconds. In practice, the Car-

Parrinello method is presently used for structure optimisations by simulated annealing rather than for dynamic simulations, which has been done so far only for a few cases.

Computational efficiency

Depending on the system under investigation, for example a metallic alloy or a molecular crystal, density functional theory can be implemented in quite different ways thus leading to efficient methods for particular materials. On the other hand, practical Hartree-Fock methods require the use of Gaussian basis functions, which can be fairly inefficient, for example for close-packed systems. Thus, in general, density functional theory tends to be computationally more efficient than Hartree-Fock calculations.

Without doubt, compared with correlated post-Hartree-Fock methods, density functional calculations are by far more efficient computationally, scaling at worst with a third power in the number of basis functions. In fact, significant effort is dedicated to the development of so-called order-N methods, i.e. methods for which the computational effort increases linearly with system size. Such methods have been successfully demonstrated, yet the pre-factor is rather large so that these methods are competitive with conventional density functional implementations only for systems with several hundred atoms [Mauri et al, 1993; Li et al, 1993].

In molecular calculations it can be important to calculate vibrational frequencies in order to determine ground state structures, transition states, and to predict infrared spectra. In Hartree-Fock theory, this approach is well established, whereas the evaluation of vibrational frequencies (i.e. the calculation of the second derivatives of the total energy with respect to nuclear displacements) for molecular density functional is been done by a finite difference technique using analytic first derivatives. This is computationally not very efficient compared with analytical methods. While this type of calculations has been used for density functional

methods within the pseudopotential plane wave approach for some time, the implementation of analytic second derivatives in localized orbital density functional calculations is a fairly recent development (Komornicki and Fitzgerald, 1993). However, this type of calculation is quite time consuming and may require supercomputer resources for larger molecules.

2.1.4 Solution of the Kohn-Sham equation

The one particle Schrödinger equation, referred to as Kohn-Sham equation is written as

$$[-\frac{1}{2}\nabla^2 + V_c(r) + \mu_{xc}(r)]\psi_i(r) = \varepsilon\psi_i(r) \qquad \textbf{(1)}$$

where $-\frac{1}{2}\nabla^2$ is the kinetic energy, $V_c(r)$ is the Coulomb energy and $\mu_{xc}(r)$ is the exchange –correlation.

This equation is derived from the three energy terms defined by $E[\rho] = T_o + U[\rho] + E_{xc}[\rho]$. The one particle wavefunctions which are the solution of the Kohn-Sham equation, are related to the total electron density as

$$\rho(r) = \sum_i n_i |\psi_i(r)|^2 \qquad \textbf{(2)}$$

where n_i is the occupation number of state *i*. The unknown wavefunction $\psi_i(r)$ is expanded in terms of known basis functions $\varphi_i(r)$ with unknown linear coefficients, c_{ij}.

$$\psi_i(r) = \sum_j c_{ij}\varphi_j(r) \quad \textbf{(3)}$$

To obtain the unknown coefficients c_{ij}, a variational procedure is applied to solve the following matrix:

$$(H - \varepsilon S)c = 0$$

where H and S have matrix elements

$$H_{ij} = \int \varphi_i^*[-\frac{1}{2}\nabla^2 + V_c(r) + \mu_{xc}(r)]\varphi_j(r)dr \quad \textbf{(4)}$$

$$S_{ij} = \int \varphi_i^*(r)\varphi_j(r)dr \quad \textbf{(5)}$$

ε=eigenvalue and c are coefficients of a solution represented as a column vector. Thus to obtain the eigenvalues and coefficients the matrix $(H - \varepsilon S)$ is diagonalised, the dimension of which is determined by the type of expansion on the wavefunction $\psi_i(r)$. The matrix can be diagonalised using the conjugate gradient scheme. The coulomb potential and the exchange correlation potential depend on the charge density, which is constructed from the one-particle wavefunction.

2.1.5 Plane-wave pseudopotential method

Any periodic function can be expanded in Fourier series, of which the convergence is determined solely by the highest frequency at which the series is terminated. Solution of the Kohn-Sham equation can be expanded into a three dimensional Fourier series

$$\psi_i^k(r) = \sum_{j=0}^{\max} C_{ij} e^{i(k+G_j).r} \quad \textbf{(6)}$$

where $\boldsymbol{G_j}$ is a reciprocal lattice vector. A large $\boldsymbol{G_{max}}$ is required for the resolution of rapid variations in the wavefunctions and charge density. These plane wave basis functions are delocalized, since they are not associated with any particular atom in the crystal, but defined over the entire unit cell. Thus the number of plane-waves to be used in computation depends on the size of the unit cell. The eigenfunctions, $\boldsymbol{\psi_i(r)}$, show nodes near atomic cores which causes convergence problems when dealing with closely packed structures, effectively rendering plane-waves expansion useless.

This problem can be handled by coupling the use of plane waves with pseudopotentials (PP) [Trollier and Martins, 1991]. Pseudopotential approximation allows the replacement of the strong electron-ion potential with a much weaker potential, a pseudopotential, which describes all the salient features of a valence electron moving through a crystal, including relativistic effects. Hence, pseudo valence electrons and pseudo ion cores now replace the original solid.

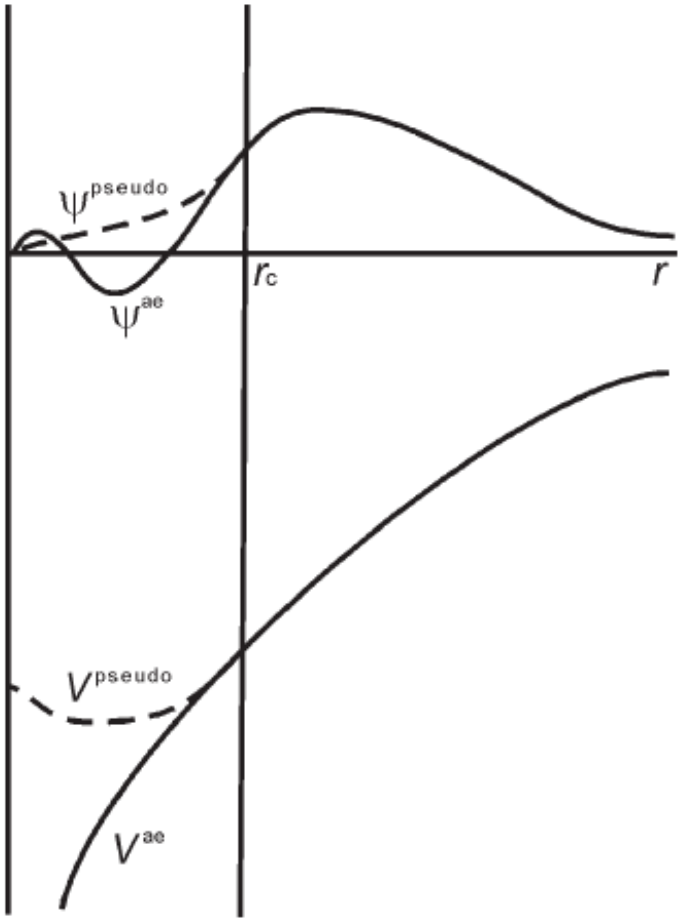

Figure 4: A schematic illustration of all-electron (solid lines) and pseudo- (dashed lines) potentials and their corresponding wavefunctions. The radius at which all-electron and pseudopotential values match is r_c

The pseudo valence electrons experience the same potential outside the core region as the original electrons, but have a much weaker potential inside the core region as Figure 4 shows. Since the potential is weaker, the solution of the Schrödinger equation is faster due to small set of plane waves required to expand the wavefunction. Local pseudopotentials are those that use the same potential for all angular momentum components of the wavefunction. The norm conserving PP by Kleinmann and Bylander [1992], are an example of the non-local PP.

To date, there has been a lot of interest in generating pseudopotentials, to increase the efficiency of the method, which will also include all the atoms in the periodic table. Recently, the ultrasoft pseudopotentials (US_PP) [Vanderbilt, 1990] implemented in plane-wave calculations covers a wide range of atoms, including the transition metals and rare earth metals, which were not well represented by the earlier PP. Some of the computer codes based on this approach are Vienna Ab initio Simulation Package (VASP) and Cambridge Serial Total Energy Package (CASTEP) (Cerius2 and Materials Studio) [http://www.accelrys.com/products]

2.2 Potential Model and Atomistic Simulations

The potential model describes the variation of energy of the system as a function of atomic co-ordinate. This energy is derived from the long-range electrostatic forces, short-range attractive and repulsive forces. A potential model that accurately describes the lattice properties is essential if quantitative results are to be obtained. This is particularly important for surfaces where it is necessary to describe the interaction at distances possibly far removed from those found in the bulk lattice [Allan, 1993]. An advantage of using the potential model over quantum mechanical calculations is that the size of the systems that can be studied is larger.

The total energy of a crystal is defined as the energy released when different ions making up the crystal are brought together from infinite distance to their lattice sites. Thus the lattice energy is made up of the electrostatic interactions between the ions and the short-range interactions, such as van der Waals attractions and short-range repulsions. In this chapter model used to describe short-range interactions in solids, including the derivation of potentials will be discussed.

2.2.1 Ionic Polarisability

Ionic polarisability is the induction of a dipole in an ions electron charge cloud when brought close to an asymmetric electric field. This dipole can affect the short-range interactions between the ions. Rigid Ion Models ignore ionic polarisability and the ions are considered to be point charges. Although this may seem simplistic, this type of model has been found to work well over a wide range of systems [Harding, 1990].

The neglect of ionic polarisability does reduce the accuracy of certain types of calculations. For example, lattice vibrations are mainly influenced by ionic polarisation, leading to the inability of the Rigid Ion Potential to predict the dynamical properties of the lattice. In addition this method is thought to be unsatisfactory when evaluating the effect of a charged defect on the lattice [Harding 1990]. A simple description of ionic polarisability can be obtained by using the point polarisable model.

2.2.2 Point Polarisable Model (PPM)

In the point polarisable model, an electric field E induces a fixed dipole μ, the size of which is related via the polarisability α.

$$\mu = \alpha E \tag{7}$$

The energy of the interacting dipoles can therefore be calculated. This approach is very simple and has been used in the calculation of defect energies [Norgett, 1971]. However this method does not account for the coupling between short-range repulsions and polarisability, leading to calculated values for defect energies being considerably lower than experiment. [Faux, 1971] showed that there is a critical distance, r_{crit}, between the approaching ions, above which their mutual interaction is divergent:

$$r_{crit} = (4\alpha_i \alpha_j)^{\frac{1}{6}} \quad \textbf{(8)}$$

The shell model can largely overcome these problems.

2.2.3 Born Model of Solids

The Born model of solids assumes that the sum of all pairwise interactions between atoms *i* and *j* gives the lattice energy of the crystal. The lattice energy is given by:

$$U(r_{ij}) = \sum_{ij}^{'} \frac{q_i q_j}{r_{ij}} + \sum_{ij}^{'} \Phi_{ij}(r_{ij}) + \sum_{ijk}^{'} \Phi_{ijk}(r_{ijk}).... \quad \textbf{(9)}$$

The first component defines the long-range electrostatic interactions and the second and third defines short-range two-body and many-body interactions. The dash above the summation is to show that the interaction where ***i=j*** is not included. It is considered adequate to calculate only the two body interactions for systems where the interactions are non-directional, such as ionic solids. However, when studying systems containing a degree of covalent bonding, the evaluation of higher body terms, bond bending and bond stretching terms is necessary to include their directionality.

2.2.4 The Coulombic Potential

Potential energy of the long-range interactions takes the form:

$$\Psi(r_{ij}) = \sum_{ij} \frac{q_i q_j}{4\pi\varepsilon_o (r_{ij} + 1)} \quad \textbf{(10)}$$

Where q_i and q_j are the charges on the ions, ε_o is the permittivity of free space and r_{ij} is the inter-ion separation. This is the coulombic interaction for long-range interactions and the short-range interactions are described using simple parameterised functions, as discussed below. The coulombic interaction has a problem of slow convergence as a function of *r*. Hence it is necessary to use mathematical models to deal with this summation.

Ewald Summation:

The approach developed by Ewald for summing long ranged potentials in periodic systems assumes that the unit cell is periodical in three dimensions and utilises the convergence properties of periodic arrays of Gaussian functions. The charge density θ for a point ion ***i*** is given by

$$\theta_i = \delta(r_i - r_{lattice}) \quad \textbf{(11)}$$

i.e. using the point ion as the origin, in any direction through the lattice the charge density at that point $\boldsymbol{r_{lattice}}$, can have a value of either 0 or 1. Each ion is then replaced by a Gaussian charge distribution of equal magnitude but opposite sign, leading to the expression below

$$\theta_i = \exp\left(\frac{(r_i - r_{lattice})^2}{\gamma^2}\right) \quad \textbf{(12)}$$

where γ is the half width of the Gaussian. This effectively neutralises each ion and so removes interactions between neighbouring charges. These charges are short ranged and can be calculated in real space. A cancelling charge of the same sign as the original charge is then added which reduces the overall potential to that of the original set of point charges. The charge density is then as given below:

$$\theta(r) = (\delta(r_i - r_{lattice}) - \exp(\frac{(r_i - r_{lattice})^2}{\gamma^2})) + \exp(\frac{(r_i - r_{lattice})^2}{\gamma^2}) \quad \textbf{(13)}$$

2.2.5 Short Range Two-Body Potential Functions

Two body potentials represent short-range interaction between two charge clouds, and can be attractive (van der Waals) or repulsive .The interaction energies, which comprise the short-range interaction term, are given by simple parameterised analytical functions. The specificity is introduced by having different parameters between different pairs of ions. Thus the model depends on using analytical functions that are of appropriate form for the interaction energies and the parameters must be carefully chosen. The kinds of functions that are successful are given below. All the analytical forms can be classified under bonded and non-bonded interactions.

Harmonic Potential:

Modelling interactions between bonded ions can be achieved by using the harmonic potential form, given below by

$$\Phi_{ij}(r_{ij}) = \frac{1}{2} k_{ij} (r_{ij} - r_0)^2 \quad \textbf{(14)}$$

In which case k_{ij} represents the bond force constant associated with the deviation from equilibrium bond separation, r_{ij} is the interatomic separation and r_o is the equilibrium separation. This potential is harmonic due to the energy being dependent on the square of the displacement of the current bond length r_{ij} from the equilibrium bond length, and is used only when the bond length does not vary much from the equilibrium.

Morse Potential:

The Morse potential is used to model covalently bonded interactions where separations vary significantly from equilibrium, such as atoms in molecular ions, displaying the anharmonic behaviour missing from the harmonic function. This potential is thus able to model systems away from their equilibrium bond distances such as point defects and surfaces or when temperature or pressure is applied. It takes the form given below:

$$V(r_{ij}) = A_{ij}(1 - \exp[-B_{ij}(r_{ij} - r_o)])^2 - A_{ij} \quad \textbf{(15)}$$

Where A_{ij} is the bond dissociation energy, r_o is the equilibrium bond distance and B_{ij} is related to the curvature of the slope of the potential energy well and can be obtained from spectroscopic data. Due to its inclusion of the bond energy, the Morse potential is often used with subtraction of the Coulomb interaction, allowing it to completely describe the bond for nearest neighbours.

Buckingham Potential:

The general form of the Buckingham potential is given by the equation below, which describes the interaction of second nearest neighbours, as it is a non-bonded pair potential.

$$\Phi_{ij}(r_{ij}) = A_{ij}e^{-(r_{ij}\frac{1}{\rho_{ij}})} - \frac{C_{ij}}{r_{ij}^6} \quad \textbf{(16)}$$

In the above equation A_{ij} represents the size of the ions whilst ρ_{ij} represents the hardness thereof, and these two terms are tied together in an effective pair potential. The first term represents the repulsive interaction between the ions and the second one the van der Waals attractive interaction of the ions. In the last term C_{ij} is the dispersion parameter that must be fitted like the other two to be able to represent the structure well. However, assigning physical meanings to potential parameters is risky because fitting procedure can not fit to individual components of the interactions, but to the whole potential surface.

Lennard-Jones Potential:

This is another form of non-bonded potential having a repulsive part and an attractive part respectively being dependent on r^{-12} and r^{-6} as in the Buckingham case. This potential is given by the expression below:

$$\Phi_{ij}(r_{ij}) = \frac{A}{r_{ij}^{-12}} - \frac{B}{r_{ij}^{-6}} \qquad \textbf{(17)}$$

The Lennard-Jones potential was originally developed to describe noble gases and later applied to intermolecular interactions in molecular systems. It is an approximation that describes the complicated nuclear and electronic repulsions, which dominate the attractive interactions at short distances.

2.2.6 Many Body Potential Functions

All of the potential functions discussed in the previous sections have been radial in nature with no account to directionality in bonding. Simulating systems in which covalency is important, multiple body interactions are commonly employed to confer directionality on the

two body bonds. This can take the form of three body interactions for σ bonding and four body interactions for π bonding.

Bond Bending:

The three body potential is used for modelling partially covalent materials. Changes in interaction energy caused by deviation from the equilibrium bond angle,θ^o, described as the angle between a central ion, *i*, and two adjoining ions j and k are modelled by the three-body potential. The potential is dependent on the square of the deviation from the equilibrium angle. The term will be zero only at the equilibrium angle and it is given by:

$$\phi_{ijk} = \frac{1}{2} k_{ijk} (\theta - \theta_o)^2 \qquad \textbf{(18)}$$

k_{ijk} is the harmonic force constant, and θ is the bond angle and θ_o is the equilibrium bond angle.

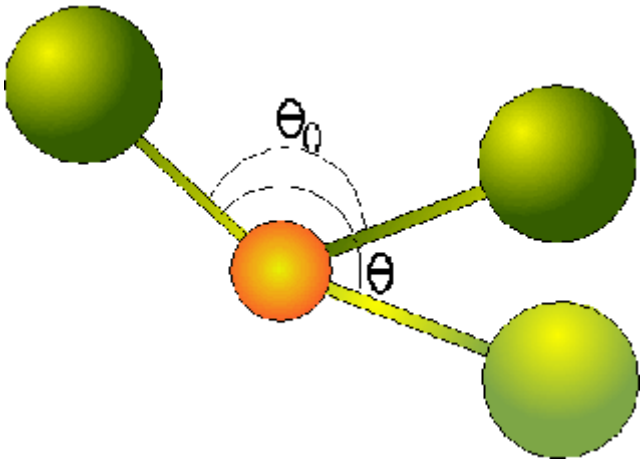

Figure 5: Representation of the three body potential or bond bending term.

Torsion:

Four body potentials or torsionals are used to model systems that have planar nature due to π bonding. The structural arrangement of four atoms i, j, k and l is shown in the figure below

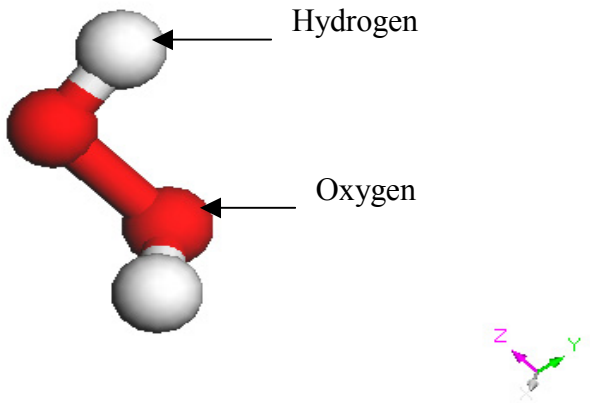

Figure 6: Description of the torsionals by four atoms

2.2.7 The Shell Model

The shell model by Dick and Overhauser (1958) successfully describes the polarisation and the physical distortion of the ion in response to an electric field. The ion is assumed to be composed of a core, representing the nucleus and core electrons, and a shell, representing the outer electrons. The core and shell carry charges that sum to the ionic charge, and are connected by an ionic spring with force constant k_i, allowing polarisation of the ion. The total interaction of the core and shell of an ion is given by the expression below:

$$\phi_i(r_i) = \frac{1}{2} k_i r_i^2 \qquad (19)$$

where r_i is the distance between the core and the shell and Y is the massless shell charge. The polarisability of the free ion is given by:

$$\alpha_i = \frac{Y^2}{4\pi\varepsilon_o k_i} \tag{20}$$

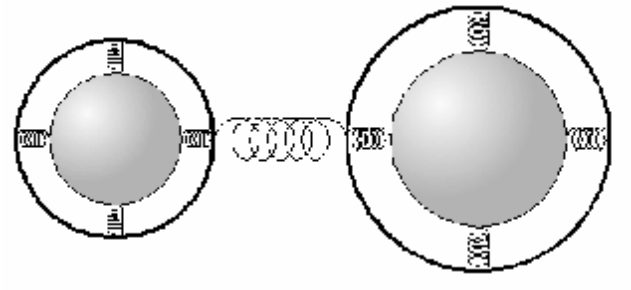

Figure 7: The shell model with balls surrounded by springs.

Short-range forces are considered to act between shells whereas the coulombic forces act between the shells and cores (except on the same ion). The Shell Model has proved very successful in the reproduction of properties such as defect energies, phonon dispersion curves and dielectric constants [Cochran, 1973]. An advantage of this method is that if the ions distort the polarisability changes. A disadvantage of the shell model is that the parameters must be obtained by empirical fitting and experimental data is not always available. In addition, the number of species involved in computer simulations is doubled and therefore the computing time is doubled. Hence, Rigid Ion Models are often used in Molecular Dynamics. Thus to model a system, knowledge of the nature of bonding is important to make a proper choice of potential functions. Once these functions are identified, their parameters could be derived.

2.3 Energy Minimisation techniques

In this study minimum energy techniques have been applied to study surface energies and the one being used in particular is Minimum Energy Techniques Applied to Dislocations, Interfaces and Surface Energies (METADISE) which takes the two dimensional periodicity into account when calculating their energies. The surface is divided into two regions in which case the regions are also divided into blocks. One region is allowed to move whilst the other is held fixed and atoms are allowed to assume their most stable positions, as the structure is relaxed.

Static lattice energy minimisations have been used in this work to calculate surface and block energies. This type of minimisation is effectively carried out at 0K since it ignores the vibrational properties of the crystal, including the zero point energy contribution. However, other methods are available which take into account the temperature of the system, like the Molecular Dynamics methods. METADISE [Watson et al, 1996] used to calculate minimum energies of the surfaces of $PtSb_2$ is partly derived from the MIDAS code developed by Tasker (1978). The crystal is considered to consist of a series of charged planes parallel to the surface and periodic in two dimensions.

Chapter 3

Electronic Structure Calculations

3.1 Introduction

Calculations carried out on both $PtSb_2$ and $PtBi_2$ were performed using planewave-pseudopotential methods embodied in CASTEP code. We performed geometry optimisations and volume relaxation on the structures, equation of states, electronic and optical properties were calculated.

3.2 Methodology

The plane-wave pseudopotential (PWP) method was used to predict the equilibrium lattice parameter, pressure-volume (equation of state (EOS)), bond lengths and internal parameters of both $PtSb_2$ and $PtBi_2$. Calculations were performed using the CASTEP code from Accelrys [www.accelrys.com/about/msi.html].

In this code, geometry optimisation is achieved by varying the hydrostatic pressure and allowing the lattice to relax using the Broyden-Fletcher-Goldfard-Shanno (BFGS) minimisation method to obtain the equilibrium geometry [Broyden, 1970, Fletcher, 1970, Goldfard, 1970, Shanno, 1970]. (BFGS) is a quasi-Newton method for energy minimization. This method minimizes a real valued function (in this case the heat of formation, ΔH_f) evaluated for the system after each SCF convergence. Electronic minimisation was performed through band-by-band conjugate gradient minimisation technique.

3.2.1 Energy cut off and k-points sampling

Some convergence tests were performed for obtaining the energy cut-off, since this is important as it determines the number of plane waves required for the calculation. In both $PtSb_2$ and $PtBi_2$ the energy cut-off obtained is 600 eV after sampling of the k-points, which

were found to be 6x6x6. These tests gave us the minimum energies for both of the structures. Figures 8 and 9 indicate the way in which the energy cut-off was chosen upon, for both $PtSb_2$ and $PtBi_2$ respectively.

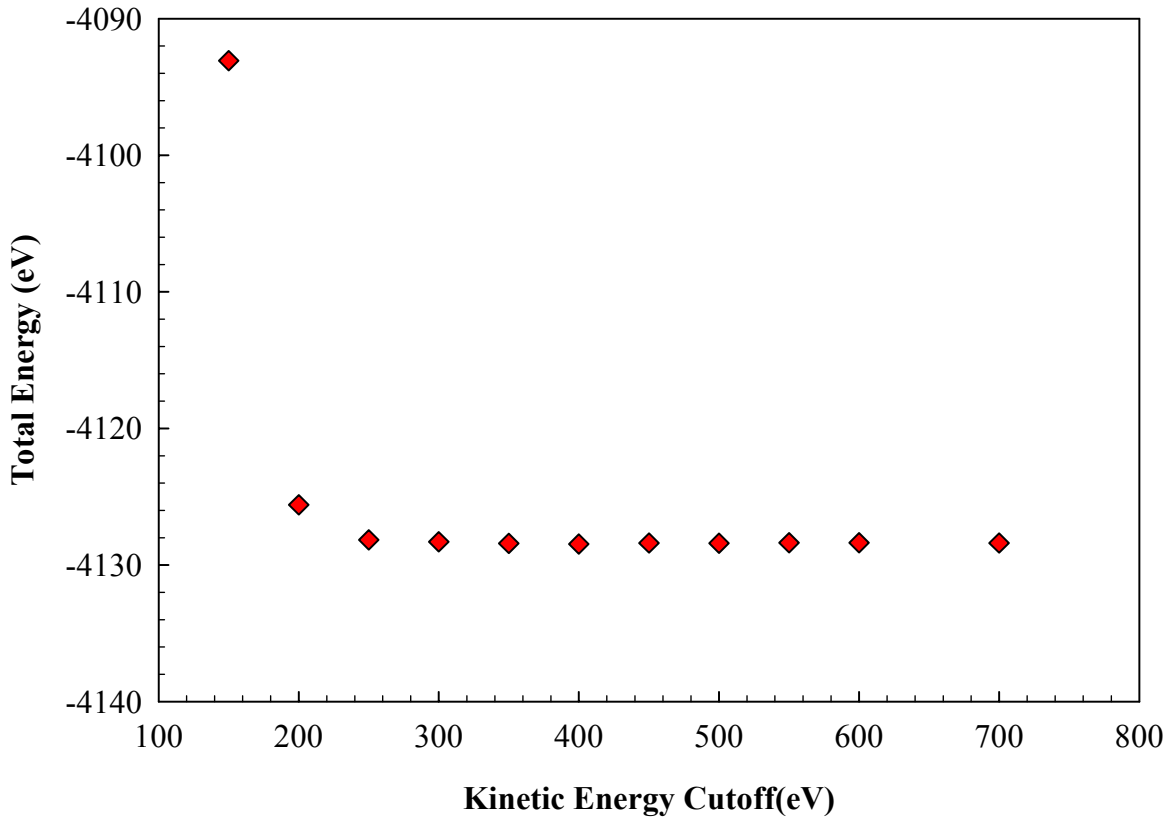

Figure 8: The variation of the total energy with kinetic energy cut-off for $PtSb_2$.

The minimum energy obtained for $PtSb_2$ is about -4130.0 eV, as opposed to that of $PtBi_2$ of approximately -4127.5 eV. In both compounds under study, the convergence of the total energies is within a few eV of the kinetic energy cut-off. Convergence is also dependent on the number of k-points for the Brilloin zone integration, which for semiconductors/insulators, a lot less number of k-points are needed, unlike for metals.

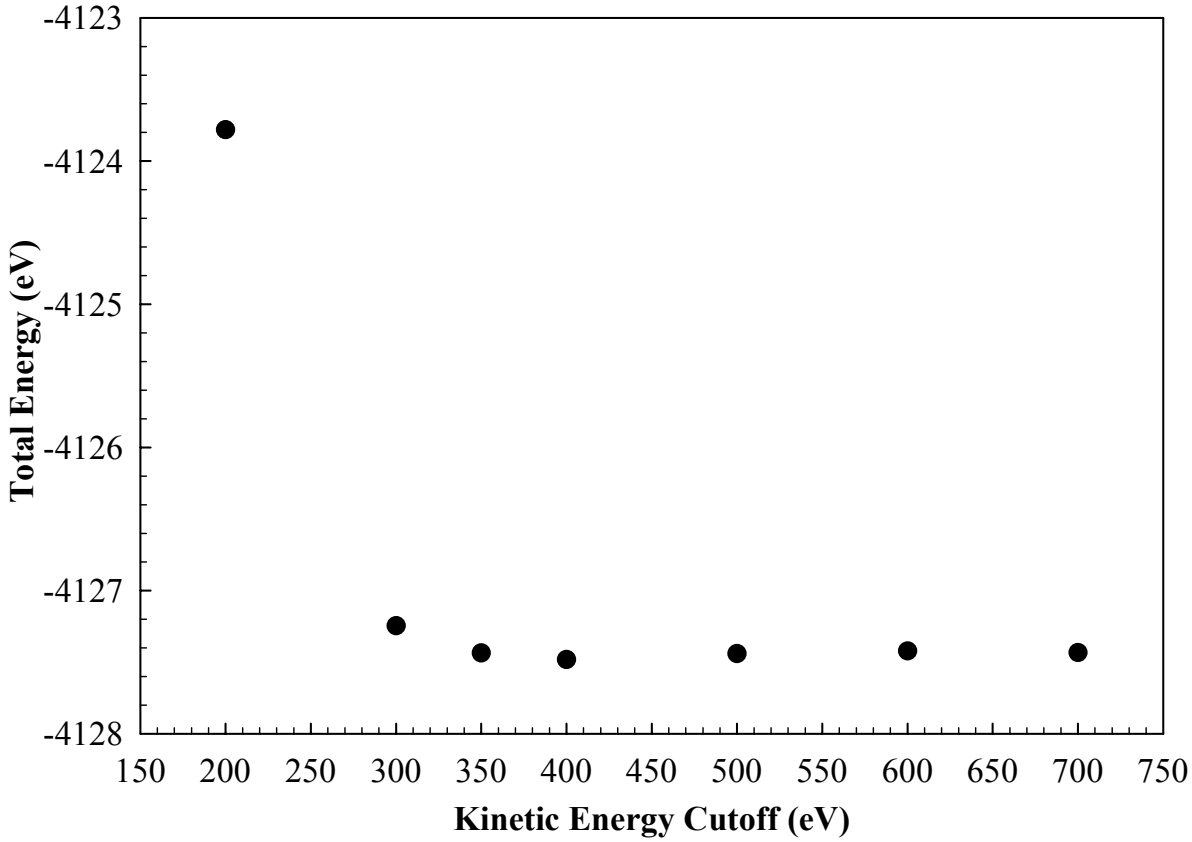

Figure 9: The variation of the total energy with kinetic energy cut-off for $PtBi_2$

3.3 Results and Discussions

In the following subsections, the results obtained are classified under the headings: structural properties, electronic properties (density of states), charge distributions and optical properties. Our calculations have been performed using Generalized Gradient Approximation of Perdew-Burke-Ernzerhof (GGA-PBE), using geometry optimisations, meaning that the internal parameters of the Sb and Bi atoms were allowed to vary. As Figures 10 and 11 indicate, it is possible to predict the lattice parameters (volumes) of systems being studied, which is equivalent to calibration in experiments.

In Figure 10 of $PtSb_2$ it is clear that the minimum of the total energy is at the lattice parameter of 6.400 Å, coming very close to the experimental value of 6.440 Å [Emtage 1965].

This is further illustrated in Figure 11 for $PtBi_2$, having an experimental lattice parameter of 6.625 Å. Our calculation corresponds to the minimum total energy found at 6.600 Å.

3.3.1 Structural Properties

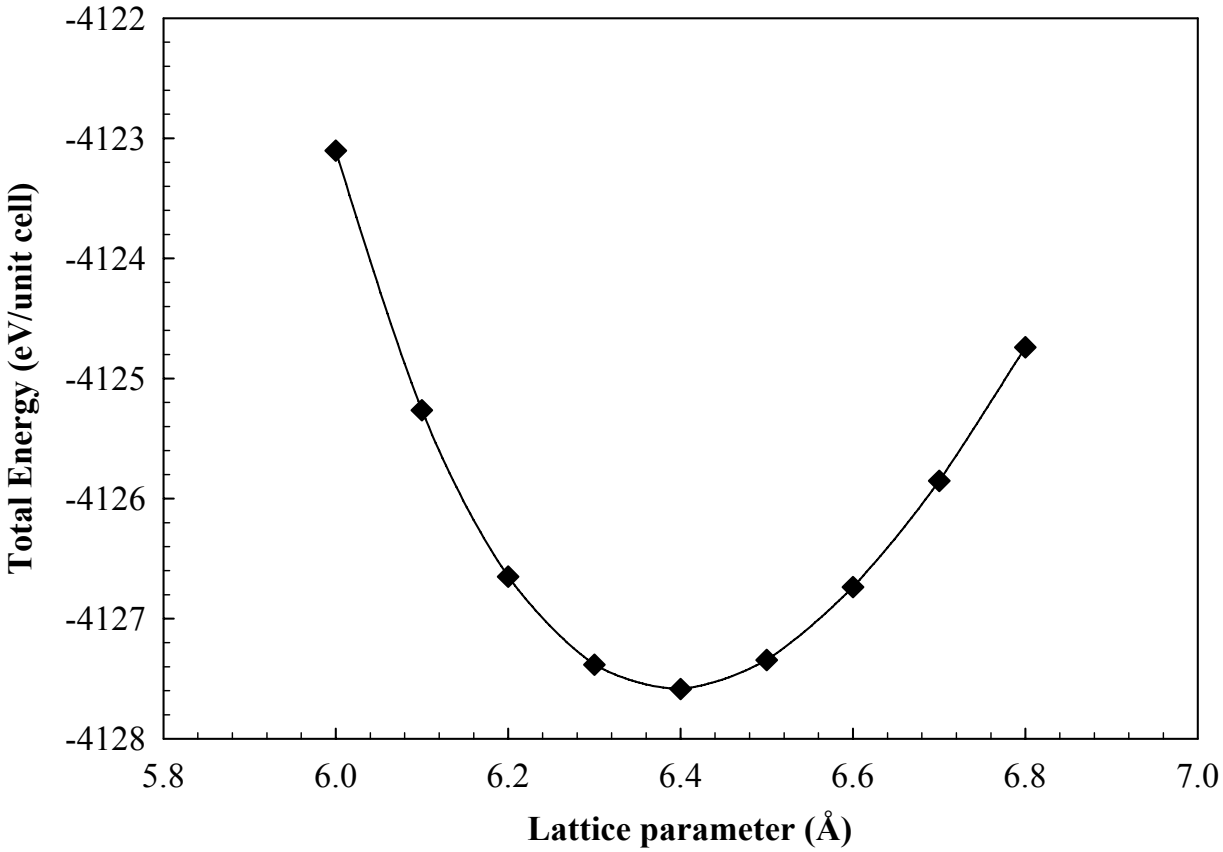

Figure 10: Total energy versus the lattice parameter for $PtSb_2$ at ambient pressure.

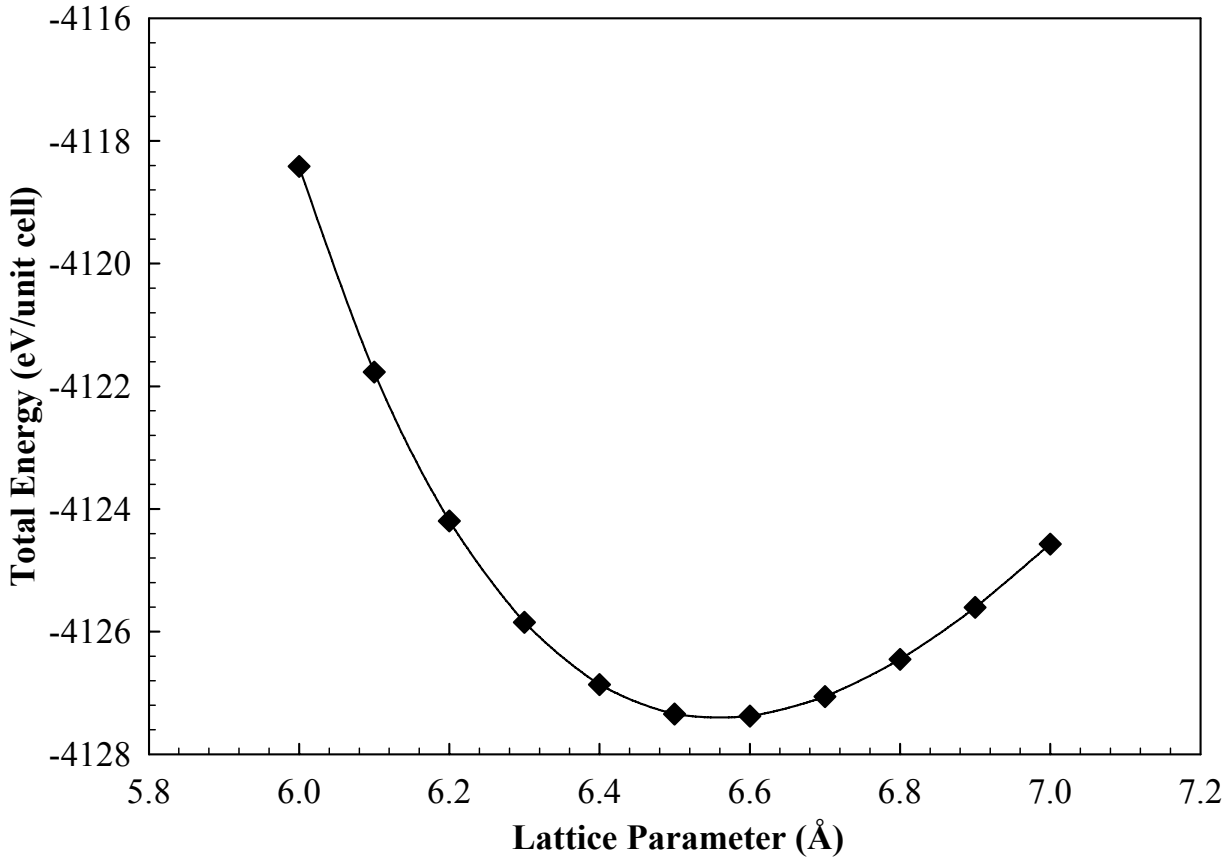

Figure 11: Total energy versus lattice parameter of $PtBi_2$

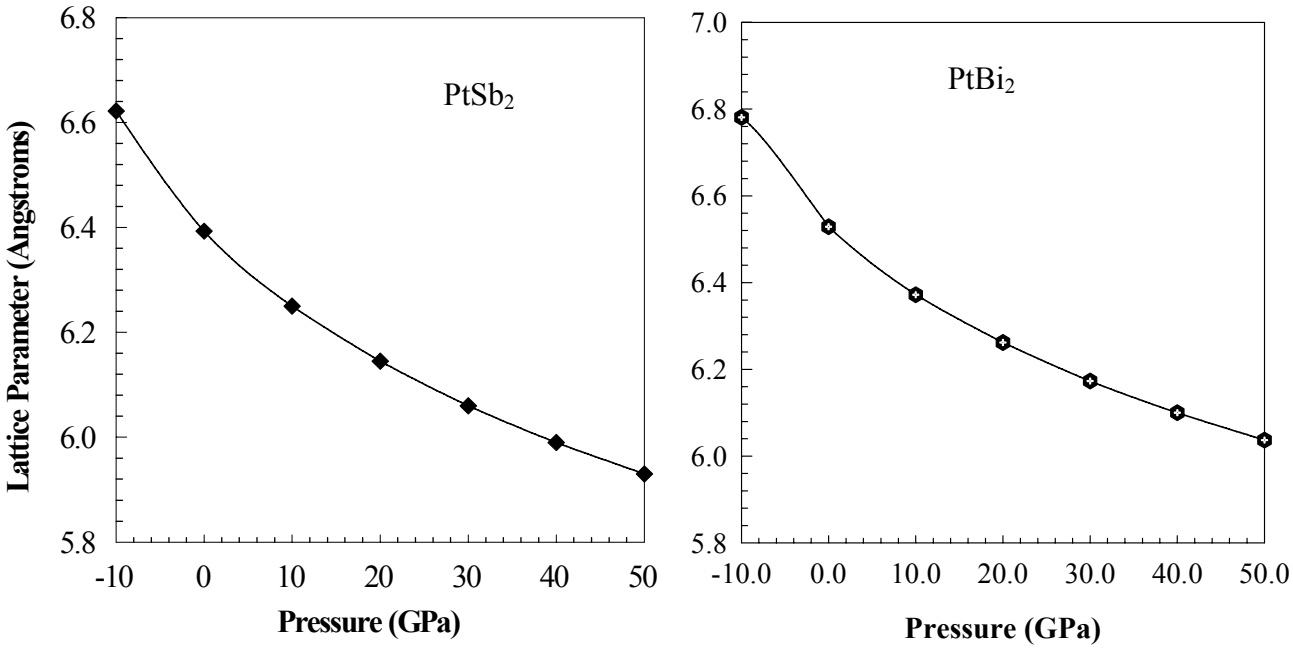

Figure 12: Lattice parameters of $PtSb_2$ and $PtBi_2$ as functions of pressure.

Pressure dependences of the lattice parameters of both $PtSb_2$ and $PtBi_2$ are given in Figure 12 and these were carried out between –10GPa and 50GPa. The observation is that both compounds decrease in size with pressure.

Table 1: Structural properties of $PtSb_2$ and $PtBi_2$.

Bond Lengths	**Calculated (Å)**	**Experimental (Å)**
Pt-Sb	2.653	-
Pt-Pt	4.520	-
Sb-Sb	2.742	2.67*
Pt-Bi	2.706	-
Pt-Pt	4.623	-
Bi-Bi	2.887	-

* [Emtage 1965]

Table 1 gives the structural parameters of both $PtSb_2$ and $PtBi_2$, calculated and experimental values. Experimental values of the bond lengths for $PtBi_2$ are not available at this stage. The Pt-Sb(Bi) bond lengths are shorter than the Sb(Bi)-Sb(Bi) lengths. Pt-Pt for $PtSb_2$ is about 0.103 Å shorter than that of $PtBi_2$ as seen in Figures 13 and 14. Corresponding bond lengths of $PtSb_2$ are shorter than those of $PtBi_2$, as is the case of the lattice parameter.

As expected, the bond lengths shorten with increasing pressure as illustrated in Figures 13 and 14. The decrease in the bond lengths for both $PtSb_2$ and $PtBi_2$ is similar throughout the pressure range. This also applies to the variation of the lattice parameters with pressure.

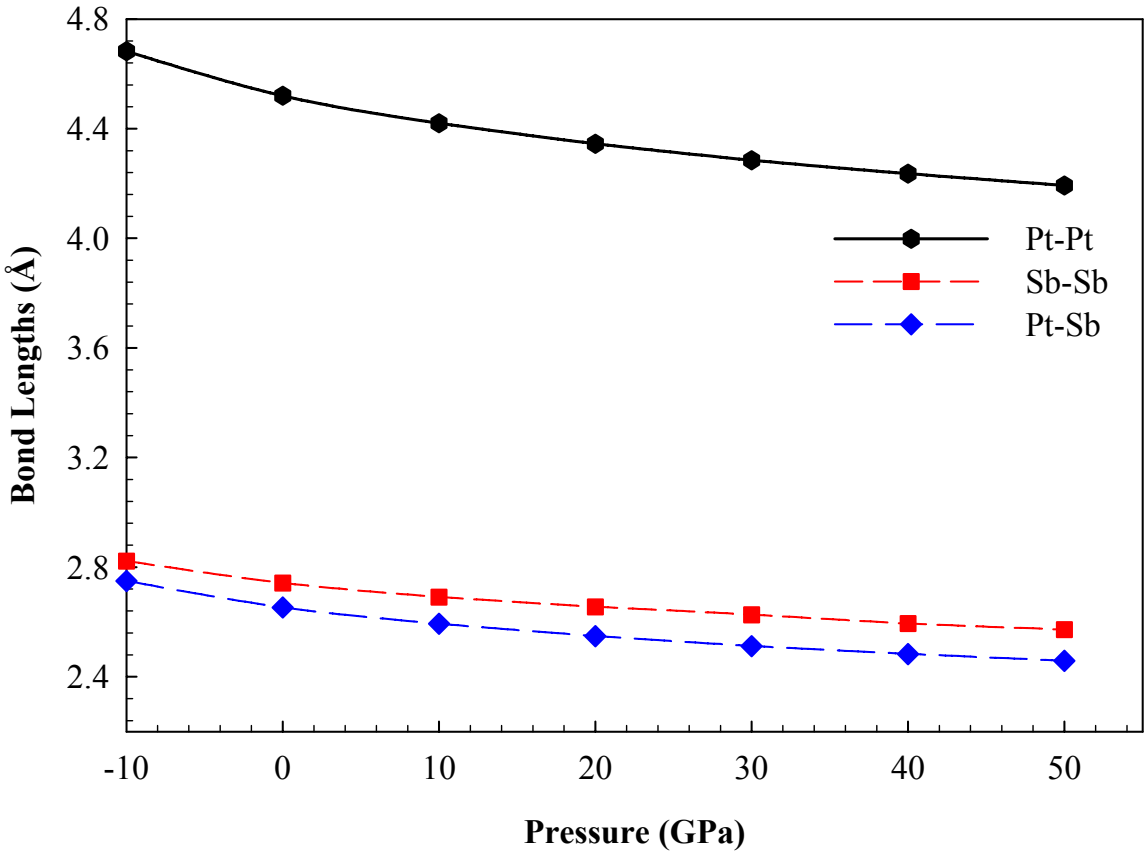

Figure 13: Bond lengths of $PtSb_2$ dependences on pressure.

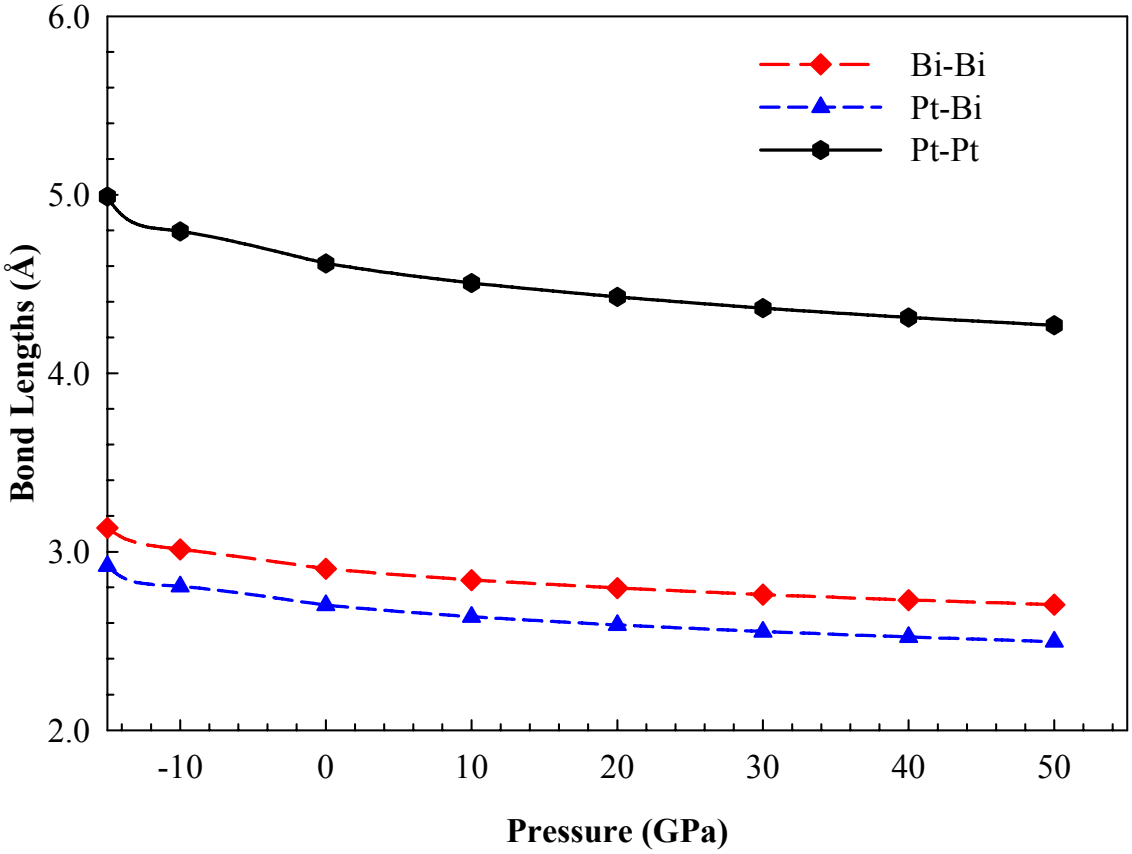

Figure 14: Bond lengths of $PtBi_2$ dependences on pressure.

$PtSb_2$ and $PtBi_2$ have different internal parameters (u), i.e., 0.375 Å and 0.371 Å as it is shown in Figure 15. As pressure is increased, the internal parameters decrease. The ambient pressure internal parameters for $PtSb_2$ and $PtBi_2$ are respectively and change by 0.267% and 0.269% at 50 GPa. The decrease in internal parameters indicate that the Sb(Bi)-Sb(Bi) positions changes with an increase in pressure.

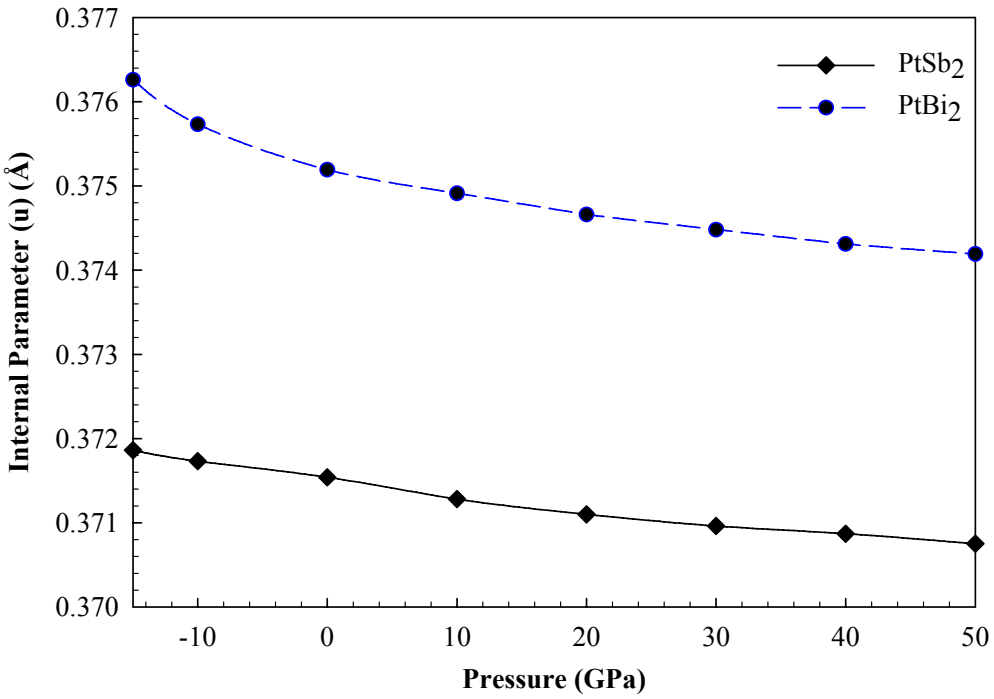

Figure 15: Internal parameters against hydrostatic pressure for $PtSb_2$ and $PtBi_2$

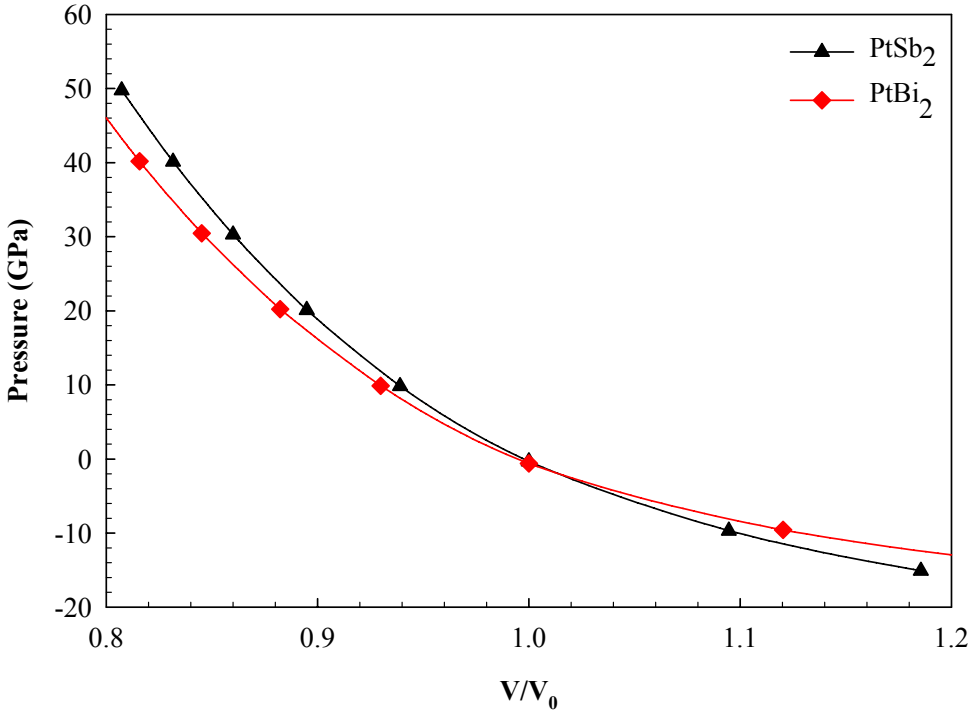

Figure 16: Equations of state of $PtSb_2$ and $PtBi_2$

3.3.2 Elastic Constants

From the equation of state in Figure 16, the bulk modulus was calculated using cubic curve fitting be 134.8 and 115.4 GPa for $PtSb_2$ and $PtBi_2$ respectively. The bulk modulus of $PtSb_2$ compares well with the experimental one, 134 GPa, deduced from the elastic constants. Elastic constants of $PtSb_2$ were also calculated by planewave pseudopotential methods and the values are given in Table 2.

Room temperature elastic constants of $PtSb_2$ [Damon et al, 1965] have been determined from sound-velocity measurements made by the pulse echo technique and the corresponding values are reflected in Table 2. There is a good correspondence between calculated and experimental elastic constants. The bulk moduli determined from calculated elastic constants and equation of states for $PtSb_2$ and $PtBi_2$ are in good agreement.

Table 2: Elastic constants

Elastic Moduli	Calculated (GPa) $PtSb_2$	Experimental (GPa) $PtSb_2$	Calculated (GPa) $PtBi_2$ (manually)
C_{11}	268.8	266.0	243.48
C_{12}	62.50	68.00	38.86
C_{44}	-	59.05	-
$C' = \frac{C_{11} - C_{12}}{2}$	103.05	99.00	-
$B = \frac{C_{11} + 2C_{12}}{3}$	131.3	134.0	107.1
B(EOS)	134.8	134.0	115.4

Damon et al (1965)

3.3.3 Electronic Properties

Density of States

Total and partial density of states for $PtSb_2$ and $PtBi_2$ will be presented in this section. The density of states calculations were carried out at 0 GPa and show that $PtSb_2$ is a semiconductor with a band gap of 0.11 eV. This value is in good agreement with the measured energy gap, which ranges between 0.07 eV and 0.11 eV [Emtage, 1965]. As shown in Figure 17, the valence part of the DOS consists of a double peak at –13 and -10 eV (bands 1–4), and a broader distribution extending from –7.5 eV up to the valence-band maximum (VBM). The lower part of the conduction band consists of a continuous distribution. A clear understanding of the features above can be obtained by studying partial densities of states. In Figure 17 the peak at –13 and -10 eV emanates predominantly from the Sb(3p) and Pt(5d) states. The broad peak below the bandgap is a contribution from the Sb(3s) and Pt(5d) states.

The portion of this broad peak, which appears immediately below the valence band maximum, consists of predominantly of the Pt(4p) and Sb(3s) states. The features of the density of states for $PtBi_2$, as depicted in Figure 19, are slightly different. Firstly the calculations show no obvious bandgap at the Fermi level, though it passes through a pseudogap. This suggests that $PtBi_2$ is metallic and stable. The valence part of the DOS consists of two isolated peaks at –12.5 and -10 eV and the partial density of states reflect contributions from the Bi(3p) and Pt(5d and 4s) states where the latter are small.

A broader band extending from –6 eV up to the valence-band maximum (VBM) is noted and mainly consists of the Bi(3s) and Pt(5d) states. As in $PtSb_2$, immediately below the Fermi level, contributions of the Pt(5d), Pt(4p) and Bi(3s) states are observed. The latter states also dominate the lower energy end of the conduction band. Figure 17 is an indication of the

electronic property of $PtSb_2$ showing that it is a semiconductor by the show of the energy gap, as projected around the Fermi level.

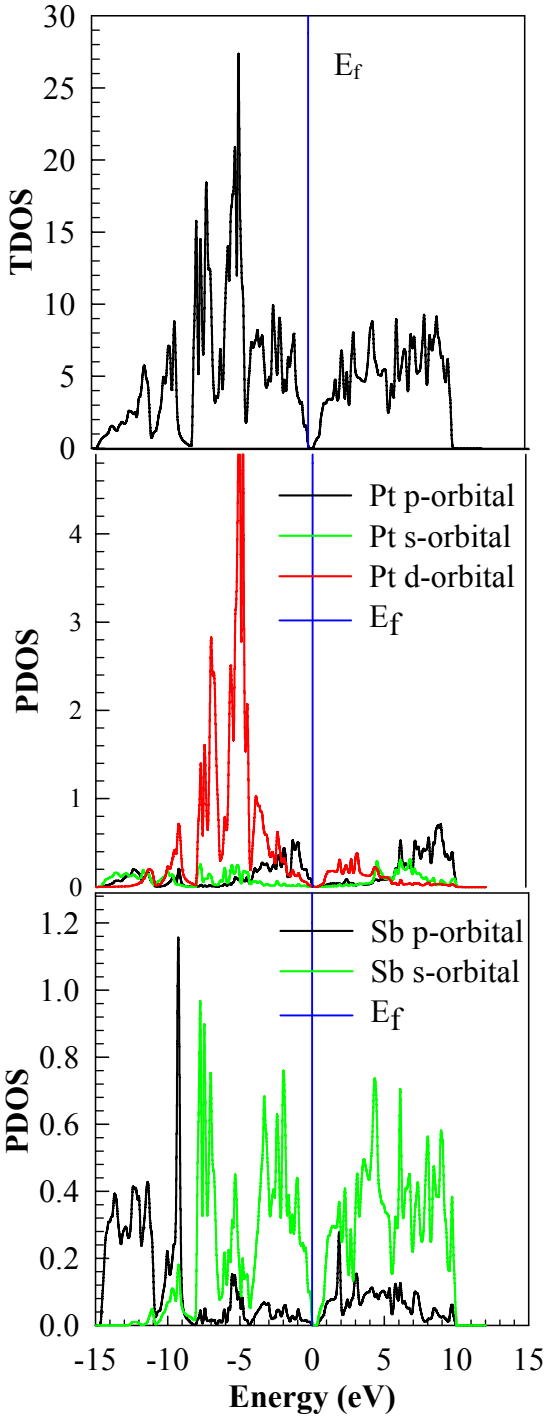

Figure 17: Partial and total density of states for $PtSb_2$.

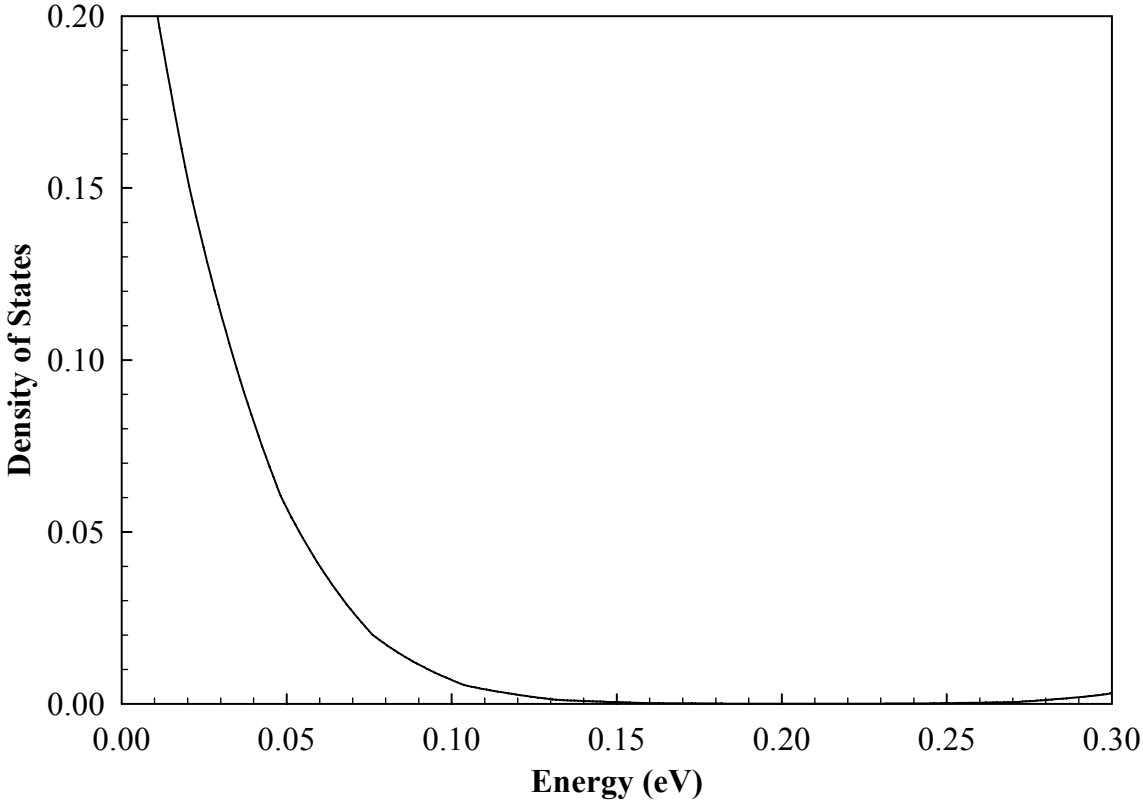

Figure 18: Finding the energy gap to 0.15 eV, obtained from the total density of states for $PtSb_2$.

Experimentally it has been determined that the energy gap ranges between 0.07 eV and 0.11 eV, and from *ab initio* calculations we have been able to find it to be approximately 0.15 eV, as indicated in Figure 18. Reynolds et al (1968) have also measured the energy gap and have found that it shows little dependence on temperature up to 300 K.

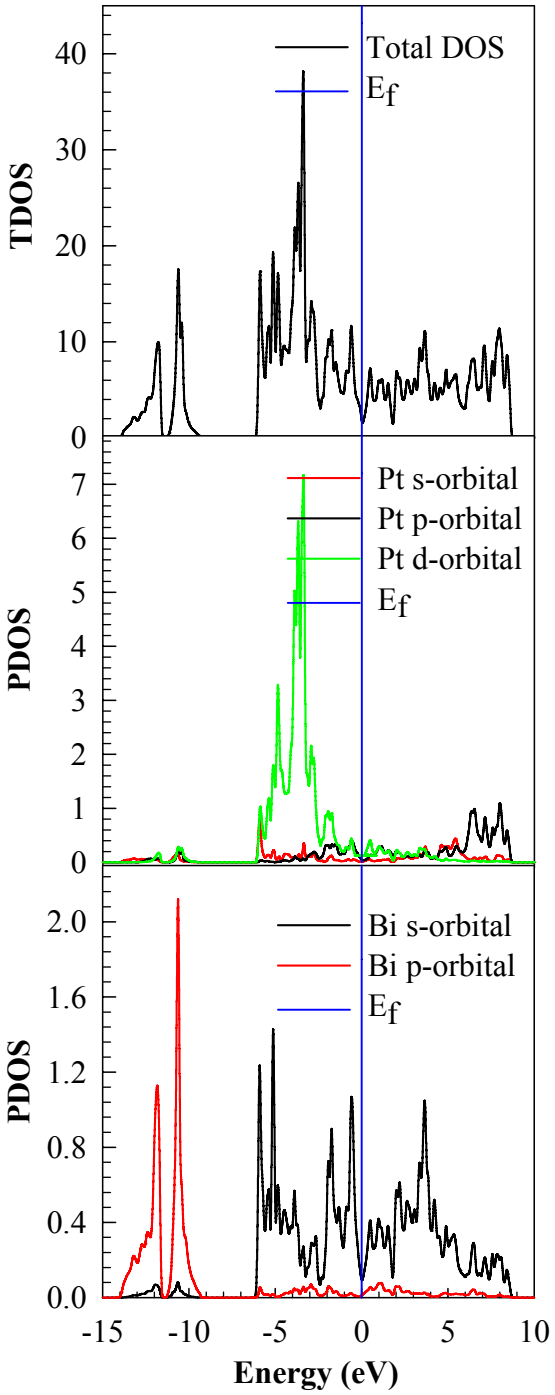

Figure 19: Partial and total density of states for $PtBi_2$.

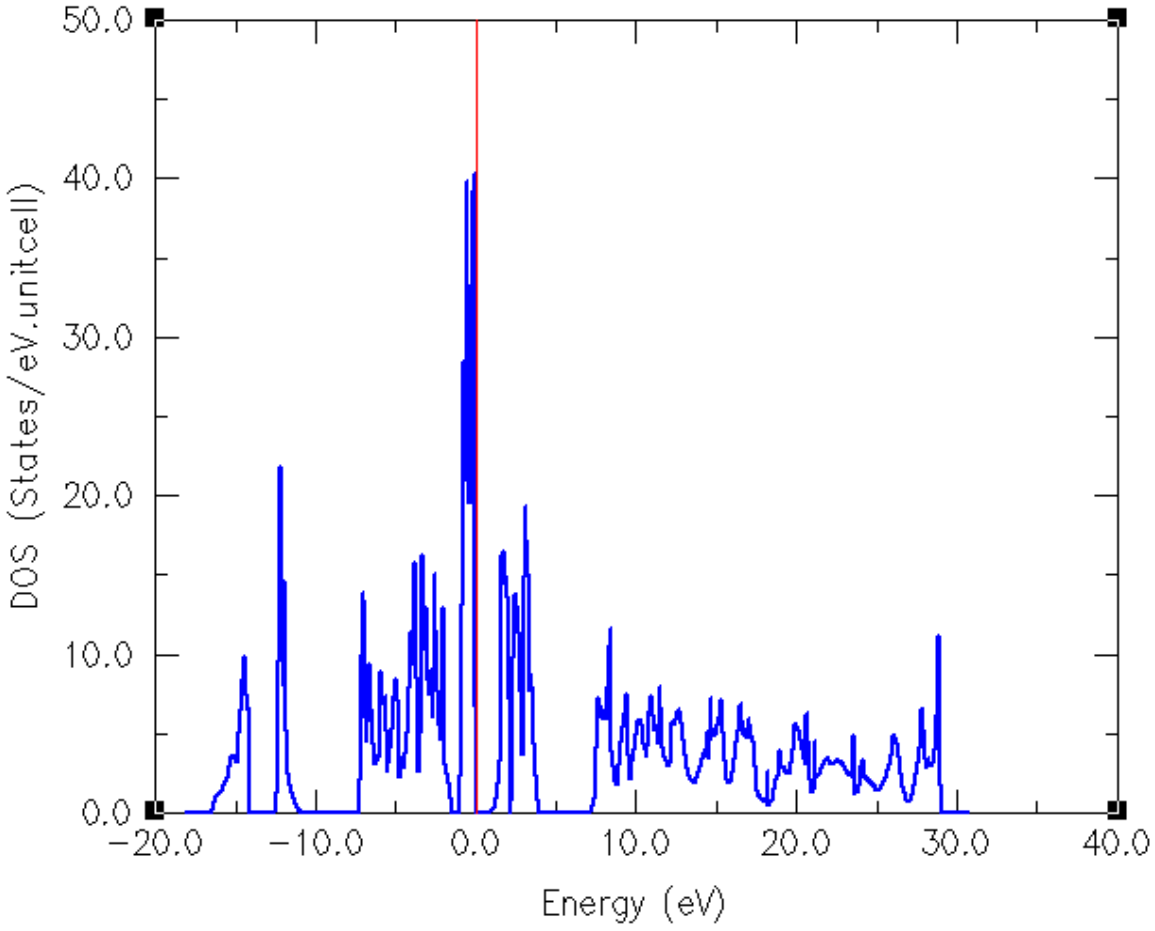

Figure 20: Total density of states of FeS_2.

FeS_2 has an indirect band gap of between 0.60 eV and 0.75 eV as obtained using GGA and LDA respectively [Sithole 2000] and the band structure also gives the indirect energy gap of 0.75 eV as the density of states. It also alluded that the energy gap depends strongly on the bonding between Fe and S owing to strong hybridisation of Fe (3d) and S (3p).

3.3.4 Charge Distribution Plots

Figures 21, 22 and 23 show the charge density differences of three pyrite compounds. The first one shows that of $PtSb_2$ followed by those of $PtBi_2$ and FeS_2. The red colour in these figures shows a charge gain, green indicates a neutral region between the atoms whilst the

blue colour signifies charge loss, from the transition metal. The orientation of these slices is along the [110] direction in all the structures.

These kinds of plots give an indication of the type of bonding that is found in a material or compound. In the case of $PtSb_2$, we can be able to analyse the bonding between Pt-Sb, Pt-Pt, and Sb-Sb. In the case of Pt-Sb, Pt-Bi, Sb-Sb and Bi-Bi there is covalent bonding. The same thing applies to other compounds like FeS_2 and $PtBi_2$. Bonding in $PtSb_2$ is mainly attributed covalency where the electrons from both the elements contribute. There is a very strong interaction between the Sb-Sb, Sb-Pt and some kind of metallic bond between the Pt atoms.

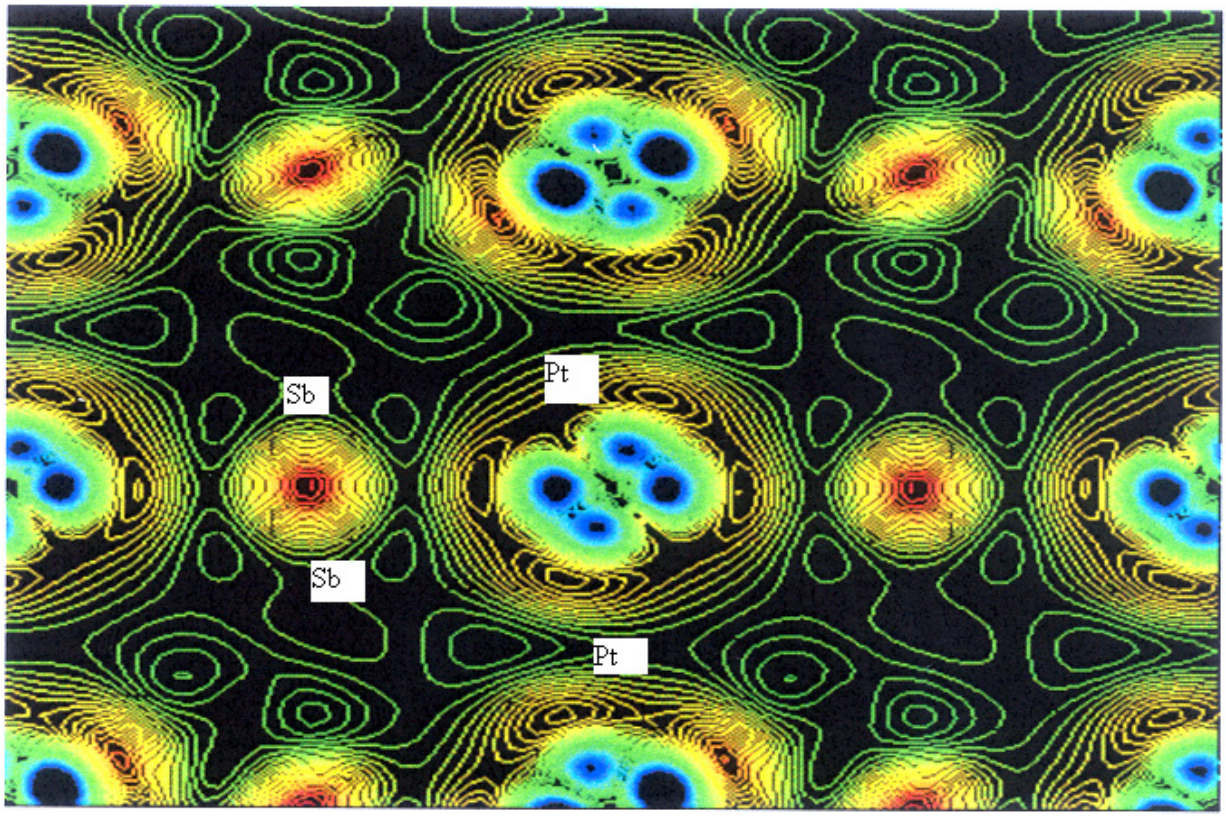

Figure 21: Charge density differences of $PtSb_2$.

In case of FeS_2, there is a high concentration of charge around the Fe atom, depicted as red, and the plots appear almost spherical [Sithole, 2000]. For all the compounds, mentioned,

strong covalent bonding is experienced between the metals and the non-metals, i.e. Fe, Pt and S, Sb, Bi. Covalent bonding is also found on the dimers whilst for metal-metal bonding it is metallic.

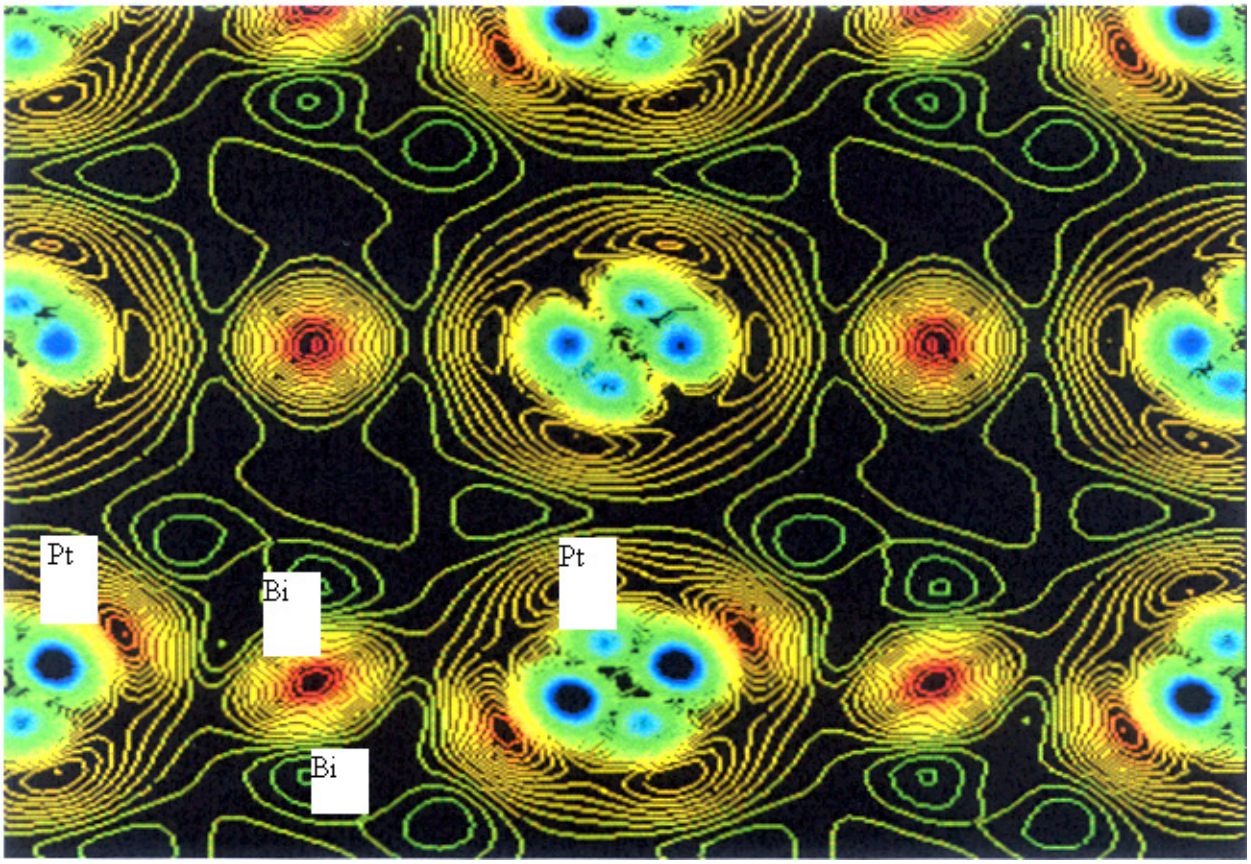

Figure 22: Charge density differences of $PtBi_2$.

The red colour around the bismuth atoms bonds indicate the accumulation of charge and this is an indication of a strong bond that is formed. Also the bonding between the Pt and Bi seem to be strong, and likely to be metallic in nature. Between the metal atoms there is a depletion of charge due to the d-orbital, and this gives a picture that there is ionic bonding.

3.3.5 Optical Properties

In general, the difference in the propagation of an electromagnetic wave through vacuum and some other material can be described by a complex refractive index.

$$N = n + ik \tag{21}$$

In vacuum, it is real and equal to unity. For transparent materials, it is purely real, the imaginary part being related to the absorption coefficient by,

$$\eta = \frac{2k\omega}{c} \tag{22}$$

the fraction of energy lost by the wave on passing through a unit thickness of the material concerned. This is derived through considering the rate of production of Joule heat in the sample.

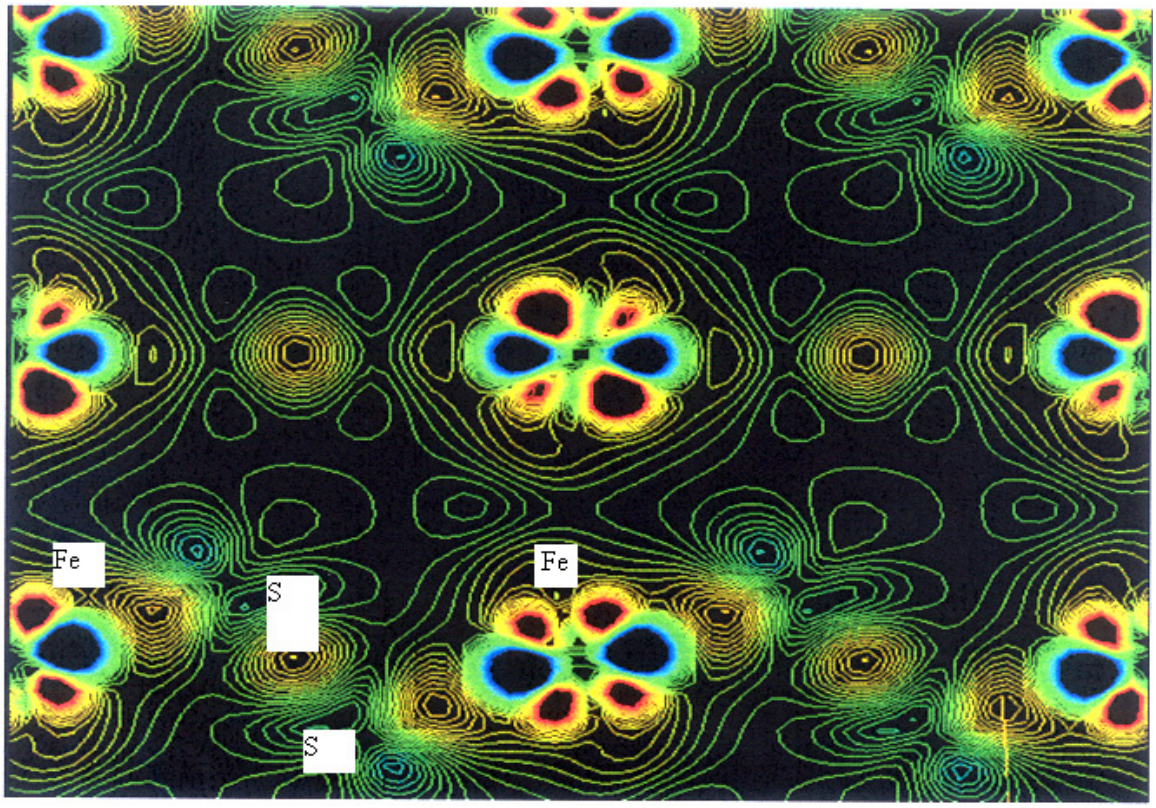

Figure 23: Charge density differences of pyrite, FeS_2.

The reflection coefficient can be obtained for the simple case of normal incidence onto a plane surface by matching both the electric and magnetic fields at the surface,

$$R = \left|\frac{1-N}{1+N}\right|^2 = \frac{(n-1)^2 + k^2}{(n+1)^2 + k^2} \quad \textbf{(23)}$$

However, when performing calculations of optical properties it is common to evaluate the complex dielectric constant, and then express other properties in terms of it. The complex dielectric constant $\varepsilon(\omega)$ is given by,

$$\varepsilon = \varepsilon_1 + i\varepsilon_2 = N^2 \quad \textbf{(24)}$$

and hence the relation between the real and imaginary parts of the refractive index and dielectric constant is,

$$\varepsilon_1 = n^2 - k^2 \varepsilon_2 = 2nk \quad \textbf{(25)}$$

A further frequent form for the expression of optical properties is the optical conductivity,

$$\sigma = \sigma_1 + i\sigma_2 = -i\frac{\omega}{4\pi}(\varepsilon - 1) \quad \textbf{(26)}$$

However, this is most useful for metals. A further property we may calculate from the complex dielectric constant is the loss function. It describes the energy lost by a point electron passing through a homogeneous dielectric material, and is given by,

$$\mathrm{Im}\left(\frac{-1}{\varepsilon(\omega)}\right) \qquad \textbf{(27)}$$

Connection to experiment

Experimentally, the most accessible optical parameters are the absorption $\eta(\omega)$, and the reflection $R(\omega)$ coefficients. In principle, given the knowledge of both, the real and imaginary parts of N can be determined, through equations 22 and 23. Equation 24 allows expression in terms of the complex dielectric constant. However, in practice, the experiments are more complicated than the case of normal incidence considered above. Polarization effects must be accounted for, and the geometry can become quite involved (for example, transmission through multi-layered films or incidence at a general angle). Only transitions between properly selected bands are allowed, i.e., only the bands with the same sign of spin.

Connection to electronic structure

The interaction of a photon with the electrons in the system under study is described in terms of time dependent perturbations of the ground state electronic states. Transitions are caused between occupied and unoccupied states by the electric field of the photon (the magnetic field effect is weaker by a factor of *v/c*). When these excitations are collective they are known as plasmons (which are most easily observed by the passing of a fast electron through the system rather than a photon, in a technique known as Electron Energy Loss Spectroscopy (EELS), since transverse photons do not excite longitudinal plasmons). When the transitions are independent they are known as single particle excitations. The spectra resulting from these excitations can be thought of as a joint density of states between the valence and conduction bands, weighted by appropriate matrix elements.

Figures 24-28 show reflectivity and absorption of $PtSb_2$, $PtBi_2$ and FeS_2. Comparison is made with the reflectivity of pyrite (FeS_2), which has been determined both experimentally and

computationally. The experimental reflectivity has been measured at different pressures as shown in Figure 28.

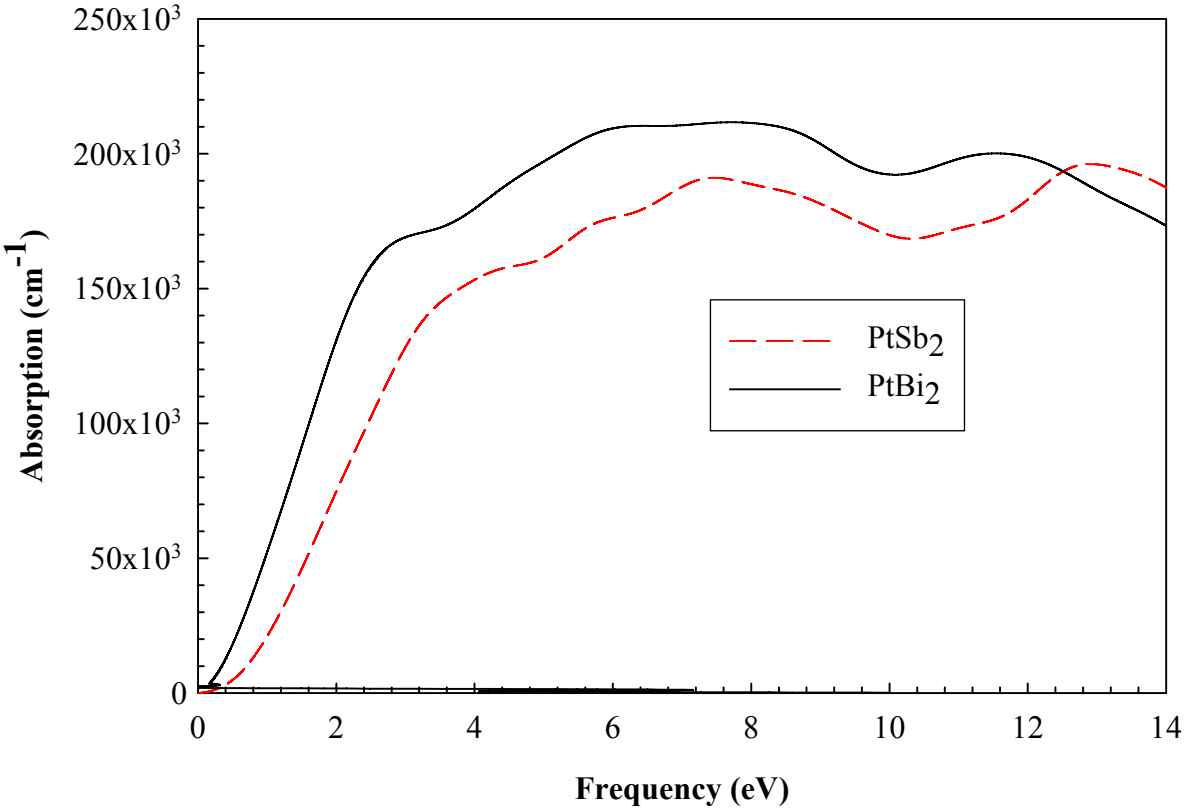

Figure 24: Calculated absorption coefficient of $PtSb_2$ and $PtBi_2$ with frequency.

The absorption versus frequency graph in Figure 24 has enabled us to determine the energy gap of $PtSb_2$ noting how it changes towards the origin. The absorption coefficient becomes ~500 cm^{-1} at the energy (frequency) of ~0.15 eV, which is comparable to the energy gap of 0.15 eV determined by density of states (DOS). Reynolds et al report that band to band optical absorption threshold is 0.11 eV at 10 K. Intrinsic absorption is small for photon energies near 0.11-0.29 eV [Reynolds 1968].

Figure 25 shows the experimental absorption coefficient of $PtSb_2$, which [O'Shaughnessy and Smith, 1970] comes close to our calculated results.

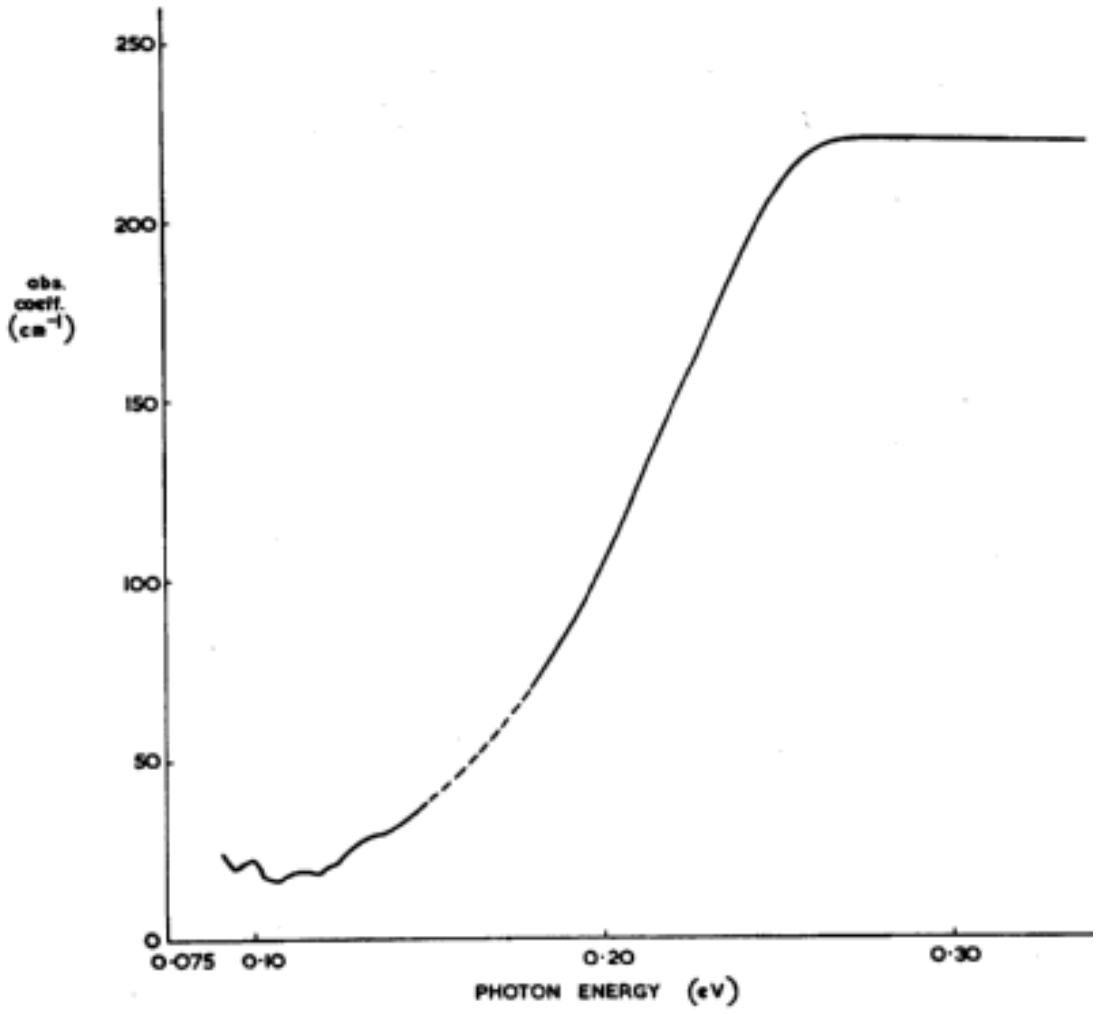

Figure 25: Experimental absorption coefficient of $PtSb_2$ with photon energy [O'Shaughnessy and Smith, (1970)].

Certain transitions occur between 0.0 eV and 15 eV with noticeable absorption peaks observed around 8 eV and 13 eV. From Figure 25 it cannot be said with certainty, which kinds of transitions are we noting, but they are likely to be associated with the Pt d-states and Sb p states. There could also be transitions between the valence and the conduction band (intraband transitions) for both occupied and unoccupied orbitals.

In the case of the calculated $PtBi_2$ absorption in observed throughout the frequency range, that is, 0-15eV, and there are possibly transitions that are taking place between the bands as

they overlap; and we could surmise that there is free movement of electrons from the valence to the conduction band. Transitions around 2.0 eV, 6.0 eV, 8 eV and 12.0 eV show strong absorption ranging from 200 000 cm^{-1} to 150 000 cm^{-1} in magnitude.

In Figure 26 the reflectivity of $PtSb_2$ is high, above 45.0 % around the frequency of 4.0 eV, and it is observed throughout the frequency range though it is smaller in magnitude. In the frequency range of interest the lowest reflectivity is just over 20.0 % near 12.0 eV.

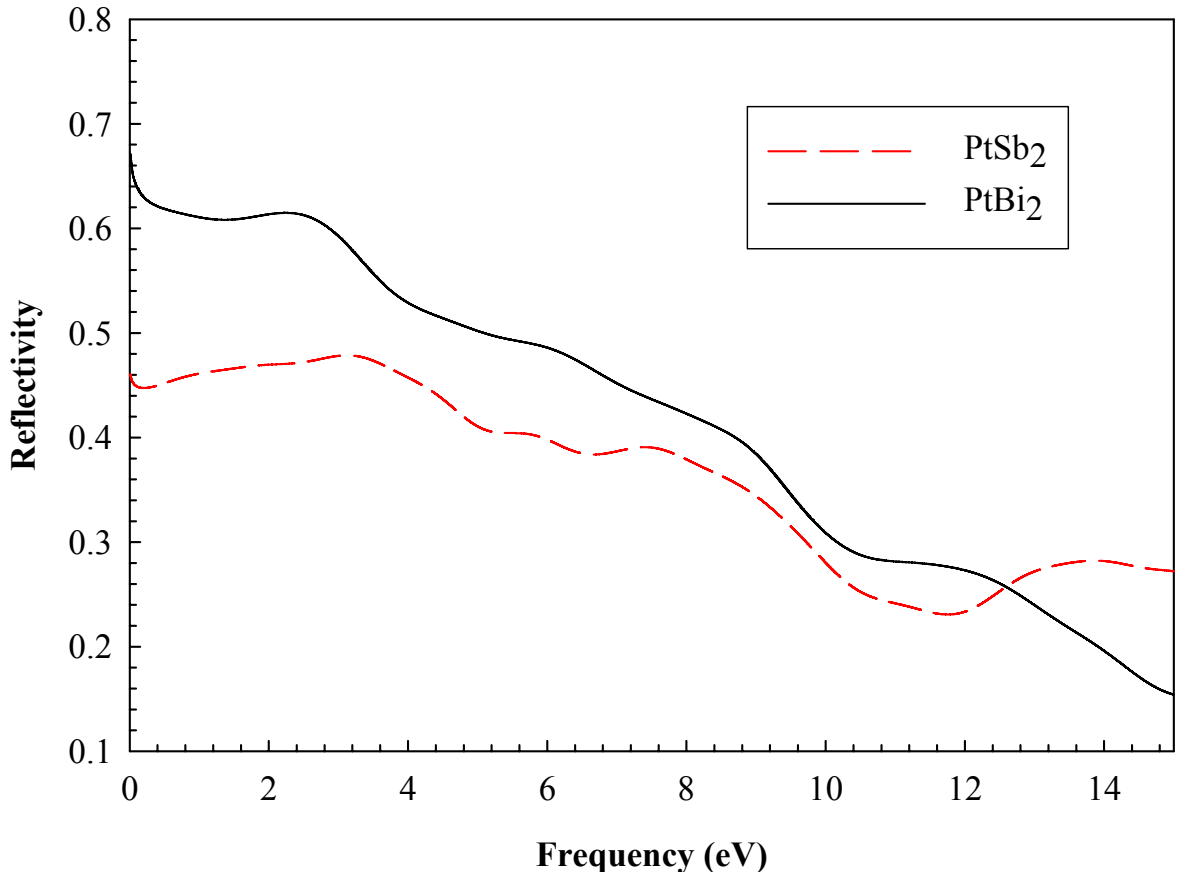

Figure 26: Calculated reflectivity of $PtSb_2$ and $PtBi_2$ with frequency.

Figure 26 gives the reflectivity of $PtBi_2$ over the frequency range 0.0 eV to 15.0 eV, and it is evident that high reflectivities occur at lower frequencies, between 0 0 eV and 3.0 eV, where

values in excess of 60.0% are attained. It can be seen that over the entire spectrum there are intra and inter-band transitions due to the shoulders appearing in the figure.

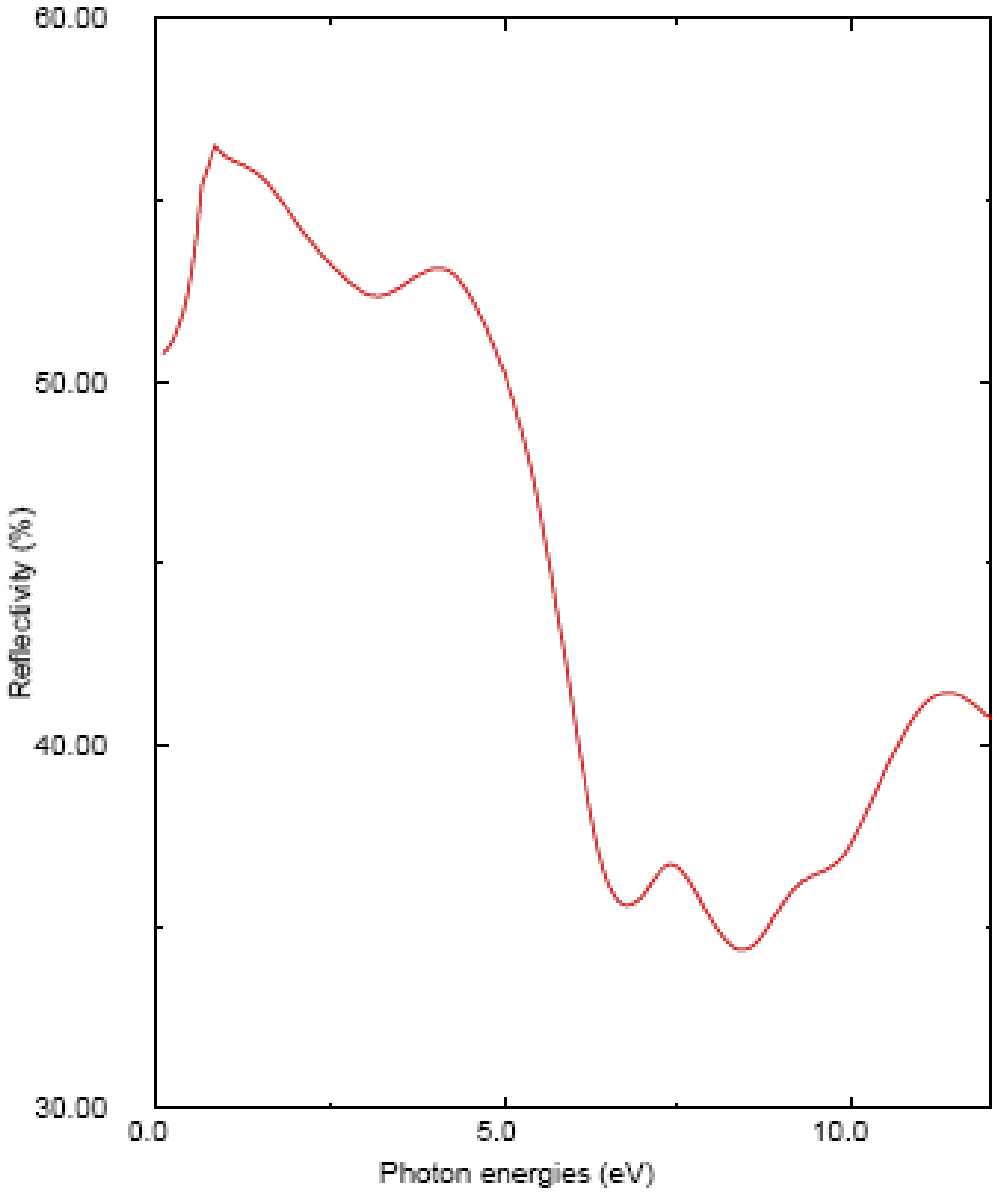

Figure 27: Calculated reflectivity of pyrite, FeS_2 with photon energy [Sithole (2000)].

The calculated reflectivity for pyrite [Sithole (2000)], between 0.0 eV and 16.0 eV, is shown in Figure 27, and can be compared with the experimental results at different pressures (Figure 28). The highest reflectivity is slightly in excess of 50.0 % for both the calculated and

experimental results, and the lowest is at about 30.0 %. The experimental reflectivity of FeS_2 shows that under high pressure the peaks are shifted to higher energy levels as shown in Figure 28.

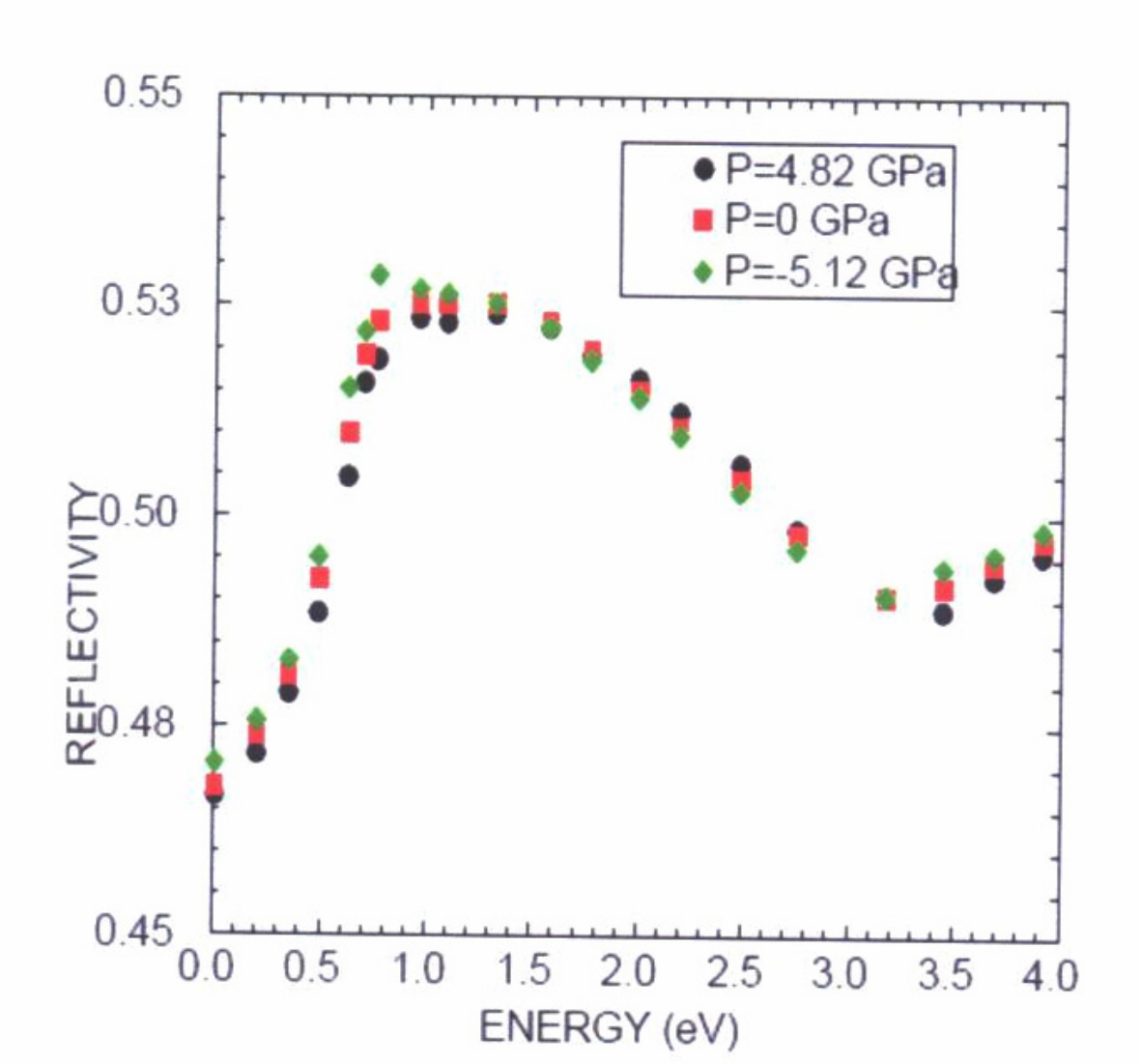

Figure 28: Experimental reflectivity of pyrite, FeS_2 [Mori and Takahashi (1997)].

Experimental reflectivity of FeS_2 performed by Mori and Takahashi, (1997) in the range 0.2 GPa and 4.2 GPa and also Ferrer et al (1990)) with energy shows a good correspondence with calculated reflectivity as depicted in Figures 27 and 28. It can hence be surmised from

the validity of the calculated FeS_2 reflectivities that those of $PtSb_2$ and $PtBi_2$ are likely to be good predictions.

3.4 Conclusion

In this chapter we have calculated the lattice parameters and elastic properties of $PtSb_2$ and $PtBi_2$. Using DFT (LDA and GGA), which are in good agreement with the available experimental results. The study has further depicted that $PtSb_2$ is a semiconductor as deduced from the calculated density of states and optical properties, and the estimated energy gap was found to be 0.15 eV, which agrees well with the experimentally determined value.

The density of states for $PtBi_2$ revealed that the material is metallic. It has been shown that the bonding between Pt-Sb(Bi) and Sb(Bi)-Sb (Bi) is covalent and that between the Pt and Pt is metallic, as deduced from charge density difference plots.

A very good agreement is found between the experimental and calculated FeS_2 and $PtSb_2$ reflectivity plots, which is a strong indication of the credibility of the ab initio techniques that we employed. $PtSb_2$ has reflectivity and conductivity quite at variance with that of $PtBi_2$ as the latter material reflects and conducts over the entire frequency range, since it is metallic.

Chapter 4

Potential Derivation and Simulation of the Surfaces of $PtSb_2$

4.1 Introduction

In this chapter we will outline steps taken in the derivation of interatomic potentials of $PtSb_2$ and their application to the study of surfaces.

4.2 Potential Derivation

In the chapter 2 the different models for the interactions between the ions were described and it was shown that for any pair of ions there are at least two parameters describing that interaction as a function of distance and angle. The specificity and reliability of this approach also depend on the quality of the parameters derived. Therefore the methods used to obtain parameters are discussed. It should be noted that this step can be by-passed by performing direct ab-initio simulations on these systems, however, the ab-initio methods can currently only handle a limited number of atoms.

4.2.1 Non-empirical

Potential parameters can also be calculated using quantum mechanical methods. In this case, the interaction energy between two ions is calculated as a function of distance. The potential parameters are then evaluated by fitting to the obtained energy surface. The most common method of calculating the interactions is via the electron gas method [Gordon and Kim, 1972] The electron density of a lattice of atoms is considered to be the sum of the electron densities of the isolated ions. The electron densities around the ions are determined via Hartree-Fock

or other electronic structure procedures. A density functional method is then used to calculate the components of the short-range energy.

Potentials derived by direct calculation are valid over a wide range of interionic separations or relative interatomic configuration, but external influences must be taken into account. Experimental data is often relied upon to modify parameters to yield reliable results.

4.2.2 Empirical

This approach uses experimentally observed structure and lattice properties to fit the parameters of the short-range functions. Taking a trial set of potential parameters and calculating a set of crystallographic, thermodynamic and dynamic data usually initialises the fitting procedure. Crystal structure must be included; other properties that can be used are cell dimensions, elastic and dielectric constants, and phonon dispersion curves. The parameters are then adjusted iteratively, usually by least squares fitting so that they reproduce known experimental values and strains are minimised. The empirical approach relies on the availability of experimental data.

A disadvantage of this type of potential is that they are fitted to equilibrium interatomic distances, thus they may not give satisfactory results in the calculation of surfaces, defects, or molecular dynamics or lattice dynamics calculations at high temperature or pressure where the separations are far from the equilibrium configuration.

4.3 Fitting Methodology

The first issue to be considered when deriving potential parameters is the matching of the calculated and observed structural parameters, which requires a least squares fitting of calculated parameters to observable properties. The greater the number and the higher the quality of observables available, the better will be the quality of determined potential

parameters. In the case of empirical potentials, typically the crystal structure, dielectric constants and elastic constants are chosen as observables. For non-empirical potentials the observables are energy at a given configuration. The approach is to adjust the parameters until the smallest sum of squares is obtained. The sum of squares, ***F***, is defined as:

$$F = \sum w\left(f_{calc} - f_{obs}\right)^2 \qquad \textbf{(28)}$$

where f_{calc} and f_{obs} are the calculated and observed quantities respectively and w is an appropriate weighting factor. The sum of squares is taken over all observables. The choice of the weighting factor depends on the magnitude and the reliability of the observable.

Fitting of the potential parameters is performed as in the case of simultaneous equations, where the constants are the observable and the unknown parameters being the potential parameters. Thus the number of parameters that could be varied at a time depends on the number of observables available. As an example, if the lattice parameter is used as the sole observable, only one parameter, say Buckingham $\boldsymbol{A_{ij}}$ could be varied at a time. The parameter is then fixed and varies $\boldsymbol{C_{ij}}$ and so on. However, for a number of observables, one can vary all parameters describing the potential function at a time and in case of the Buckingham potential, $\boldsymbol{A_{ij}}$, $\boldsymbol{C_{ij}}$, and $\boldsymbol{\rho_{ij}}$ could be varied simultaneously.

A minimum sum of squares does not always lead to accurate prediction of other properties, which were not used as observables, for example, phonon frequencies. This condition could be occur when the structure is at a local minimum rather than the global minimum, and the structure will show instabilities, such as distorted structure and or imaginary phonon frequencies.

4.4 Types of Surfaces

Surfaces can be divided into two classes, those that are polar and those that are non-polar as shown in Figures 29 and 30. Non-polar surfaces are the easiest and most reliable to model, since no corrections need to be made to compute the surface energy (which is the energy required to cleave the crystal in order to create the surface) or attachment energy (the energy released when a growth slice is attached to the surface).

Accurate modeling of polar surfaces requires special attention, as it is necessary to neutralize the dipole in some way, either mechanically, environmentally or chemically. Mechanical neutralization involves moving some ions from one face to another to counteract the dipole; chemical neutralization removes some of charge by attaching new charged species, such as hydroxy groups to the surface; while environmental neutralization is effected by polarization of the surrounding solvent.

A type I surface, represented in Figure 29, has each plane consisting of anions and cations in a stoichiometric ratio. Therefore each plane has an overall zero charge which implies no dipole moment perpendicular to the surface. A type II stacking sequence in Figure 29 has charged planes, but the repeat unit consists of several planes which when considered together have no dipole moment perpendicular to the surface. In both type I and type II surface the electrostatic energy converges with the increase in region size. Thus it is important to calculate surface energies for different region sizes and obtain minimum surface energy for convergence.

The final type, type III, Figure 30 however, alternately charged planes are stacked and produce a dipole moment perpendicular to the surface if cut between any of planes. In nature these surfaces are stabilized by defects and/or adsorbed species. We can generate a stoichiometric surface by removing half of the ions in the surface layer at the top of the

repeat unit and transferring them to the bottom Figure 30, thereby producing a highly defective structure.

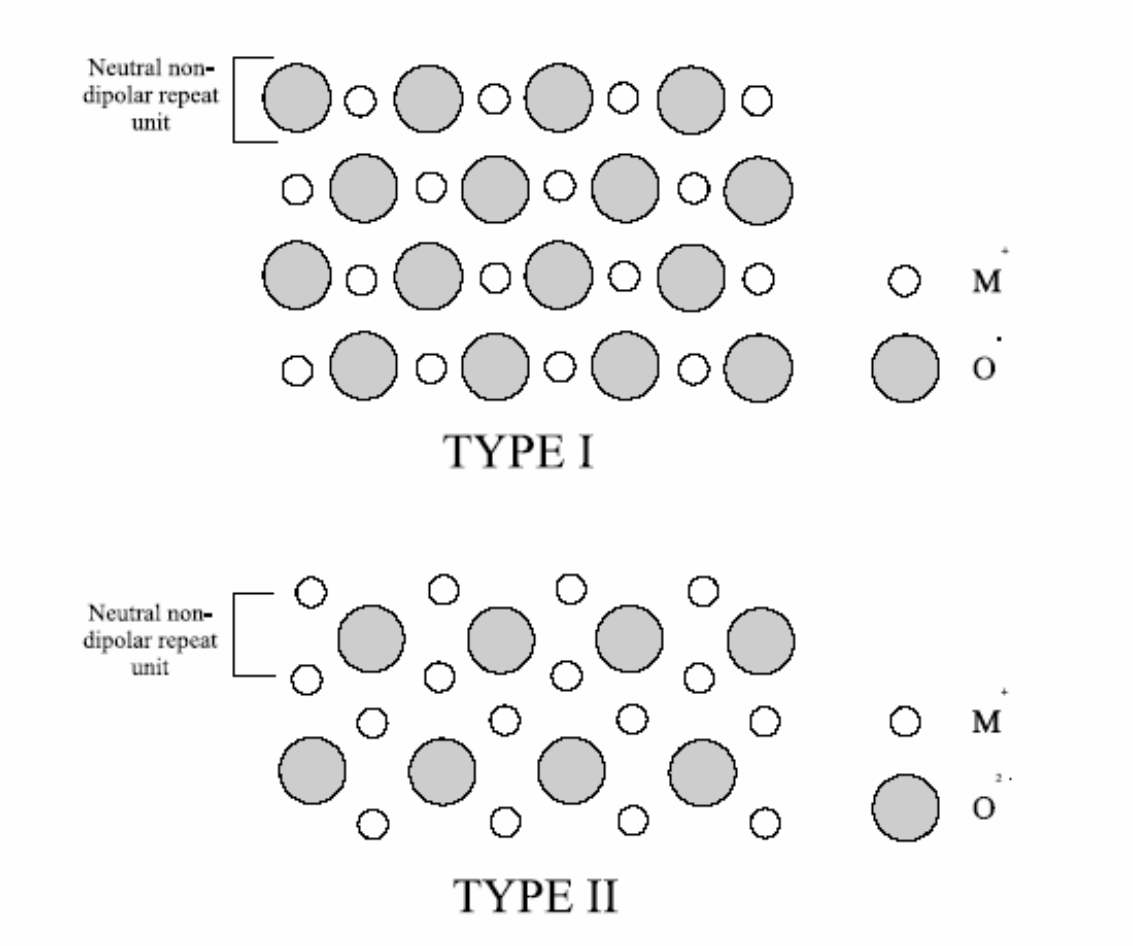

Figure 29: Types I and II surfaces

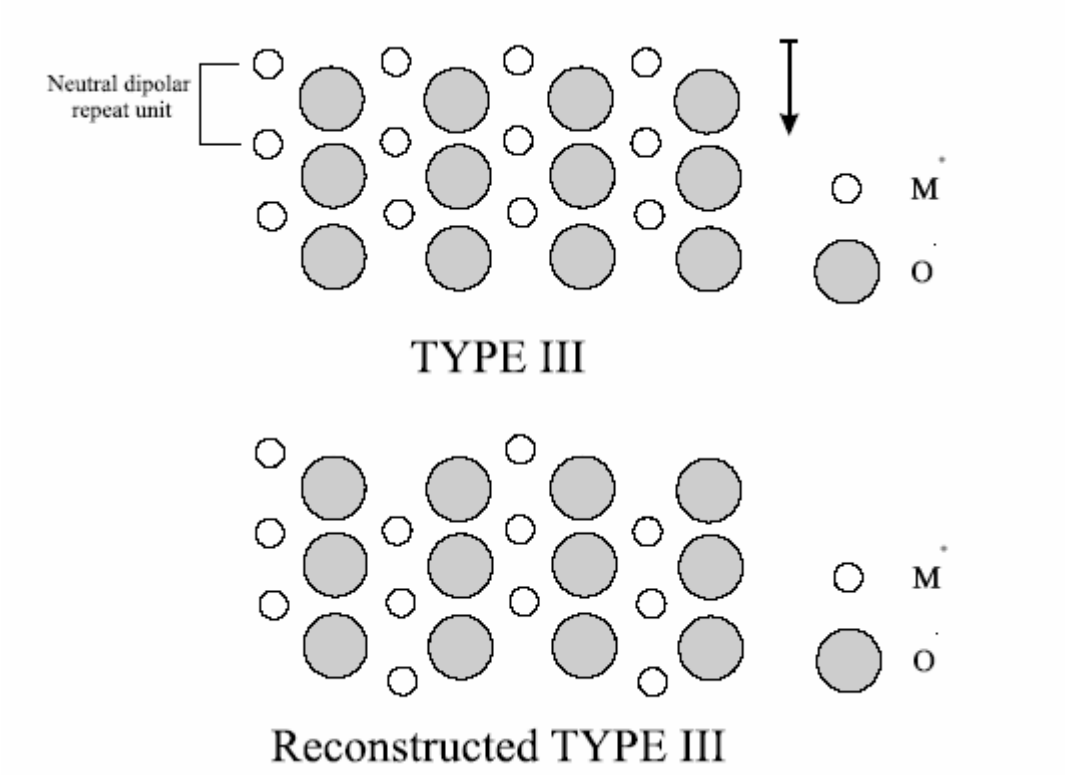

Figure 30: Type III surfaces

The crystal is then divided into two blocks, each of which is divided into two regions, I and II, as shown in Figure 31. The ions in region I are allowed to relax explicitly while those in region II are fixed at their equilibrium bulk positions, although the two region IIs are allowed to move relative to each other. It is necessary to include region II to ensure that the potential of an ion at the bottom of region I is modelled correctly [Tasker, 1979]. A surface is created when block II is removed with the top of region I as the free surface. Interfaces such as stacking faults and grain boundaries can be studied by fitting two surface blocks together in different orientations.

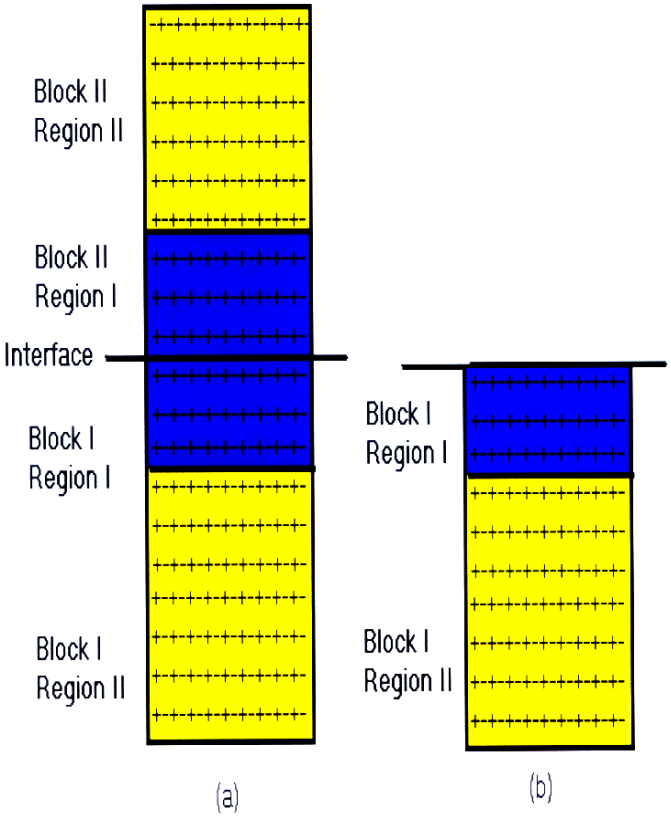

Figure 31: The two-region approach used in METADISE. (a) The complete crystal and (b) half the crystal revealing the surface.

4.5 Results and Discussion

In this section we give the calculated surface energies and bulk properties of $PtSb_2$ obtained by energy minimisation method using METADISE code.

4.5.1 Bulk Properties of $PtSb_2$

The bulk properties of $PtSb_2$ were obtained using the energy minimisation code GULP (General Utility Lattice Program) [Gale, 1996, 1997, 2003]. Dependences of the elastic constants and bulk modulus with temperature and pressure were obtained using GULP, as shown in Figures 32, 35, 36 and 37.

Table 3: Interatomic potentials for $PtSb_2$.

Morse (bonded)	**De (eV)**	**a_o (Å)**	**r_o(Å)**
Sb-Sb	4.9655	1.011	2.762
Buckingham (non-bonded)	**A_{ij} (eV)**	**ρ_{ij} (Å)**	**C_{ij} (eVÅ^6)**
Sb_2-Sb_2	342064.086595	0. 226518	183.54707
Pt-Sb	1686174.889654	0.172432	0.00
Three-body Potential	**k_b (eV.rad^{-2})**	**θ_o (degrees)**	
Sb-Sb-Pt	8.151451	103.0	

Cut off distance 35 Å

Table 3 gives the interatomic potentials, which are robust and produces bulk properties consistent with experiment as shown in Table 4. These potentials were derived using the GULP code. In Table 4 a validation of our results is presented for the lattice parameter, volume, and internal parameter and bond lengths. D_e is the equilibrium dissociation energy of the molecule (measured from the potential minimum) and a_o and r_o is the bond length and equilibrium bond length respectively. Other parameters have their usual meaning as explained in Chapter 2.

Table 4: Calculated and experimental structural parameters for $PtSb_2$.

Parameter	Calculated	Experimental
Lattice parameter (Å)	6.441	6.440
Volume ($Å^3$)	267.2	267.1
Internal parameter (Å)	0.3438	0.3752
Bond Lengths (Å)		
Sb-Sb	2.703	2.670
Pt-Sb	2.678	2.642
Elastic constants (GPa)		
C_{11}	262.2	266.0
C_{44}	57.91	59.05
C_{12}	64.07	68.00
Bulk Modulus (GPa)	130.1	134.0
Shear Modulus (GPa)	99.05	N/A
Young's Modulus (GPa)	182.2	N/A
Poisson's ratio	0.267	N/A

Table 4 gives the relationship of calculated and experimental structural parameters of $PtSb_2$, and they all agree within 10 %. The lattice parameter gives an error of 0.2 % while the internal parameter has a percentage difference of 9.1 %. Bond lengths are giving errors in the region of 1.2 and 1.3 %, which is reasonable enough compared to the experimental values. C_{11} and C_{44} are in excellent agreement with experiment and C_{12} gave an error of 6.1 %.

These values were obtained by fitting as explained in Section 4.3 (Fitting Methodology) and gives good agreement with experimental values, as the interatomic parameters derived in Table 3 are reproducing lattice and structural parameters well.

Temperature and Pressure dependences of Elastic Constants

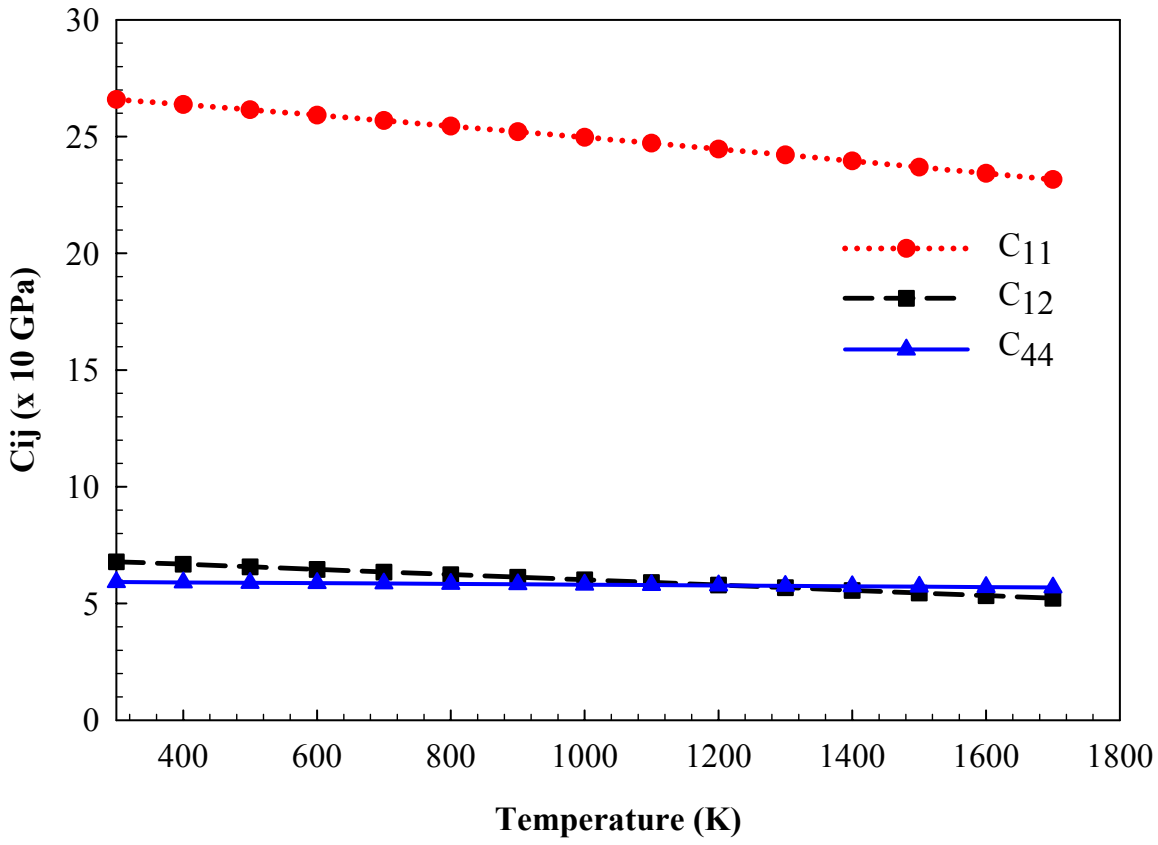

Figure 32: The calculated temperature variation of elastic constants for $PtSb_2$.

All the elastic constants decrease linearly with temperature until 1200K. This is apparent by the sudden change at around the melting point, i.e. ~1200K, as when the temperature increases the elastic constants decreases. Elastic constants C_{11} and C_{12} show some less appreciable change at about 1200K. An anomalous behaviour is displayed by C_{44} at around 1200K, as it seems not to decrease with increasing temperature.

As other studies have shown [Sithole, 2000], especially for FeS_2 (pyrite), the melting temperature of materials can be observed by plotting the elastic constants against temperature. Ngoepe et al (1990, 1992) also carried studies of LaF_3 using Brillouin scattering techniques and found that elastic constants decrease linearly with temperature, and this is ascribed to lattice expansion. These changes are attributed also to anharmonicity in the lattice vibration

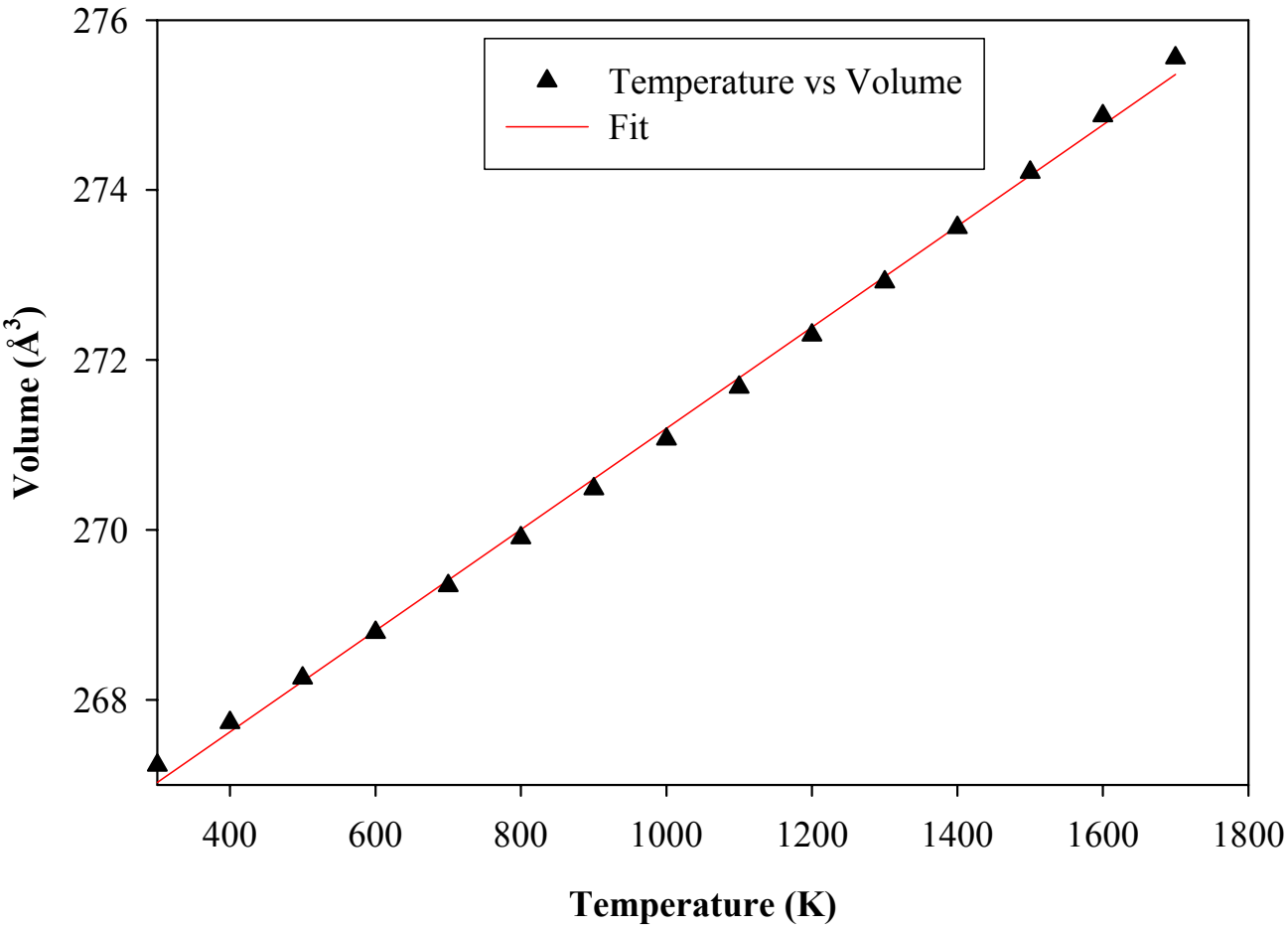

Figure 33: The calculated variation of the lattice parameter with temperature for $PtSb_2$.

For all real structures the volume increases with increasing temperatures is depicted in Figure 33 for $PtSb_2$. This relationship bears testimony to the rule, $T = \frac{PV}{Nk_b}$ where T is

the temperature, P, pressure, V, volume, N, number of particles and k_b the Boltzmann constant.

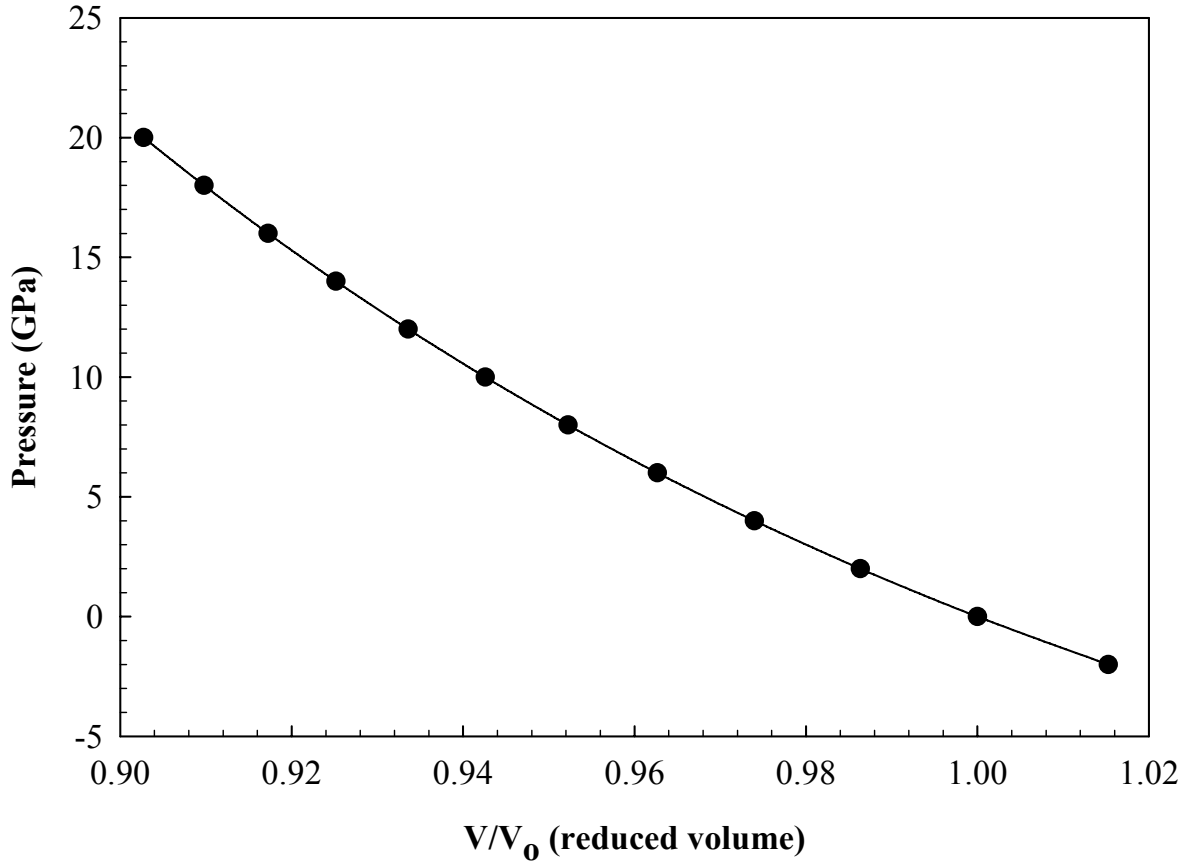

Figure 34: The calculated equation of state for PtSb2.

In Figure 34 the equation of state is shown and has enabled us to calculate the bulk modulus of $PtSb_2$ using the Birch-Murnaghan fit [Birch, 1947, Murnaghan. 1944]. The bulk modulus obtained using derived interatomic potentials is 138.9 GPa, close to the one found by planewave pseudopotential method of 134.8 GPa. The Birch-Murnaghan fit is obtained from the equation relation pressure to the reduced volume ,(Vo/V), given by:

$$P(V) = \frac{3}{2} B_O [(\frac{V_O}{V})^{\frac{7}{3}} - (\frac{V_O}{V})^{\frac{5}{3}}] \{1 + \frac{3}{4}(B'_O - 4)[(\frac{V_O}{V})^{\frac{2}{3}} - 1]\} \quad \textbf{(29)}$$

where B'_O is the first derivative of the bulk modulus and B_o is the bulk modulus at zero pressure, Vo the equilibrium volume while V is the volume. Fitting to the Murnaghan EOS and taking the derivative at zero pressure, yield the bulk modulus

$$B = -V_O (\frac{dP}{dV}) \quad \textbf{(30)}$$

Thus we are able to determine the bulk modulus at any pressure for materials under study.

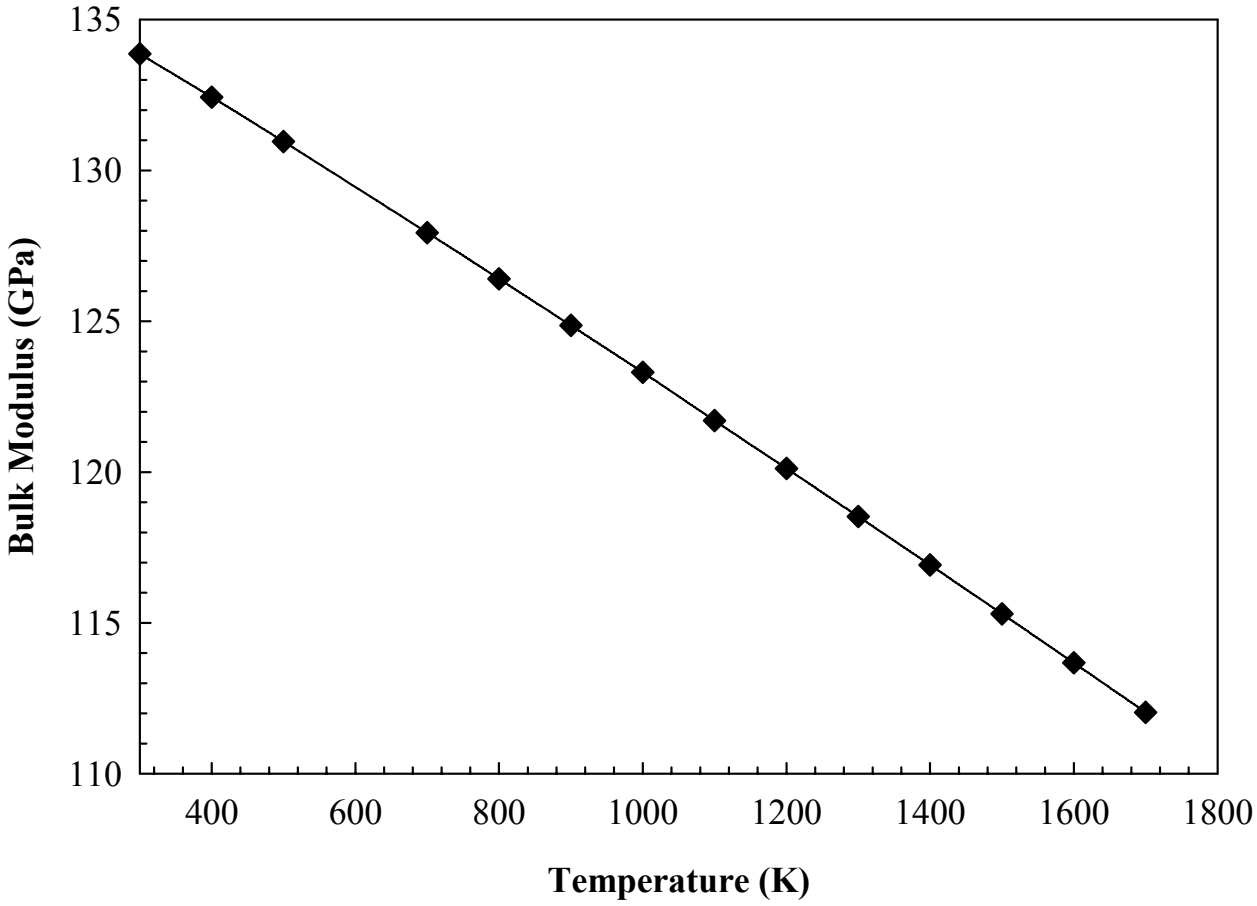

Figure 35: The calculated bulk modulus as a function of temperature for $PtSb_2$.

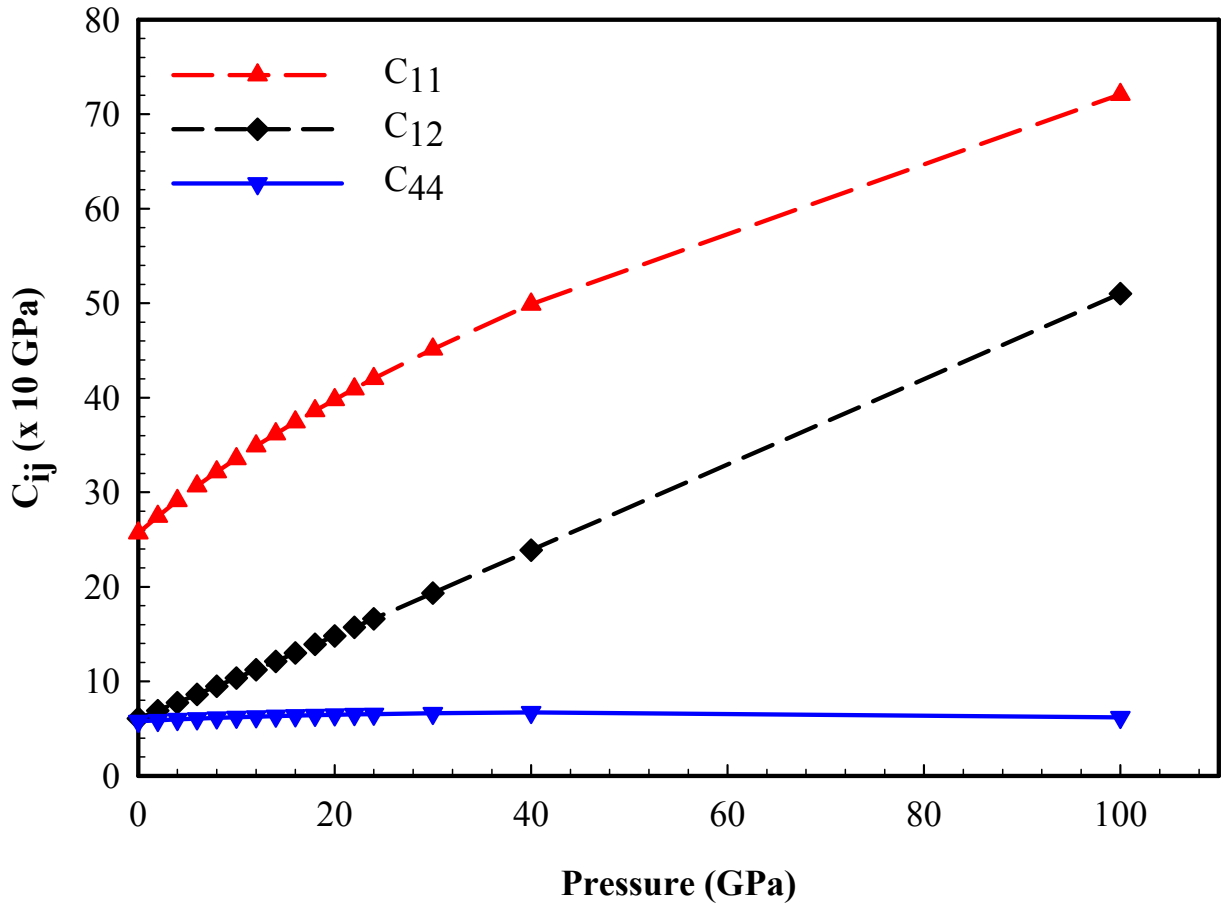

Figure 36: The calculated pressure variation of elastic constants for $PtSb_2$.

The bulk modulus follows the same trend as the elastic constants as shown in Figure 37. Pressure dependence of bulk modulus also follows the trend as displayed in Figure 37. Figure 36 shows change of the elastic constants of $PtSb_2$ with pressure. There is a marked increase of the C_{11} and C_{12} elastic constants with pressure in contrast to the C_{44}, as is the figure indicates. The fact that C_{44} seem not to increase with increasing pressure or decrease with increasing temperature could signal some interesting feature of $PtSb_2$ which needs further investigation.

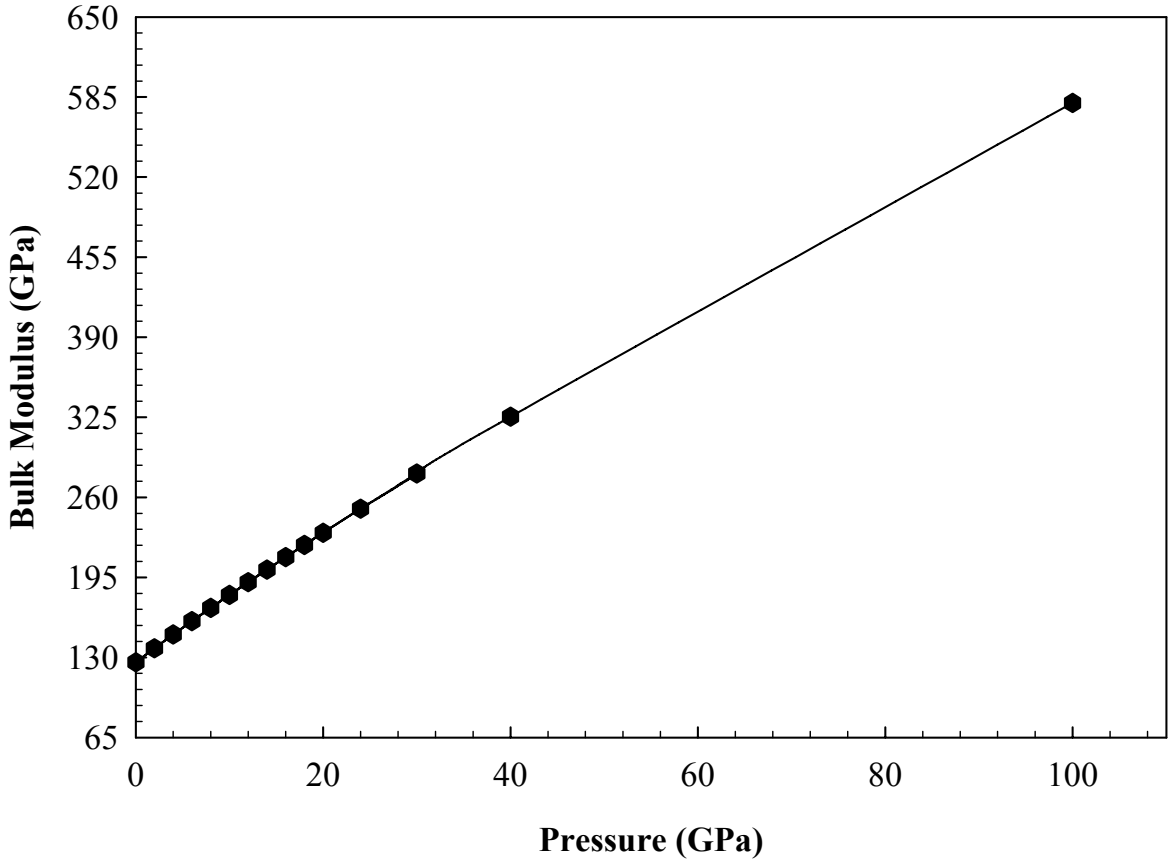

Figure 37: The calculated bulk modulus as a function of pressure for $PtSb_2$.

Figure 37 also shows the relationship between the bulk modulus and pressure, which is similar to that of elastic constants, particularly C_{11}. Comparison can be drawn with FeS_2 calculated results, [Sithole, 2000], but no experimental results are available for pressure work of the elastic moduli.

4.5.2 Surface Properties

The surface energy γ is a measure of the thermodynamic stability of the surface with a low, positive value indicating a stable surface. It is given by:

$$\gamma = \frac{U_s - U_b}{A} \qquad \textbf{(31)}$$

Where U_s is the energy of the surface block of the crystal, U_b is the energy of an equal number of atoms of the bulk crystal and A is the surface area. The energies of the blocks are essentially the sum of the energies of interaction between all atoms. The long-range Coulombic interactions are calculated using the Parry technique [Parry, 1975, Parry, 1976] whereas the short-range repulsions and Van der Waals attraction are described by parameterised analytical expressions.

Table 5 gives the calculated surface energies of $PtSb_2$ from the derived set of potentials, employing energy minimisation technique METADISE. It can be noted that the Sb terminated (100) surface is more stable than the others, with the least stable being (111) Sb terminated after (111) Pt terminated one. In the appendix the (100) surface slices/cuts are given for different terminations.

The equilibrium surface morphology of a crystal is determined by the surface energy of the most stable, or the most dominant surface structure. According to Wulff [1901], the equilibrium shape of a crystal is determined by the surface energies of its various surfaces, in such a way that the equilibrium morphology is the shape of the crystal with minimum surface free energy. If the crystal is limited in space by n flat faces, then:

$$\frac{\sigma_1}{h_1} = \frac{\sigma_2}{h_2} = \frac{\sigma_3}{h_3} = ... = \frac{\sigma_i}{h_i} = \frac{\sigma_n}{h_n} \qquad \textbf{(32)}$$

where σ_i is the specific free energy of the i^{th} face and h_i is the distance from the centre of the crystal to the plane of the i^{th} face [Tauson et al. 1989] and is normal to the face. Hence the height of the face is directly proportional to its specific free energy. At zero Kelvin, the

specific free energy is approximately equal to the surface energy as calculated by static lattice simulations. Thus the surface energies can be assumed to determine the equilibrium morphology of the crystal as follows:

$$E_s = \sum \gamma_i A_i \text{ =minimum for constant volume} \qquad \textbf{(33)}$$

where $\boldsymbol{E_s}$ is the excess energy for the surface defined by Stoneham (1976) and $\boldsymbol{\gamma_i}$ and A_i are the surface energy and the surface energy of the i^{th} crystallographic face.

Table 5: Surface energies of $PtSb_2$

Surface termination	$\gamma_{unrelaxed}$ **(J.m^{-2})**	$\gamma_{relaxed}$ **(J.m^{-2})**
{100} Pt	2.374	2.271
{100} Sb	0.948	0.933
{110} Sb	1.679	1.629
{110} Pt	1.477	1.432
{111} Pt	3.054	2.466
{111} Sb	3.232	2.586

Similar surface energies were calculated with the DFT based ab initio codes and are with METADISE results in Table 6. A slight percentage difference is observed for the two methods employed, but generally there is an overall agreement. As in the other set of potentials for which their surface energies are given in the table preceding the previous one,

the (100) Sb terminated surface has the lowest surface energy as regards the others, with (111) Sb terminated surface having the highest surface energy in the case of METADISE, but for CASTEP the highest is the (111) Pt surface with the energy of 1.528 $J.m^{-2}$.

It is found that the {100} Sb terminated has the lowest energy (0.933 $J.m^{-2}$) and is the most stable as compared to the least stable (2.586 $J.m^{-2}$) {111} Sb terminated surface. We only looked at the low-index surfaces, as they are the ones that will tell us more about the fastest growing faces when considering crystal growth and morphology of the structure. But from what is known the surface with the lowest surface energy grows slowest whilst the one with the highest surface energy grows fastest. The cut-off for the potential was taken to be 35 Å.

Table 6: Surface energies of $PtSb_2$ in $J.m^{-2}$.

Surface termination	**CASTEP**	**VASP**	**METADISE**
100 Sb	0.809	0.950	0.933
111 Sb	1.027	1.990	2.586
111 Pt	1.528	1.900	2.466
110 Sb	0.884	1.390	1.628
110 Pt	1.462	2.400	1.432
100 Pt	1.247	1.840	2.271

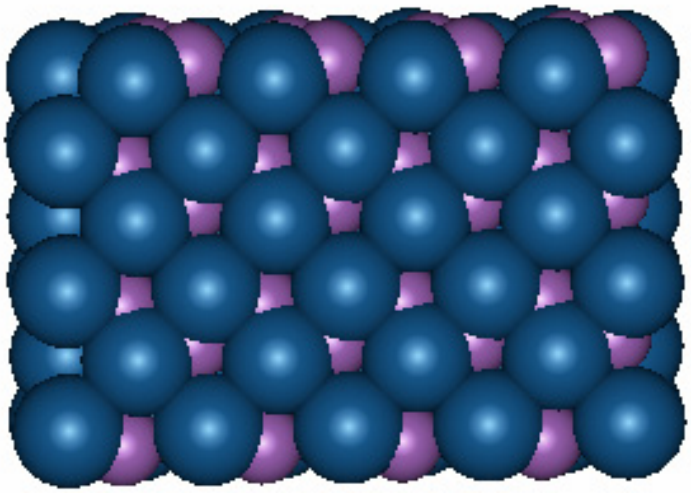

Figure 38: Sb terminated (100) surface of $PtSb_2$ before relaxation.

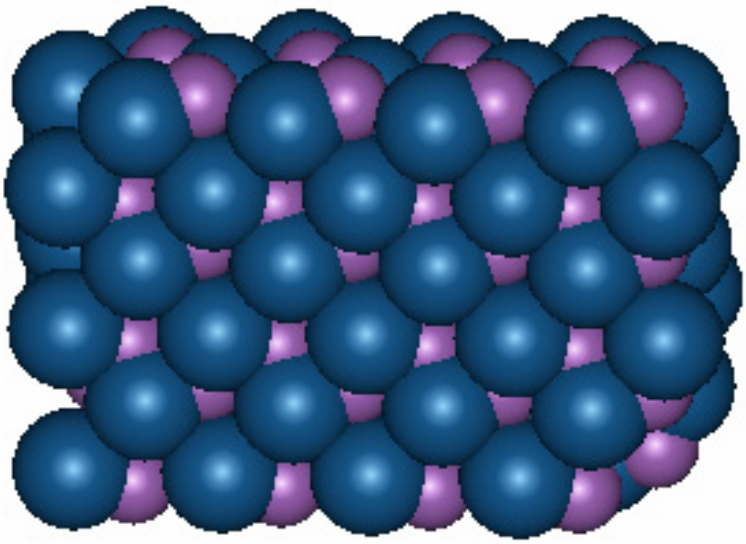

Figure 39: Sb terminated (100) surface of $PtSb_2$ after relaxation.

Figures 38, 39, 40 and 41 gives the simulated low index surfaces employing energy minimisation technique, i.e., METADISE, and it was found that relaxation of the atoms is between 0.03 Å and 0.07 Å, which is not quite significant.

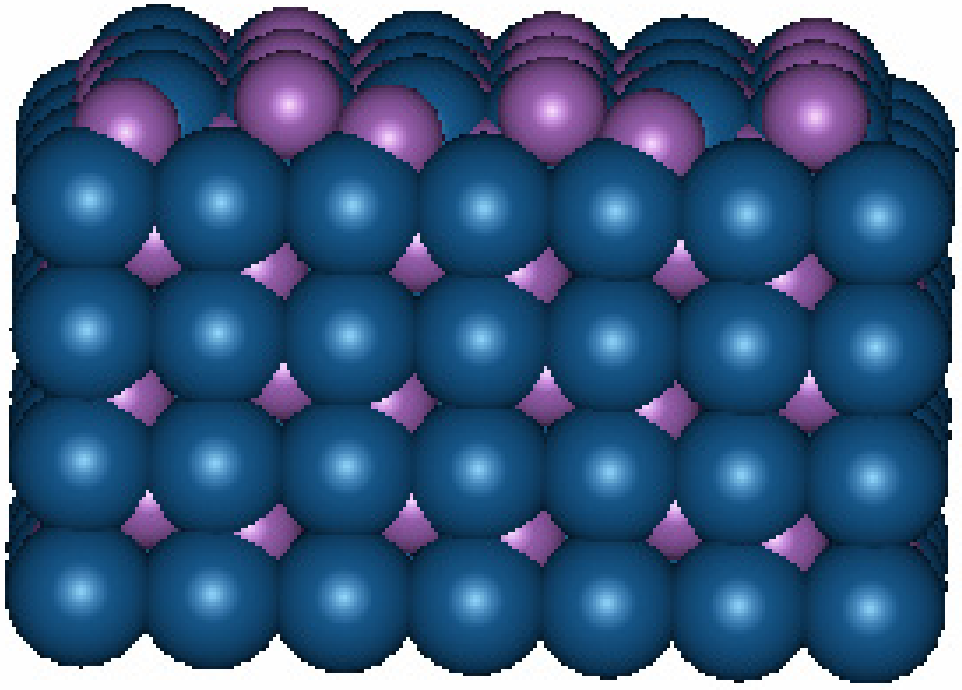

Figure 40: Sb terminated (110) surface of $PtSb_2$ before relaxation

The relaxation is quite observable by looking at the surface energy differences for relaxed and unrelaxed calculations. For the most stable (100) Sb surface the energy difference is 0.015 J.m2 and the least stable surface (111) Sb it is 0.646 Jm^2. For other surfaces we obtained intermediate values.

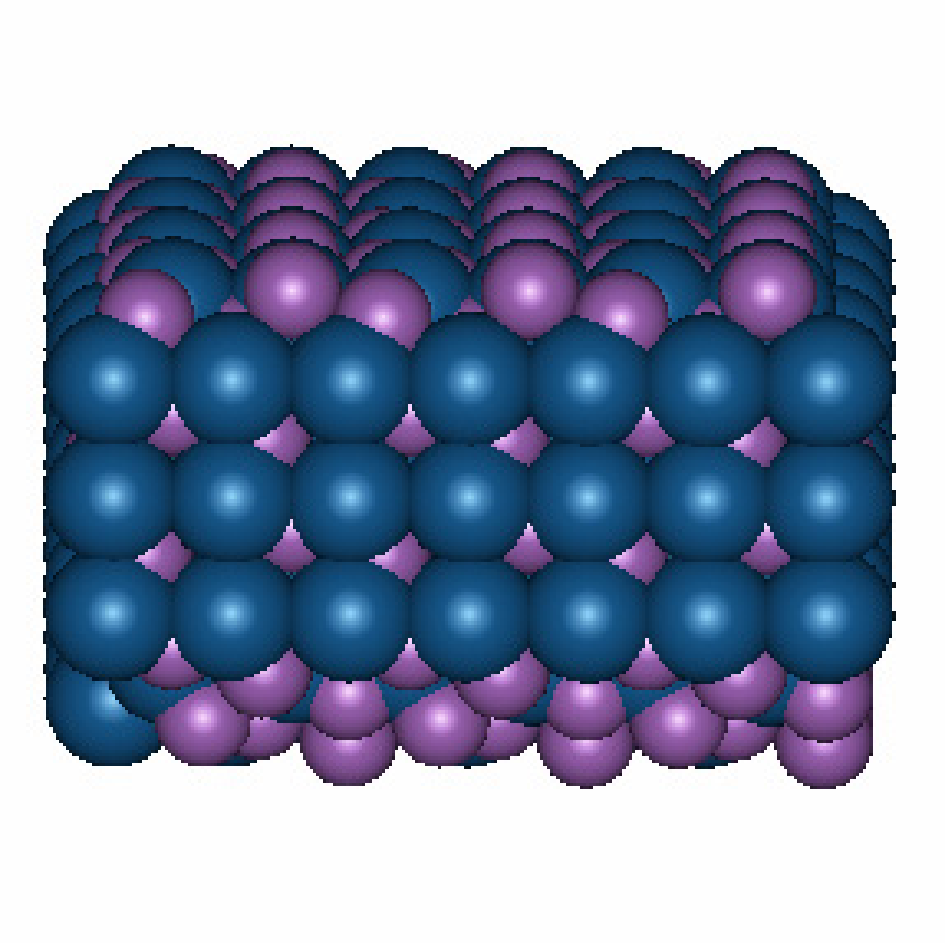

Figure 41: Sb terminated (110) surface of $PtSb_2$ after relaxation

4.6 Conclusion

From the above, it is abundantly clear that the sets of potentials that we derived work very well for both the bulk structure and the surfaces. Unfortunately there are no surface energies found experimentally to compare with but we feel confident that what we have calculated using the present set of potentials reproduces the bulk structural properties very well. We saw that the {100} Sb terminated surface is the most stable one as compared to the others, with the {111} Pt terminated the least stable or unstable, with the highest surface energy amongst the other surfaces. Elastic constants decrease linearly with an increase in temperature, whilst they increase proportionately with an increase in pressure.

Chapter 5
Conclusions

In the previous chapters we have been able to use different techniques, ab initio (Density Functional Theory, GGA-PBE and LDA) and atomistic simulation methods (Free Energy Minimisation (METADISE. From this study we were able to investigate several electronic and thermodynamic properties of the pyrite structures ($PtSb_2$ and $PtBi_2$). The equation of state (EOS) enabled determination of the bulk modulus, which agrees very well to that obtained from calculated elastic constants, which in turn accords well with experimental results.

Our ab initio calculations predicted the energy band gap from the density of states (electronic) and also from the absorption graphs, which has a relationship with the energy gap. The electronic structures indicate the band gap to be dependent on the hybridisation of the metal 4d orbitals and metalloids 3p orbitals. The charge distribution plots further indicate shows that the Pt- (Sb, Bi), Sb-Sb and Bi-Bi bonding in the structures is mainly covalent. We also observed that bond lengths of $Pt(Sb,Bi)_2$ and the internal parameters decrease linearly with hydrostatic compression.

In the atomistic simulation study we managed to derive the first interatomic potentials using the code GULP (General Utility Lattice Programme), which we then employed in the calculation of surface energies using METADISE code. The interatomic potentials reproduced the structure well and yielded elastic constants that are in excellent agreement with experimental results. We also carried out high pressure and high temperature dependences on structures and elastic properties, which normally occur under laboratory conditions, or under extreme conditions in the earth's mantle/crust. Surface energy calculations generally showed the {100} Sb terminated surface to be the most stable and the

second most stable surface is {110} Pt terminated surface. Our model also shows that at high temperatures the Sb are diffusing faster than the Pt for the surfaces.

5.1 Recommendation for Future Work

The next study of $PtSb_2$ should consider the hydration of surfaces and also the interaction of other ligands in terms of their reactivity with these minerals. In the case of $PtBi_2$ the study of surfaces should be pursued, as there are available potentials, which need to be refined to cater for the fact that the material is a metallic mineral.

Appendix

Surface Slices

This section shows various possible cuts for each surface in geversite ($PtSb_2$). The miller index shows the surface, e.g. Miller 1 0 0 represents the {100} surface, and the height is the depth of the surface, whilst other terms like charge are self-explanatory. Each code has its unique arrangement of atoms, which could be classified under three types of surface as discussed in Section 4.4 (Types of Surfaces).

Below is the part that gives the surface cuts of $PtSb_2$, and similar ones can be obtained for other surface cuts like the {110} and {111} surfaces and so are not shown.

Miller Index: 1 0 0

NORMAL AXIS 1.000000000000000 0.0000000000000000E+00
0.0000000000000000E+00

PLDRAW: Code (3) with dipole = 8.8817841970012523E-16

height	charge	atom arrangement
0.0	-2.0	SBSB
0.2	0.0	
0.4	0.0	
0.6	0.0	
0.8	4.0	PT--PT
1.0	0.0	
1.2	0.0	
1.4	0.0	
1.6	-2.0	SBSB
1.8	0.0	
2.0	0.0	
2.2	0.0	
2.4	0.0	
2.6	0.0	
2.8	0.0	
3.0	0.0	
3.2	-2.0	SBSB
3.4	0.0	
3.6	0.0	
3.8	0.0	
4.0	4.0	PT--PT
4.2	0.0	
4.4	0.0	
4.6	0.0	

4.8 -2.0 SBSB

Miller Index: 1 0 0

Normal Axis 1.000000000000000 0.0000000000000000E+00

0.0000000000000000E+00

PLDRAW: Code (6) with dipole = 1.7763568394002505E-15

height charge atom arrangement

0.0 2.0 PT

0.2 0.0

0.4 0.0

0.6 0.0

0.8 -2.0 SBSB

1.0 0.0

1.2 0.0

1.4 0.0

1.6 0.0

1.8 0.0

2.0 0.0

2.2 0.0

2.4 -2.0 SBSB

2.6 0.0

2.8 0.0

3.0 0.0

3.2 4.0 PT--PT

3.4 0.0

3.6 0.0

3.8 0.0

4.0 -2.0 SBSB

4.2 0.0

4.4 0.0

4.6 0.0

4.8 0.0

5.0 0.0

5.2 0.0

5.4 0.0

5.6 -2.0 SBSB

5.8 0.0

6.0 0.0

6.2 0.0

6.4 2.0 PT

Miller Index: 1 0 0

Normal Axis 1.000000000000000 0.0000000000000000E+00

0.0000000000000000E+00

PLDRAW: Code (9) with dipole = 1.7763568394002505E-15

height charge atom arrangement

0.0 -2.0 SBSB

0.2 0.0

0.4 0.0

0.6 0.0

0.8 4.0 PT--PT

1.0 0.0

1.2 0.0

1.4 0.0

1.6 -2.0 SBSB

1.8 0.0

2.0 0.0

2.2 0.0

2.4 0.0

2.6 0.0

2.8 0.0

3.0 0.0

3.2 -2.0 SBSB

3.4 0.0

3.6 0.0

3.8 0.0

4.0 4.0 PT--PT

4.2 0.0

4.4 0.0

4.6 0.0

4.8 -2.0 SBSB

Miller Index: 1 0 0

Normal Axis 1.000000000000000 0.0000000000000000E+00

0.0000000000000000E+00

PLDRAW: Code (12) with dipole = -1.7763568394002505E-15

height	charge	atom arrangement
0.0	2.0	PT
0.2	0.0	
0.4	0.0	
0.6	0.0	
0.8	-2.0	SBSB
1.0	0.0	
1.2	0.0	
1.4	0.0	
1.6	0.0	
1.8	0.0	
2.0	0.0	
2.2	0.0	
2.4	-2.0	SBSB
2.6	0.0	
2.8	0.0	
3.0	0.0	
3.2	4.0	PT--PT
3.4	0.0	
3.6	0.0	
3.8	0.0	
4.0	-2.0	SBSB
4.2	0.0	
4.4	0.0	

4.6	0.0	
4.8	0.0	
5.0	0.0	
5.2	0.0	
5.4	0.0	
5.6	-2.0	SBSB
5.8	0.0	
6.0	0.0	
6.2	0.0	
6.4	2.0	PT

References

M. P. Allen, and D. J. Tildesley, *Computer Simulation of Liquids*, Clarendon Press, Oxford Science Publications (1987)

N.L.Allan, *et al,* J Chem.Soc.:Faraday Trans.,**95**,273,(1993)

N. L. Allinger, Y. H. Yuh, J.-H. Lii, J. Am .Chem Soc. **111**, 8551 (1989)

O. K. Andersen, Phys. Rev. B **12**, 3060 (1975)

J. Andzelm and E. Wimmer, J. Chem. Phys. **96**, 1280 (1992)

M. Aoki, Phys. Rev. Lett. **71**, 3842 (1993)

M. Aoki, P. Gumbsch, and D. G. Pettifor, Computer Aided Innovation of New Materials,

W.Cochran , The dynamics of atoms in crystals, ed. Coles B.R., Edward Arnold, (1973)

F Birch, Physical Review**, 71**, 809-824 (1947).

N. H. de Leeuw, S. C. Parker, H. M. Sithole, and P. E. Ngoepe, J. Phys. Chem. B **104**, 7969 (2000).

M. Doyama, J. Kihara, M. Tanaka, and R. Yamamoto, editors, North-Holland, Amsterdam p. 1457 (1993).

G. B. Bachelet, D. R. Hamann, and M. Schlüter, Phys. Rev. B **26**, 4199 (1982).

E. J. Baerends, D. E. Ellis, and P. Ros, Chem. Phys. **2**, 41 (1973).

A. Balková and R. J. Bartlett, J. Chem. Phys. **96**, 3739 (1992).

G. A. Baraff and M. Lannoo, Rev. Phys. Appl. **23**, 863 (1988).

M. I. Baskes, Proceedings of the International Conference on Computer-assisted Materials Design and Process Simulation, Tokyo, The Iron and Steel Institute of Japan (1993) p. 219

A. D. Becke, Phys. Rev. A **38**, 3098 (1988).

S. F. Boys, Proc. R. Soc. A**200** (1950).

J. L. Brédas F. Meyers, B. M. Pierce, and J. Zyss, J. Am. Chem. Soc. **114**, 4928 (1992).

K. M. Brommer, M. Needles, B. Larson, and J. D. Joannopoulos, Phys. Rev. Lett. **68**, 1355 (1992).

C.G. Broyden, J. Inst. Math. Appl, **6**, 76. (1970).

R. Car and M. Parrinello, Phys. Rev. Lett. **55**, 2471 (1985).

C. R. A. Catlow and A. N. Cormack, Int. Rev. Phys. Chem. **6**, 227 (1987).

C. R. A. Catlow and J. M. Thomas, Phil. Trans. R. Soc. Lond. A **341** (1992)

.C.R.A.Catlow, E.Kotomin (Eds), Computational Materials Science, NATO Science Series III, Vol.187, Computer Modelling of Fluids Polymers and Solids, Vol.293, (1990)

M. L. Cohen and V. Heine, Solid State Physics **24**, 37 (1970)

D. G. Coronell and K. F. Jensen, J. Computer-Aided Materials Design **1**, 3 (1993)

D.H.Damon, R. C. Miller, and A. Sagar, Phys.Rev 138,2A, (1965)

A.Dargys and J.Kundrotas, J.Phys.Chem.Solids, Vol 44, 3, (1983)

M. S. Daw and M. I. Baskes, Phys. Rev. B **29**, 6443 (1984)

W.A.Deer, R.A.Howie, J.Zussman, An introduction to the rock forming minerals, Longman, Harlow, UK, (1992)

B. Delley, J. Chem. Phys. **92**, 508 (1990)

M. J. S. Dewar and W. Thiel, J. Am. Chem. Soc. **99**, 4899 (1977)

D. A. Dixon, in Computer Applications in Applied Polymer Science II: Automation, Modeling, and Simulation, T. Provder, editor, ACS Symposium Series No. **404**, 147 (1989)

D. A. Dixon and B. E. Smart, Chem. Eng. Comm. **98**,173 (1990)

R. Dovesi , V. R. Saunders, and C. Roetti, CRYSTAL 92 User Manual, University of Turin, Italy, and SERC Daresbury Laboratory, UK; August 17 (1992)

P.R.Emtage, Phys.Rev Vol.138 No 1A (1965)

A.Ennaoui, H.Tributsch, Solar Cells, 13, 197, (1984)

V.Eyert, K.H.Hoch, S.Fietcher, and H.Tributsch, Phys. Rev B, 57(11), 6350, (1998)

I.D .Faux , J. Phys. C, **4**, L211, (1971)

E. Fermi, Z. Phys. **48**, 73 (1928)

I.J. Ferrer, D.M. Nevskaia, C. de las Heras, C. Solid State Commun., **74**, 913, (1990)

R. Fletcher, Comput. J., **13**, 317, (1970)

V. Fock, Z. Phys. **61**, 126 (1930) and ibid. **62**, 795 (1930)

T. Forester and W. Smith (DL POLY, DLPOLY, CCP5 Program Library, Daresbury Lab., UK, (1994)

A. J. Freeman and R. Wu, J. Magn. Magn. Mater **104-107**, 1 (1992)

C. L. Fu and A. J. Freeman, J. Mag. Magn. Matls. **54-57**, 777 (1986)

C. L. Fu, A. J. Freeman, E. Wimmer, and M. Weinert, Phys.Rev.Lett. **54**, 2261 (1985)

J.D. Gale, Phil. Mag. B, **73**, 3, (1996)

J.D. Gale, *JCS Faraday Trans.,* **93**, 629 (1997)

J.D. Gale and A.L. Rohl, *Mol. Simul.*, **29**, 291 (2003)

J. G. Gay, J. R. Smith, and F. K. Arlinghaus, Phys. Rev. Lett. **42**, 332 (1979)

D. Goldfarb, *Math. Comp*, **24**, 23*,* (1970)

X. Gonze, D. C. Allan, and M. P. Teter, Phys. Rev. Lett. **68**, 3603 (1992)

O. Gunnarsson, B. I. Lundqvist, and S. Lundqvist, Solid State Commun.**11**, 149 (1972)

J.H.Harding, *Rep.Prog.Phys.,**53**,1403*,(1990)

J. Harris, Phys. Rev. B **31**, 1770 (1985)

D. R. Hartree, Proc. Camb.Phil. Soc. **24**, 89 (1928)

R. Haydock, V. Heine, and P. J. Kelly, J. Phys. C **5**, 2845 (1972); **8**, 2591 (1975)

W. J. Hehre, L. Radom, P. Schleyer, and J. A. Pople, *Ab initio molecular orbital theory*, John Wiley & Sons, New York (1986)

P. Hohenberg and W. Kohn, Phys. Rev. **136**, B864 (1964)

W.Jaegerman, H.Tributsch, J. Appl. Electrochem, 13, 743, (1983)

K. S. Kim, M. A. Moller, D. J. Tildesley, and N, Quirke, Molecular Simulation **13**, 77 (1994)

D. D.Koelling and G. O. Arbman, J. Phys. F **5**, 2041 (1975)

D. D. Koelling and B. N. Harmon, J. Phys. C **10**, 3107 (1977)

A. Komornicki and G. Fitzgerald, Chem. Phys. **98**, 1399 (1993)

W. Kohn and N. Rostoker, Phys. Rev. **94**, 1111 (1954)

W. Kohn and L. J. Sham, Phys. Rev. **140**, A1133 (1965)

J. Korringa, Physica **13**, 392 (1947)

J. Labanowski and J. Andzelm, editors, Density Functional Methods in Chemistry, Springer-Verlag, New York, (1991)

M. Lannoo and P. Friedel, *Atomic and Electronic Structure of Surfaces. Theoretical Foundations*, Springer Series in Surface Science 16, Ed. M. Cardona, Springer Verlag, (1991)

I. Lefebvre, M.Lannoo, and G. Allan, Phys. Rev. B **39**, 13518 (1989)

Z. H. Levine and D. C. Allan, Phys. Rev. Lett. **66**, 41 (1991)

X. -P. Li, R. W. Nunes, and D. Vanderbilt, Phys. Rev. B **47**, 10891 (1993)

P. S. Mangat, P. Soukiassian, K. M. Schirm, L. Spiess, S.-P. Tang, A. J. Freeman, Z. Hurych, and B. Delley, Phys. Rev. B **47**, 16311 (1993)

J. Maple, J., U. Dinur, A. T. Hagler, Proc. Nat. Acad. Sci. USA **85**, 5350 (1988)

F. Mauri, G. Galli and R Car, Phys. Rev. B **47**, 9973 (1993)

M. Methfessel, Phys. Rev. B **38**, 1537 (1988)

N. Mori, H. Takahashi, High Pressure Research in Mineral Physics, eds. M.H. Manghnani and Y. Syono, American Geophysical Union, 341, (1987)

V. L. Moruzzi, J. F. Janak, and A. R. Williams, *Calculated Electronic Properties of Metals*, Pergamon Press, NY (1978).

C. Mottet, G. Tréglia, and B. Legrand, Phys. Rev. B **46**, 16018 (1992).

F.D. Murnaghan, Proceedings of the National Academy of Sciences, **30**, 244-247, (1944).

L. P. Nielsen, F. Besenbacher, I. Stensgaard, E. Laegsgaard, C. Engdahl, P. Stoltze, K. W. Jacobsen, and J. K. Nørskov, Phys. Rev. Lett. **71**, 754 (1993).

P.M.Nikolic et al, Jpn.J.Appl.Phys.Vol 36, (1997)

M.J. Norgett , J Phys. C., 4,298,(1971)

P. M. Oppeneer, T. Maurer, J. Sticht, and J. Kübler, Phys. Rev. B **45**, 10924 (1992)

J. O'Shaughnessy, Solid State Communications, Vol 8, (1970)

D.E. Parry, Surf. Sci. 49, 433 (1975)

D.E. Parry, Surf. Sci. 54, 195 (1976)

M.C. Payne, M. P. Teter, D. C. Allan, and J. D. Joannopoulos, Reviews of Modern Physics **64**, 1045 (1992)

M.C.Payne, J. D. Joannopoulos, D. C. Allan, M. P. Teter, and David H. Vanderbilt, Phys Rev.Lett, 56, 2656, (1986)

J. P. Perdew, Phys. Rev. B. **33**, 8822 (1986)

J.C. Phillips, Phys. Rev. **112**, 685 (1958)

D. Pines, Solid State Physics **1**, 367 (1951)

C Priester, Journal de Physique III **1**, 481 (1991)

C. Priester, G. Allan, and M. Lannoo, Phys. Rev. B **37**, 8519 (1988)

T. J. Raeker and A. E. DePristo, Inter. Rev. in Phys. Chem. **10**, 1 (1991)

Reynolds et al, J.Phys.Chem.Solids, Vol. 29, (1968)

H. Sambe and R. H. Felton, J. Chem. Phys. **62**, 1122 (1975)

E. Salomons, P. Bellon, F. Soisson, and G. Martin, Phys. Rev. B **45**, 4582 (1992)

H. M. Sithole, PhD Thesis, University of the North, (2000), Unpublished

H. M. Sithole, P.E. Ngoepe, K. Wright, Phy. Chem. Minerals, **30** 615-619, (2003)

D.F. Shanno, Math. Comp., **24**, 647 (1970)

H. L. Skriver, The LMTO Method, Springer Verlag (1984)

J. C. Slater, Phys. Rev. **51**, 846 (1937)

J. C. Slater, Phys. Rev. **81**, 385 (1951)

J. C. Slater and G. F. Koster, Phys. Rev. **94**, 1498 (1954)

J. C. Slater, *Quantum Theory of Molecules and Solids Vol. 4*, McGraw-Hill, New York (1974)

J. J. P. Stewart, J. Computer-Aided Mol. Design **4**, 1 (1990)

I. Stich, M. C. Payne, R. D. King-Smith, J.-S. Lin, and L.J. Clarke, Phys. Rev. Lett. **68**, 1351 (1992)

V.L. Tauson, Mineralogiceskij 11, 30 (1989).

W.M.Temmerman, P.J.Durham, and D.J.Vaughan, Phys. Chem. Minerals, 20, 248, (1993)

L. H. Thomas, Proc. Camb. Phil. Soc. **23**, 542 (1926)

S. B. Tlali, H. M. Sithole, B. A. Mathe, L. M. Kotane, P. E. Ngoepe, Phys. Stat. Sol (c), **1**, No11, 3073-3076 (2004)

N. Troullier and J. L. Martins, Phys. Rev. B **43**, 1993 (1991).

P. Turchi and F. Ducastelle, The Recursion Method and Its Applications, D. G. Pettifor and D. L. Weaire, editors, Springer-Verlag, Berlin (1985) p.104

D. Vanderbilt, Phys. Rev. B 41 (Rapid Communications), 7892 (1990).

W. F. van Gunsteren, and P. K. Weiner, *Computer Simulation of Biomolecular Systems*, ESCOM, Leiden (1989)

L.Verlet Phys Rev A 159:98-103 (1967)

U. von Barth and L. J. Hedin, Phys. C **5**, 1629 (1972)

C. S. Wang and J. Callaway, Phys. Rev. B **8**, 4897 (1974)

E. Wimmer, J. Computer-Aided Materials Design **1**, 215 (1993)

E. Wimmer, A. J. Freeman, M. Weinert, H. Krakauer, J. R. Hiskes, and A. M. Karo, Phys. Rev. Lett. **48**, 1128 (1982)

E. Wimmer, H. Krakauer, and A. J. Freeman, in Electronics and Electron Physics, ed. by P.W. Hawkes, Vol. **65**, p. 357, Academic Press, Orlando (1985).

G.Wulff , *Z. Kryst. Mineral.* **34**, 449, (1901).

www.accelrys.com/about/msi.htm

www.accelrys.com/products/

J. Yu, A. J. Freeman, and J.-H. Xu, Phys. Rev. Lett. **58**, 1035 (1987)

G.L.Zhao, J.Callaway, and Hayashibara M., Phys. Rev B., **48**, 15781 (1993)

Papers and Posters Presented at Local and International Conferences

1. S.S.Mangwejane, P.E.Ngoepe, and H.M.Sithole, "Electronic Studies of $PtSb_2$ (geversite)", Materials Modelling Meeting, University of the North, 2001
2. S.S.Mangwejane, P.E.Ngoepe and S.C.Parker, "Computational Molecular Dynamics studies of $PtSb_2$ with special emphasis on variation of temperature". South African Institute of Physics, 47th Annual Conference 23-27 September 2002, University of Potchefstroom, Potchefstroom.
3. S.S.Mangwejane, P.E.Ngoepe and S.C.Parker, "Atomistic and Ab initio studies of bulk and surface properties of $PtSb_2$". South African Institute of Physics, 48th Annual Conference, 25-27 June 2003, University of Stellenbosch, Stellenbosch.
4. S.S.Mangwejane, P.E.Ngoepe and S.C.Parker, "Atomistic and Electronic simulation studies of $PtSb_2$". 4th International Workshop on Surface and Interface Segregation, 17-22 August 2003, iThemba Labs, Faure.
5. S.S.Mangwejane, P.E.Ngoepe and S.C.Parker, "Atomistic and Electronic simulation studies of $PtSb_2$", Interscience, 1-3 October 2003, University of the North, Sovenga
6. S.S.Mangwejane, P.E.Ngoepe and S.C.Parker , Ab initio Studies of Electronic and Optical Properties of $PtSb_2$ and $PtSb_2$" South African Institute of Physics, 49th Annual Conference, 28 June–02 July 2004, University of the Free State, Bloemfontein.
7. P.E.Ngoepe, S.P.Ntoahae, S.S.Mangwejane, H.M.Sithole, S.C.Parker and K.V.Wright "Atomistic Modelling of Metal Sulphides" European Materials Research Society Spring Meeting, 24-28 May 2004, Strasbourg, France.